Alma Mater Studiorum – Universitá di Bologna

Dottorato di Ricerca in

Meccanica e Scienze Avanzate dell'Ingegneria: Progetto n. 1
"Disegno e Metodi dell'Ingegneria Industriale e Scienze Aerospaziali"

Ciclo XXIII

Settore scientifico-disciplinare di afferenza: ING-IND/04

Crashworthiness and composite materials: development of an experimental test method for the energy absorption determination and implementation of the relative numerical model

Presentata da: Francesca Garattoni

Coordinatore Dottorato:
Chiar.mo Prof. Franco Persiani

Relatore:
Ing. Enrico Troiani

Esame finale anno 2011

We are all in the gutter,
but some of us are looking at the stars.
O. Wilde

Abstract

In this PhD thesis the crashworthiness topic is studied with the perspective of the development of a small-scale experimental test able to characterize a material in terms of energy absorption.
The material properties obtained are then used to validate a numerical model of the experimental test itself.
Consequently, the numerical model, calibrated on the specific material, can be extended to more complex structures and used to simulate their energy absorption behavior.
The experimental activity started at University of Washington in Seattle, WA (USA) and continued at Second Faculty of Engineering, University of Bologna, Forlì (Italy), where the numerical model for the simulation of the experimental test was implemented and optimized.

Sommario

In questa tesi di dottorato, il tema della crashworthiness è studiato nell'ottica di sviluppare un test di caratterizzazione del materiale su piccola scala, eseguibile in laboratorio, da utilizzare per la successiva validazione di un modello numerico.
Il modello numerico, opportunamente calibrato sulle caratteristiche del materiale, renderà possibile estendere le proprietà di assorbimento di energia a strutture di grande scala, riducendo tempi e costi di progettazione.
L'attività sperimentale iniziata presso i laboratori della Univeristy of Washington a Seattle, WA (USA) è proseguita presso i laboratori della Seconda Facoltà di Ingegneria dell'Università di Bologna, dove è stato ottimizzato il modello numerico per la simulazione del test sperimentale.

Acknowledgements

The research activity performed during these years would not have been possible without the help and support of many people.

In particular I would like to acknowledge:

Dr. Enrico Troiani, who led my research and gave me both technical and personal support during tough days.

Ing. Gianluca Molinari, a brilliant brain and great person I would have been lost without.

Ing. Paolo Proli, the more helpful extra hands I could ever have asked for.

Staff at the A&A dept. of the University of Washington, for the technical support and the possibility they gave me to feel like home at their facilities.

Besides the formal acknowledgements, other important persons that shared with me these years have to be mentioned.

My dear ladies (in alphabetical order, so no preferences) Daniela, Francesca, Sara and Valentina: what would I have done without your support and our endless talks about shoes?

The staff at MaSTeR Lab: Ivan and Lorenzo, you guys have driven me mad for three years, but life in the office would not have been so good otherwise.

And in the end, the most important acknowledgment: mom and dad.

Thanks for everything.

You know what I mean.

Contents

Preface

The advent of composite materials in primary aircraft structures has recently put the accent on the lack of data about the behavior of these structures under operative loads. As a matter of facts, the introduction of composite materials makes the data obtained from experience of incidents and accidents of existing aircraft, usually traditional aluminum structures, no longer sufficient or representative.

Moreover, this growing interest of the aeronautical industry for the use of composite materials in primary structures requires reliable tools for the design of these structures according to the requirements of occupants safety and crashworthiness.

In order to define an appropriate and useful tool for the design in crashworthiness, the purposed achievements of this PhD research are the development of an experimental test method for the energy absorption determination and the implementation of its relative numerical model.

To pursue these aims, the work will be articulated in two parts: experimental tests and numerical simulations.

In the experimental test part, different experimental test methods will be compared in terms of reliability, reproducibility of results and insensitivity to external factors through an extensive test campaign. Also, the experimental campaign will help the definition of the guidelines of a reliable test procedure.

The results obtained from the experimental tests will be used as a benchmark for the numerical model.

In the numerical simulations part, a virtual model of the test configuration defined as the most reliable, will be realized with a commercial finite elements software (Abaqus/Explicit). The model will implement a progressive failure analysis in order to simulate the macroscopic behavior of the experimental test during the crushing process. The numerical simulation is also asked to give an approximation of the experimental test specific energy absorption progress.

Throughout this PhD thesis, the reader will find the contemporary use of different Unit Systems: both English Units and the International System of Units. This happens because the most of the experimental part of the work presented in this PhD thesis was developed at the Aeronautics and Astronautics department facilities of the University of Washington in Seattle, WA (USA).

Chapter 1

Crashworthiness

> Crashworthiness: the ability of a craft, or one of its components, to sustain a crash event with minimal, or otherwise acceptable, damage to the occupants, cargo and structure.
>
> MIL-HDBK-17

1.1 Principles of crashworthiness

The overall objective of designing for crashworthiness is to eliminate injuries and fatalities in relatively mild impacts, and to minimize them in all severe collisions. A crashworthy vehicle will also control the extent of crash impact damage. By minimizing personnel and material losses, crashworthiness conserves resources, improves effectiveness, and increases confidence of the end-users [1].

This objective can be reached either by modifying the structural geometry of the assembly, or by introducing specific load-limiting devices in the structure to dissipate kinetic energy.

The new design philosophy replaces the more traditional "the stronger, the better" that is far from optimal when the objective is the protection of passengers or cargo in the event of an accident, because massive and stiff structures do not dissipate energy during the impact but they convey it to the occupants. It is therefore preferable to design a vehicle to collapse in a controlled manner, ensuring a safe dissipation of an adequate amount of kinetic energy.

The new structure, designed in accordance with the crashworthiness requirements [2], must ensure the four necessary conditions for survival as stated in [1], which are:

- maintaining sufficient occupant space;
- providing adequate occupant restraint;

- employing energy-absorption devices
- allowing for safe post-crash egress from the craft.

Traditionally, in the particular case of aircrafts, the energy-absorption devices are steel or aluminum structural elements; these materials allow a controlled collapse of the structure during which they absorb energy by folding or hinging, involving extensive plastic deformation.

The current trend of substituting metals with composites can improve the energy absorption performances of the devices [3, 4], but it introduces several problems due to the complexity of failure mechanisms that can occur within the material and the combination of fracture mechanisms that lead to structural failure. The overall response of the structure, moreover, is highly dependent not only on the failure mechanisms, but on a number of parameters including the geometry of the structure and the material system.

1.2 Regulations

Crashworthiness is a design philosophy that is applicable to every transportation field, from aircrafts to trains getting through the automotive industry.

Regarding aircrafts, the crashworthiness topic is discussed principally in FAA's Advisory Circular 20-107B "Composite aircraft structure" [2].

The purpose of the Advisory Circular (AC) is to file a set of guidance points which are not mandatory or regulatory in nature. The guidelines purposed in the AC are one of the many means of showing compliance with the provisions of Title 14 of the Code of Federal Regulations (14 CFR) parts 23, 25, 27 and 29 regarding airworthiness type certification requirements for composite aircraft structures involving fiber reinforced materials.

The procedures outlined in the AC provide guidance material for composite structures, particularly those that are essential in maintaining the overall flight safety of the aircraft, and are considered acceptable to the FAA showing compliance with certification requirements of civil composite aircrafts.

The crashworthiness of the aircraft is dominated by the impact response characteristic of the fuselage [2]. Regulations, in general, evolve based on either experience gained through incidents and accidents of existing aircraft or in anticipation of safety issues raised by new designs. In the case of crashworthiness, regulations have evolved as experience has been gained during actual aircraft operations. Fleet experience has not demonstrated a need to have an aircraft level crashworthiness standard. As a result, the regulations reflect the capabilities of traditional aluminum aircraft structure under survivable crash conditions. This approach was

satisfactory as aircrafts have continued to be designed using traditional construction methods. With the advent of composite structures, this historical approach may no longer be sufficient to substantiate the same level of protection for the passengers as provided by similar metallic design.

The AC states that special conditions are anticipated for transport category airplanes with composite fuselage structure to address crashworthiness survivability. The impact response of a composite fuselage structure must be evaluated to ensure the survivability is not significantly different from that of a similar-sized aircraft fabricated from metallic materials. Impact loads and resultant structural deformation of the supporting airframe as well as floor structures must be evaluated. Four main criteria areas should be considered in making such an evaluation:

1. occupants must be protected during the impact event from release of items of mass (e.g. overhead bins);
2. the emergency egress paths must remain following a survivable crash;
3. the acceleration loads experienced by occupants during a survivable crash must not exceed critical thresholds;
4. a survivable volume of occupant space must be retained following the impact event.

The criticality of each of this four criteria will depend on the particular crash conditions: for example, the loads and accelerations experienced by passengers may be higher at lower impact velocities where structural failures have not started to occur.

1.3 Energy absorption and failure mechanisms

To better understand the phenomenon of energy absorption, few key-terms need to be pointed out. Referring to figure 1.1a, the typical behavior of a crushed structure is represented: F is the applied force and l is the shortening of the structure (or stroke). A plot of the applied force history is also produced for every test (figure 1.1b); referring to this exemplar plot, the most important features that regulate the energy absorption behavior are:

- *stroke*, also referred to as *crush* or *displacement*, is the amount (length) of structure or material being sacrificed during the impact event;
- *peak force* (F_{max}), also known as maximum load, is the maximum point on the load-stroke or force-displacement diagram;
- average crush force (F_{avg}), or *sustained load*, is the displacement- or time-average value of the crush force;

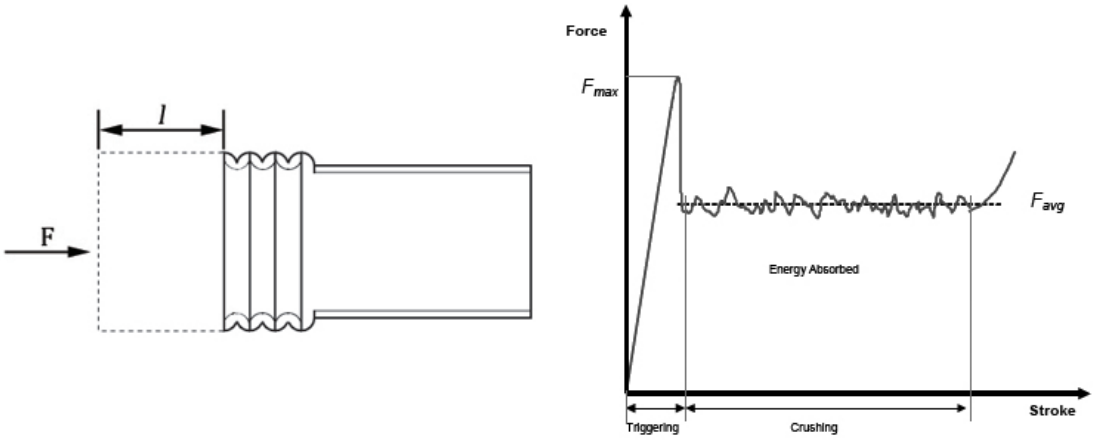

(a) (b)

Figure 1.1: Typical representation of (a) a crushed structure and (b) its relative load-displacement plot

- crush initiator, also known as *trigger mechanism*, is a design feature that facilitates the progressive collapse of the structure avoiding the tendency of composite materials to fail in an unpredictable and sometimes unstable manner;

- *Energy Absorption* (EA) is the total area under the load-stroke diagram

$$EA = \int F dl \tag{1.1}$$

- Specific Energy Absorption (SEA) is the energy absorbed per unit mass of crushed structure expressed in J/g

$$SEA = \frac{EA}{\rho\ A\ l} \tag{1.2}$$

  where ρ is the density of the material, A the cross-sectional area and l the stroke.

The specific energy absorption (SEA) will be the main parameter for the evaluation of both test reliability and material efficiency throughout the whole dissertation.

The specific energy absorption strongly depends on the mode the structure fails. As a matter of fact, two different crushing modes can occur: the catastrophic failure mode and the progressive failure mode.

The catastrophic failure mode occurs when unstable intralaminar or interlaminar crack growth occurs and it is characterized by a sudden increase in load to a peak value followed by a low post failure load.

The progressive failure mode is when the failure is controllable and progresses through the body at the loading speed. In this case, a trigger is provided at one end of the structure. A trigger is a stress concentrator that causes the failure to initiate at a specific location; it reduces the initial load peak that accompanies failure initiation followed by a stable collapse.

The advantages of a progressive failure are that the energy absorbed in a progressive crush is larger than the one absorbed in a catastrophic failure. Furthermore, a structure designed to react to loads produced by progressively failing energy absorbers is lighter than structures designed to react to loads produced by catastrophically failing energy absorbers.

According to Farley [5], the crushing mode is an indication of how efficiently the structure, or the specimen in the case of a coupon-size test, is being crushed. The understanding of the crushing response includes how energy-absorption capability is affected by both the mechanical properties of the constituent material and the specimen structure; moreover, Farley states that also the crushing speed can affect the energy-absorption capability of a structural element made of composite material in the same way the strain rate can affect the mechanical response of a material.

Referring to his studies on composite tubular specimens (1989), Farley identifies four different crushing modes: all of them are exhibited by brittle composite material, while only the last one is showed by ductile composites.

1. *Transverse shearing* or *fragmentation mode*

   It is characterized by a wedge-shaped laminate cross section with one or multiple short interlaminar and longitudinal cracks that form partial lamina bundles (figure 1.2). The main energy absorption mechanism is fracturing of lamina bundles; when fragmentation occurs, the length of the longitudinal and interlaminar cracks are less than that of the lamina. The mechanism results efficient when the characteristic length of the crushed material is short.

   The mechanism that controls the crushing process is the transverse lamina bending strength. It is a function of the fiber stiffness and strength: if the fiber mechanical response is a function of strain rate, then the energy-absorption capability is a function of crash speed.

2. *Brittle fracturing*

   The brittle fracturing crushing mode (figure 1.3) exhibits the same principal energy-absorption mechanism of the transverse shearing mode, that is to say the failure of the lamina bundles.

   However, the characteristic length of the interlaminar cracks in the brittle fracturing crushing mode is between one and ten times the laminate thickness. The longer the fractured lamina bundle is, the less efficient the crushing

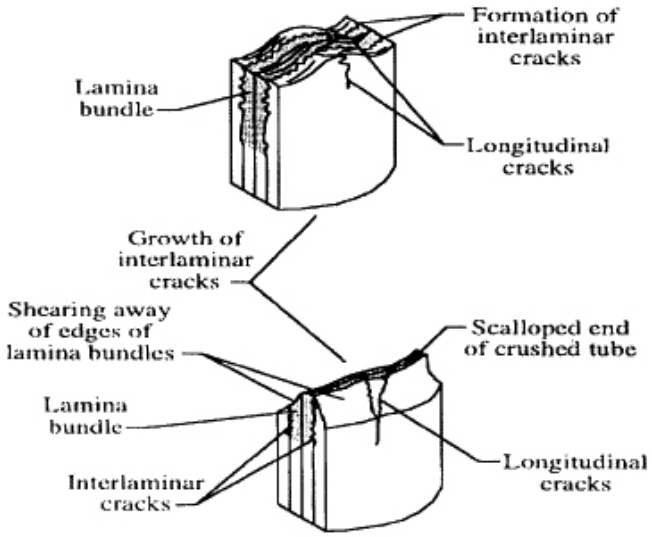

Figure 1.2: Transverse shearing or fragmentation mode [5]

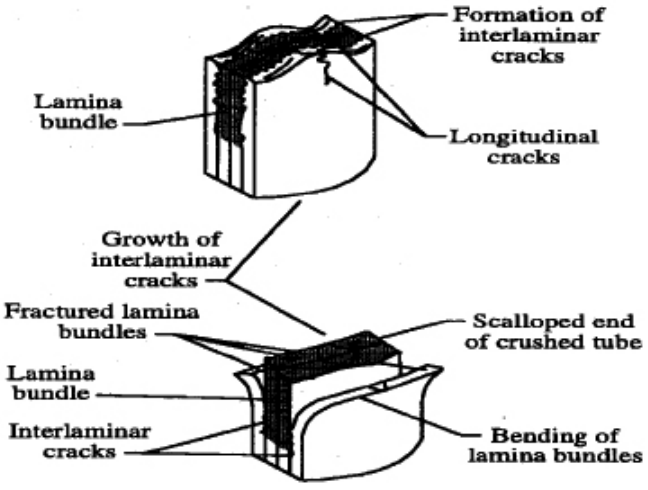

Figure 1.3: Brittle fracturing [5]

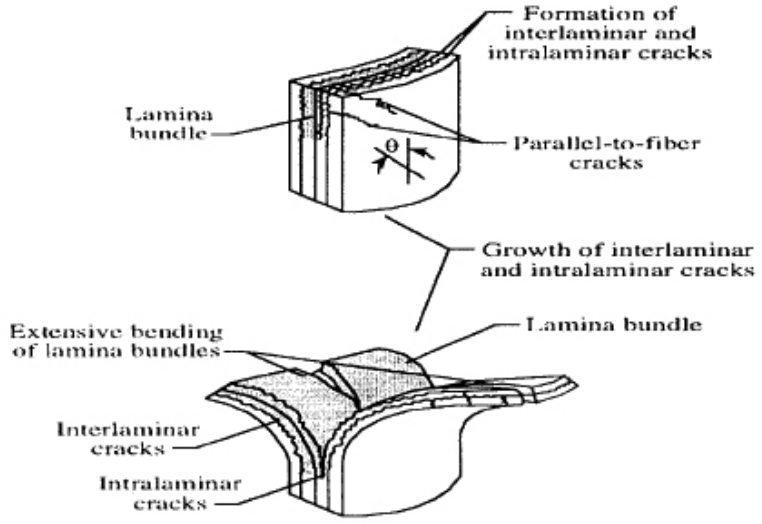

Figure 1.4: Lamina bending or splaying mode [5]

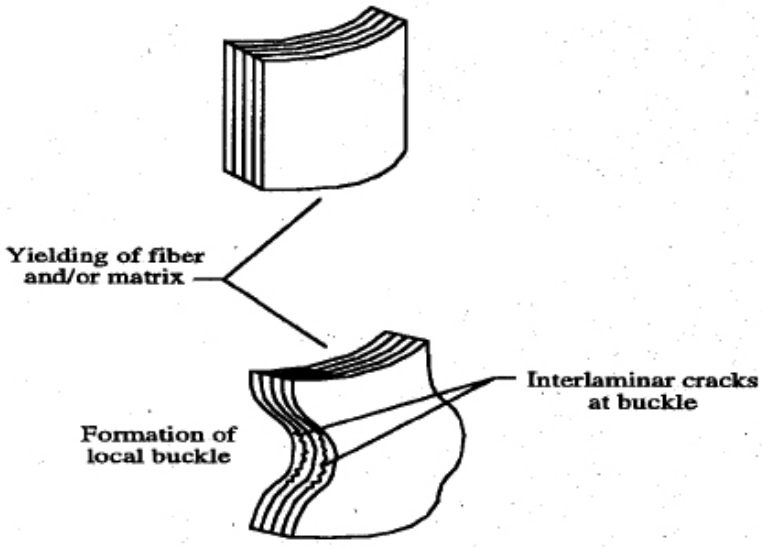

Figure 1.5: Local buckling or progressive folding [5]

mode is. Lamina bundles in brittle fracturing crushing mode exhibit some bending and usually fracture near the base. When a fracture of lamina bundle occurs, the load is redistributed within the specimen and the cyclic process of crack growth and lamina bundle fracture is repeated.

The controlling mechanism for the brittle fracturing mode is double: matrix strength and lamina bundle tensile strength. The first controls the interlaminar, intralaminar and parallel-to-fiber crack growth, while the second controls the fracture of the lamina bundle. In the latter, the mechanical response of the lamina bundle is primarily a function of the mechanical properties of either the fiber (for the 0° lamina bundle) or the matrix (90° lamina bundle or low fiber volume fraction material).

3. *Lamina bending* or *splaying mode*

   Lamina bending (figure 1.4) is characterized by very long interlaminar, intralaminar and parallel-to-fibers cracks but the lamina bundles do not fracture. The principal energy absorption mechanism is crack growth. While the three kinds of cracks form and grow in their own peculiar mode, the lamina bundles exhibit significant bending deformation but do not fracture. The lengths of interlaminar, intralaminar and parallel-to-fiber cracks are generally greater than ten times the laminate thickness. The long length of the lamina bundles and the lack of their fracturing result in an inefficient crushing mode.

   The matrix strength is the controlling mechanism of the lamina bending crushing mode. It controls the interlaminar, intralaminar and parallel-to-fiber crack growth. Considering that many polymeric matrix materials exhibit a mechanical response that is function of the strain rate, in the lamina bending crushing mode the crushing speed will affect the energy-absorption capability because the energy absorbed through matrix crack growth is a significant portion of the total energy absorption.

4. *Local buckling* or *progressive folding*

   Local buckling (figure 1.5) is characterized by the formation of local buckles by means of plastic deformation of the material. The mode is exhibited by both brittle and ductile fiber reinforced composite material. Ductile fiber-reinforced composites remain intact after being crushed and thereby demonstrate post-crushing integrity. The post-crushing integrity is a result of fiber and matrix plasticity and fiber splitting. Brittle fiber-reinforced composites exhibit the local buckling crushing mode only when the interlaminar stresses are small compared to the strength of the matrix, or the matrix has a higher failure strain than the fiber, or the matrix exhibits plastic deformation under high stress. Mechanisms like plastic yielding of the fiber and/or the matrix control the crushing process for progressive folding. The local buckling mode is generally an inefficient crushing mode for thin-walled specimens.

The crushing mechanism that controls this crushing mode is the matrix non-linear stress-strain response. If the material is brittle, the local buckling is exhibited only if the matrix has a high failure strain. With ductile materials, the material property that controls the local buckling crushing response can be either fiber or matrix stiffness.

Physics and mechanics of the crashworthiness of composite structures involve several issues. The local strength, energy absorbing characteristics, and multiple, competing failure modes need to be addressed for composite structures made from anisotropic, quasi-brittle, composite materials. As a result, the accelerations and load histories experienced by passengers and equipment on a composite aircraft may differ significantly from that experienced on a similar metallic aircraft unless specific considerations are designed into the composite structure.

Considering a need for comparative assessments with metal structures and a range of crash conditions, analysis with sufficient structural test evidence is often needed for transport applications. Analysis requires extensive investigation of model sensitivity to model parameters and test also requires investigation of test equipment sensitivity appropriate to composites. Model validation may be achieved using a building block approach, culminating in an adequately complex test.

The development of the first stage of the building block approach is the purposed achievement of this thesis: in the following chapters the development of a coupon-size test and its implementation in a finite element environment will be presented.

The aim of this work is to define a test that is sensitive neither to the equipment used to perform it, nor to the environment where it is performed. Once the experimental test is defined, the study of its numerical model is presented.

Chapter 2

Experimental tests

All life is an experiment.
The more experiments you make the better.

R. W. Emerson

2.1 Introduction

According to the AC 20-107B, the strength of a composite structure should be reliably established, incrementally, through a program of analysis and a series of test conducted using specimens of varying levels of complexity, from coupons to full size structure.

Crush tests can be carried out in two different ways: quasi-static and impact conditions.

In quasi-static conditions, the specimen is crushed at a constant speed. This is not a true simulation of a crash condition, because in a real crash condition the structure is subjected to a decrease in crushing speed, from the initial impact speed to rest. Assuming that many materials used in crashworthy structures are rate sensitive, that means that their energy absorption capability is a function of crushing speed, the quasi-static test may not lead to an accurate value of the amount of energy absorbed.

The advantages of the quasi-static test are that it simple and easy to control and that it does not require the expensive equipment necessary to record the crash event as it happens in the impact test.

Its main disadvantage is that this kind of test may not be a true simulation of the actual crash conditions, but it has to be evaluated material by material.

In the impact test, on the other hand, there is a true simulation of the crash event, as the crushing speed decreases from the initial impact velocity to rest because of the energy absorbed by the specimen.

The advantage of the impact test is that it is a true simulation of the crash condition since it takes into account the stress rate sensitivity of materials.

The major disadvantage of this test is that the crushing process takes place in a fraction of second, so expensive equipment as high-speed cameras are necessary to study the crushing at its best.

The most of the tests performed in this work are quasi-static tests. The reasons of this choice are principally:

- the low cost of the equipment needed to perform the test;
- the simplicity of control of the test procedure, easily performable in a university laboratory;
- the possibility of studying the fracture mechanisms of composite materials, which are not rate sensitive.

Few impact tests have been performed, though, as a comparison for the energy-absorption results obtained with quasi-static tests to demonstrate the reliability of the latter.

In this chapter, the first level of analysis will be described and discussed: a wide range of coupons has been tested to determine the energy absorption capability of carbon fiber reinforced plastics.

The tests were performed according to different methodologies found in literature. The test methods were compared in terms of reliability, easiness of setup and sensitivity to external factors, finally a procedure with a new concept of self-supporting specimens was defined and will be purposed as a standard method.

2.2 Test methodologies

In literature, it is possible to find only a limited number of attempts of coupon size test methods for composite materials. They can be divided into two main categories based on the kind of specimen they use:

- flat specimen test [6–9];
- self-supporting specimen test, usually thin-walled tubes [5, 10–13].

The flat specimen test method consists generically in a flat coupon crushed in between two anti-buckling supports; the anti-buckling support is provided by dedicated test fixtures like the ones developed by the Army Research Laboratory (ARL) [6] (figure 2.1) or the University of London [8, 9] (figure 2.2).

The ARL fixture (figure 2.1a) presents a movable platen (top plate), fitted with linear bearings, that slides on four guide rods which are fixed in a base plate. The

specimen is in contact with, and supported by, four knife-edges that fit into their support posts. The knife-edges constrain the specimen along its full height and can host only specimens of a fixed thickness and width (figure 2.1b).

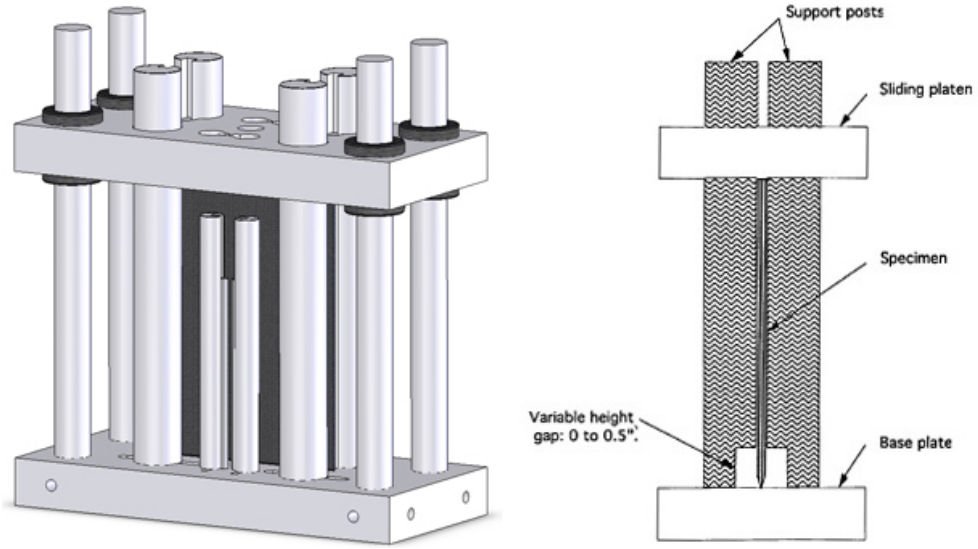

(a) (b)

Figure 2.1: Anti-buckling fixture developed by ARL – NASA: (a) isometric view and (b) schematic side view [6]

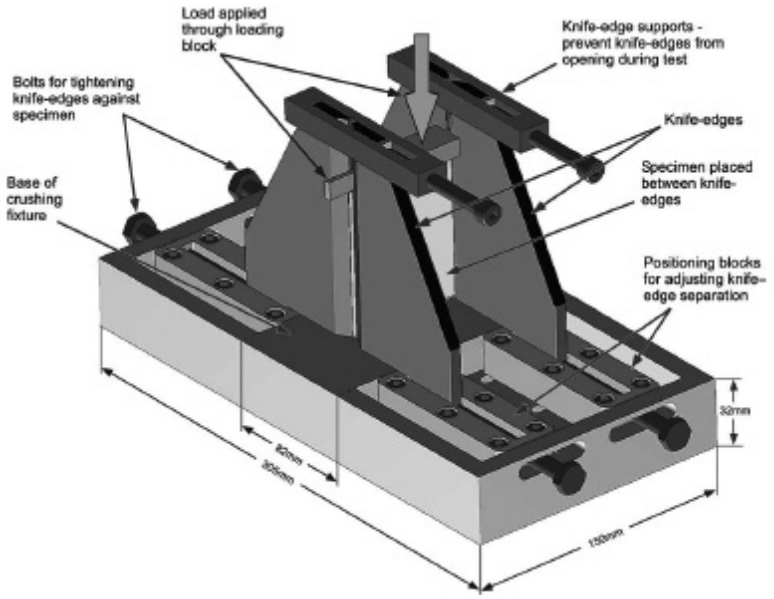

Figure 2.2: Modified ARL fixture by University of London [8]

The specimens used in the ARL test method are flat rectangular plates with two different trigger mechanisms: the so-called steeple (figure 2.3 left) and notch (figure 2.3 right).

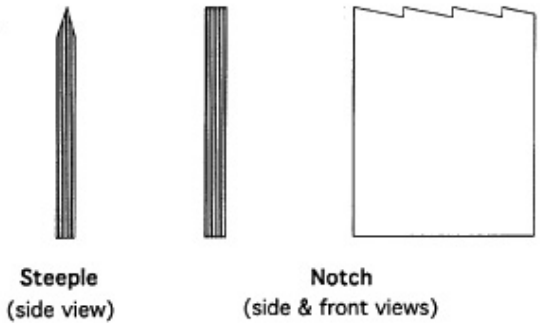

Figure 2.3: Trigger mechanisms [6]

Both of the trigger mechanisms worked successfully, leading to a sustained crush of the specimen; the steeple trigger characterized the load-displacement history plot with a double peak during the initial loading phase, probably due to the formation of a long central crack that divides the specimen in two fronds, but it did not affect the result of the test in terms of energy absorption (figure 2.4).

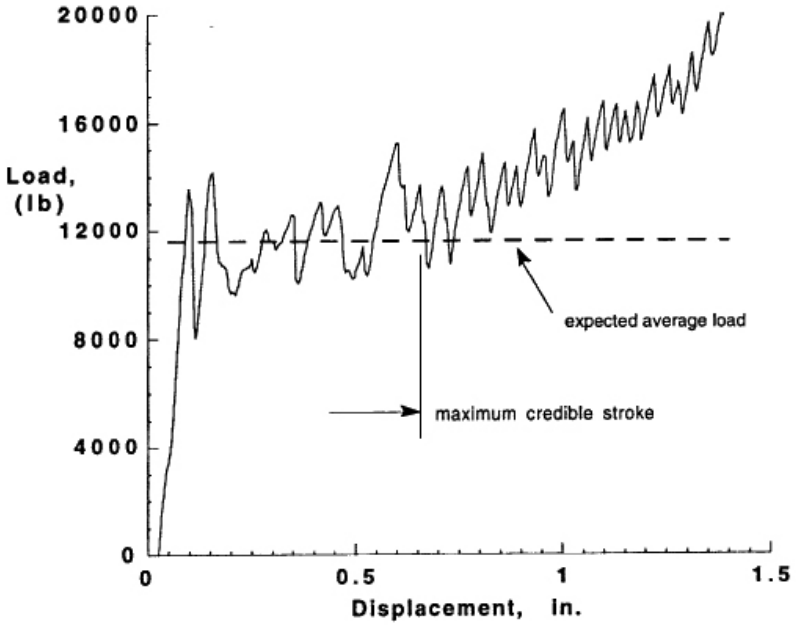

Figure 2.4: Typical crushing response obtained by ARL tests [6]

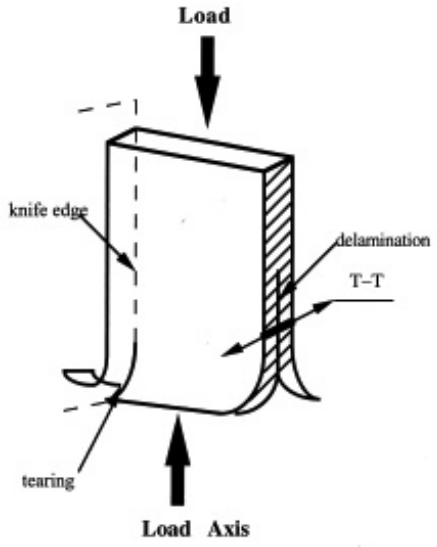

Figure 2.5: Fronds tearing phenomenon [9]

The first configuration of the fixture constrained the specimen along its full height and this led to phenomena of fronds tearing (figure 2.5); those phenomena are the reason why the SEA value rose steadily during the test instead of being constant as expected (figure 2.4).

The test method developed by ARL was recently revised by a research group at University of London [8, 9].

The fixture was modified introducing movable knife-edges to allow for different plate widths and thicknesses (figure 2.2); however, this new configuration, does not resolve the limitation of the tearing of the fronds already recorded with the original fixture design.

An effort to understand the reliability of the ARL test method was made by Bolukbasi and Laananen [11] comparing the energy absorption behavior of both flat specimens tested with the ARL fixture and two self-supporting geometries: an angle stiffener and a C-channel stiffener (figure 2.6).

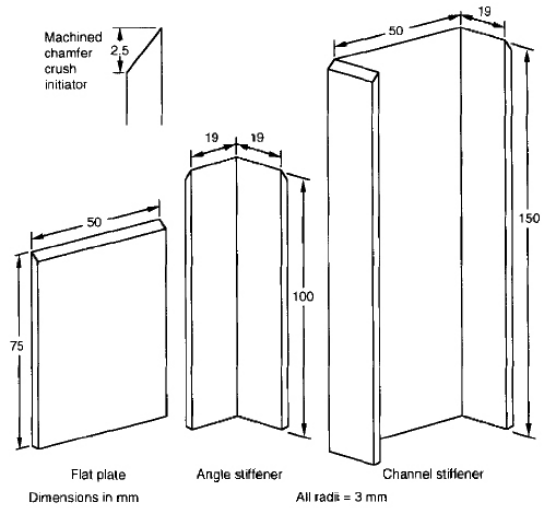

Figure 2.6: Flat specimen and stiffeners tested by Bolukbasi and Laananen [11]

The three specimen configurations were realized with the same material system and layup; the crush initiator mechanism was common to all the geometries. All the specimens were crushed under the same quasi-static conditions.

The experimental results obtained by Bolukbasi and Laananen evidenced that the flat plates supported by the fixture absorb a higher amount of energy than the self-supporting specimens.

The self-supporting specimen test method eliminates the need of an anti-buckling fixture and all its related issues, like the phenomenon of fronds tearing or the arbitrary closing force of the knife-edges. The test method is similar to the one with flat specimens but simpler, in fact the specimen is crushed between two plates fixed to the load cell actuator.

Figure 2.7: Crushed square tube

Different shapes of self supporting specimens can be found in literature: from a simple tube, round or square (fig. 2.7), to sinusoidal webs (fig. 2.8) [5], getting to complex C-shaped tube-segments like the ones developed by DLR [10] (fig. 2.9).

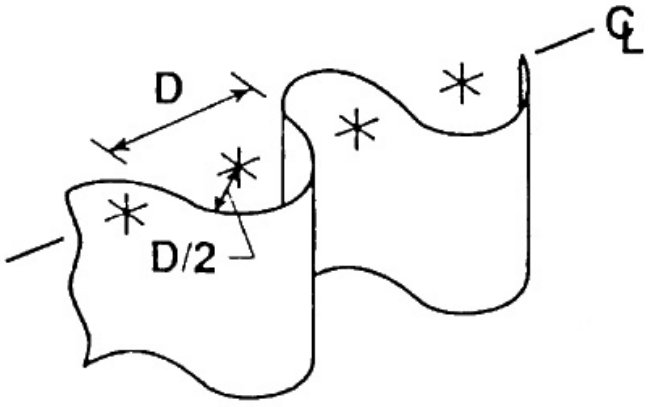

Figure 2.8: Tangent half-circle tube beam (sine-wave beam) [5]

The manufacture of tubes is more complex than that of flat specimens, requiring an internal mandrel around which the plies have to be wrapped. The alternative shape of DLR specimens gave a hint to override the mandrel complication of self-supporting specimens manufacture, but to increase its stability, the specimen is mounted with adhesive in a contoured aluminum base.

The experimental tests on carbon/epoxy specimens gave reproducible crush failures (figure 2.10), involving fracture mechanisms that lead to a progressive crush and a constant level of sustained load, that is preferable to the slightly increasing sustained load registered with flat specimens constrained in their fixture.

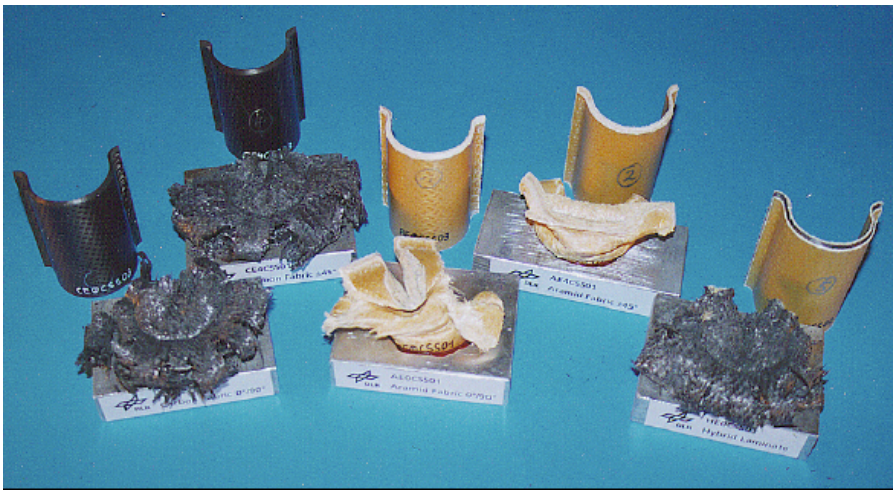

Figure 2.9: Examples of DLR self-supporting specimen shape [10]

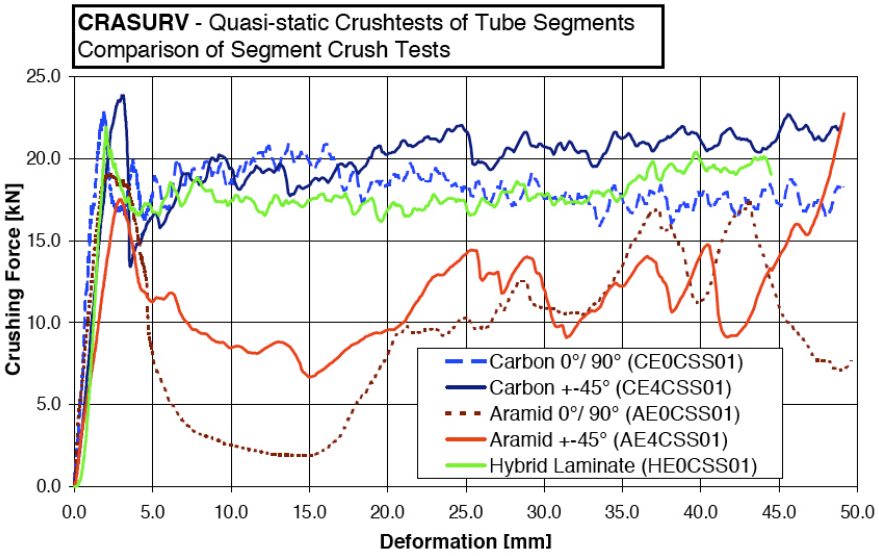

Figure 2.10: Measured load deformation curves of DLR tests with tube segments [10]

2.3 Test campaigns

Five different test campaigns were performed to collect data:

1. first session of tests with flat specimens crushed in a ARL inspired fixture;
2. second session of tests with flat specimens with the ARL fixture and improved anti-buckling supports;
3. first session of tests with self-supporting specimens in three different shapes;
4. flat specimens crushed with a new design fixture;
5. second session with self supporting specimens with innovative layups.

The results of each campaign were used to better define the following campaign and the test method.

The most of the tests were performed at the laboratories of the Aeronautics and Astronautics department of the University of Washington, Seattle, WA (USA) while the second session with self supporting specimens was totally developed and realized at MaSTeR Lab – Material Structure Technology Research Laboratory at the Second Faculty of Engineering, University of Bologna, Forlí (Italy).

2.3.1 Flat specimen part I

The first set of tests on the energy absorption capability were intended as a feasibility study using an anti-buckling fixture similar to the ARL one (figure 2.11).

A generic carbon fiber reinforced plastic (epoxy) material was tested; the density of the material is 1.55 g/cm^3.

The specimen dimensions were 3 in x 4 in to fit into the knife-edges of the fixture. The thickness was around 0.092 in, relative of a $[0/90]_{4s}$ layup. Two kinds of trigger were tested: arrow (A) (figure 2.12a) and sawtooth (S) (figure 2.12b).

The specimens were crushed at different speeds of 0.5, 1.5 and 10 in/sec; with the chosen speeds, the tests can be classified as impact tests. The unsupported length (h) was tested in a range from 0 to 1.5 in (figure 2.13).

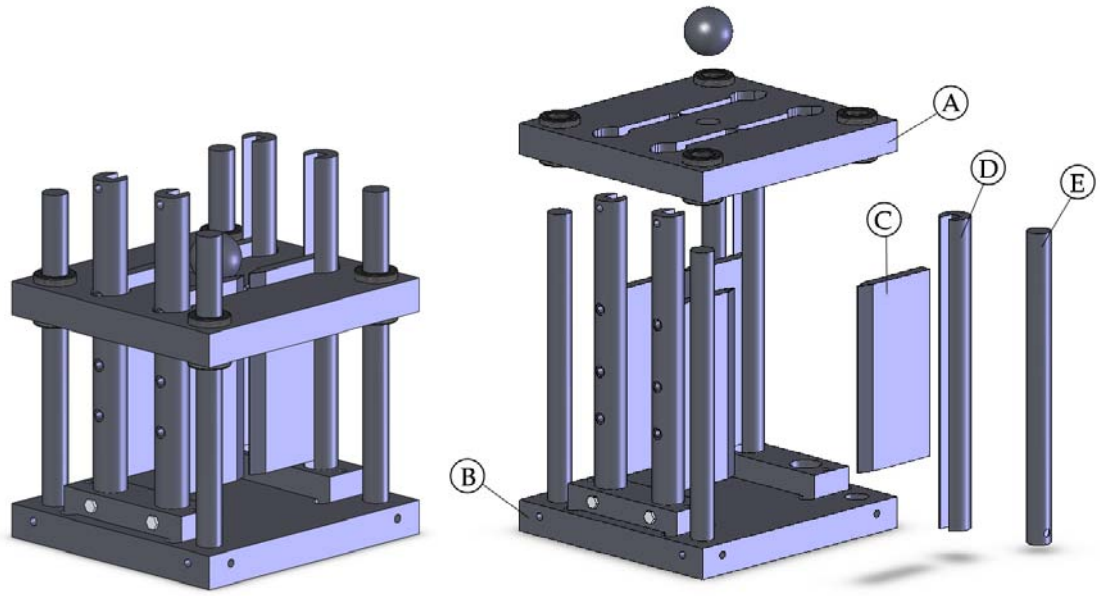

(a) (b)

Figure 2.11: Anti-buckling fixture inspired to the ARL – NASA one: (a) closed view and (b) main components: A - top plate; B - bottom plate; C - knife-edge; D - support rod; E - guide rod

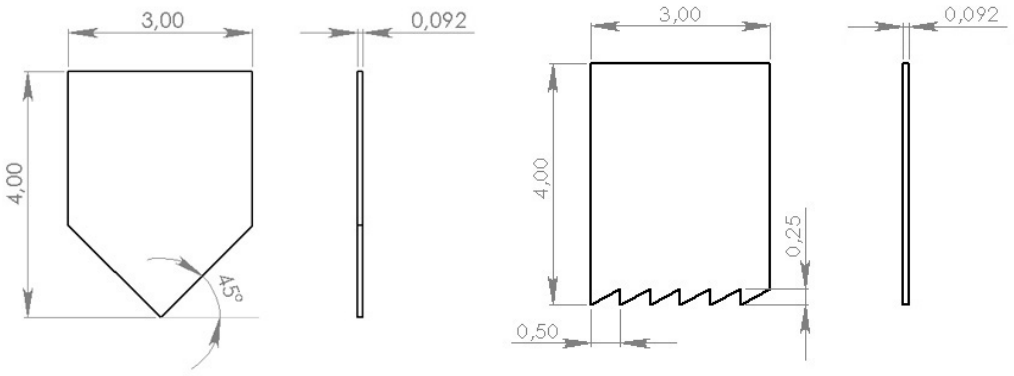

(a) Arrow specimen (b) Sawtooth specimen

Figure 2.12: Specimens

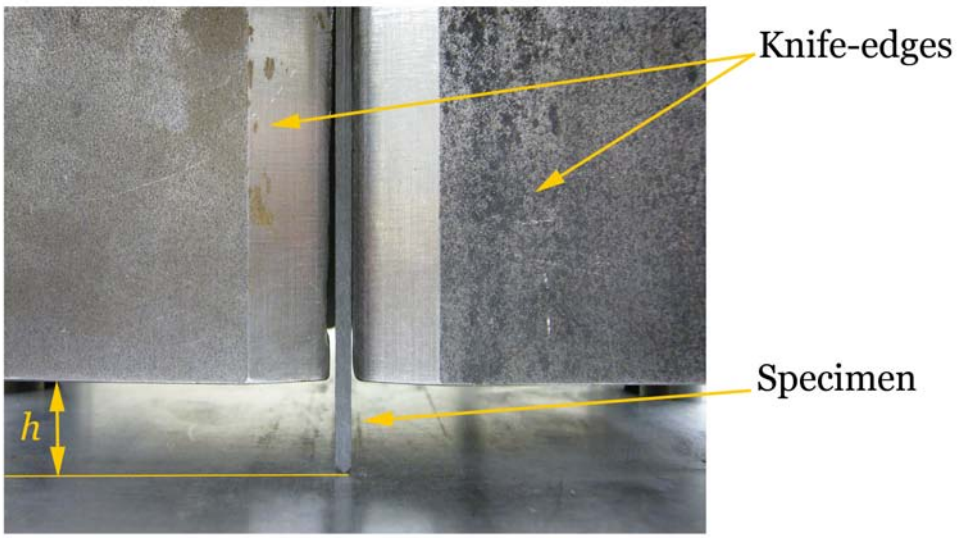

Figure 2.13: Sideview of a specimen constrained between knife-edges; h is the unsupported length

A summary of the tests performed is in table 2.1: trigger is either arrow (A) or sawtooth (S), v is the crushing speed measured in in/sec and h is the unsupported length of the specimen.

Test ID	Trigger	v [in/sec]	h [in]
2	A	0.5	1.5
3	A	0.5	0.5
4	A	10	0.5
5	S	1.5	0.5
6	A	1.5	0

Table 2.1: Flat specimen tests part I - Test summary

The results obtained are shown in table 2.2 and in figure 2.14. In figure 2.14, the results are presented as a function of the increasing unsupported length of the specimen.

For each configuration, only a test was performed at this stage of the test campaign.

Test ID	Trigger	v [in/sec]	h [in]	SEA [J/g]
2	A	0.5	1.5	18.366
3	A	0.5	0.5	12.714
4	A	10	0.5	23.955
5	S	1.5	0.5	17.117
6	A	1.5	0	113.567

Table 2.2: Flat specimen tests part I - Results

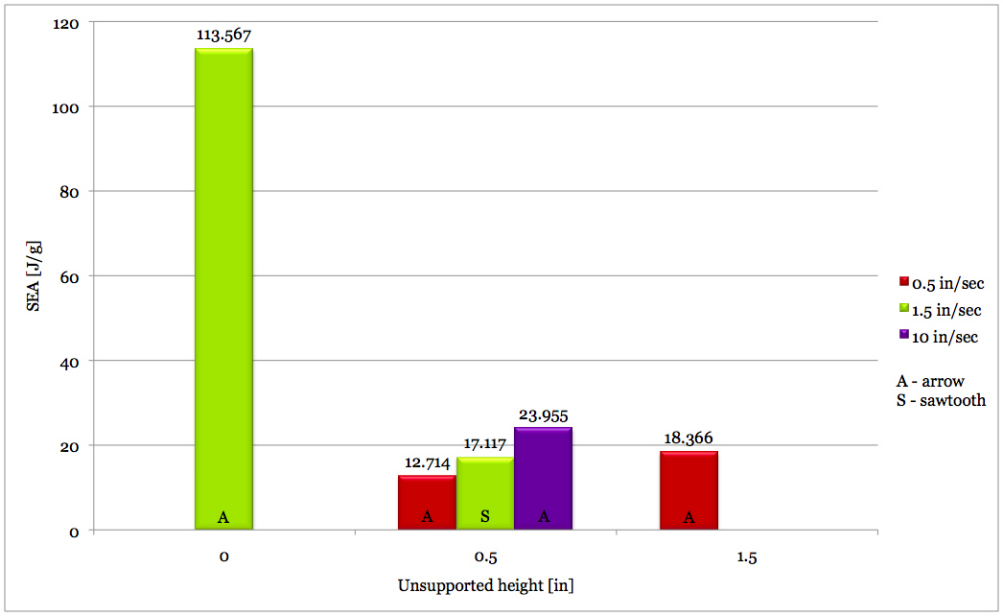

Figure 2.14: Flat specimen tests part I - Results

From the results obtained, the following aspects of the test method can be picked out:

- the higher amount of energy absorbed is shown when the specimen is constrained along its full height;
- referring to the data with 0.5 in of unsupported height, the crushing speed does not seem to significantly affect the energy absorption;
- it seems that there is no considerable difference between the two trigger mechanisms, strictly referring to the energy absorbed, comparing again the results of the series with the knife-edges at 0.5 in;
- the knife-edges height can influence the energy absorption result of the test.

The above considerations are the starting point for further investigations mainly focused on the influence of the knife-edges height.

2.3.2 Flat specimen part II

The main objective of this tests session is the identification of a reliable configuration of test setup in terms of trigger mechanism, knife-edges height and crushing speed.

The material system used to produce the specimens was the same generic carbon fiber reinforced plastic used in the part I of the flat specimens tests.

Two sizes of specimens were tested: the regular size of 3 in x 4 in, that fits into the knife-edges of the ARL-like fixture (figure 2.11), and a narrow version of the regular specimen that measures 1 in x 4 in, in order to evaluate possible scaling effects. Both kind of specimens have a $[0/90]_{4s}$ layup, that corresponds to a mean thickness of 0.092 in.

To sustain the narrow specimens, a new feature was added to the existent fixture: a pair of plates that fitted the original of the knife-edges and that presented two narrower knife-edges on the side in contact with the specimen (figure 2.15). The two plates were inserted in the fixture as shown in figure 2.16.

The specimens were triggered in four different manners (figure 2.17): arrow (A) , sawtooth (S), chamfer (CH) and steeple (ST). A specimen without trigger (NT - no trigger) is also tested.

The crushing speeds were of 0.5 and 1.5 in/min and 1.85 in/sec. The first two speeds classify the test as quasi-static, while with the speed of 1.85 in/sec the test is considered dynamic, therefore an impact test.

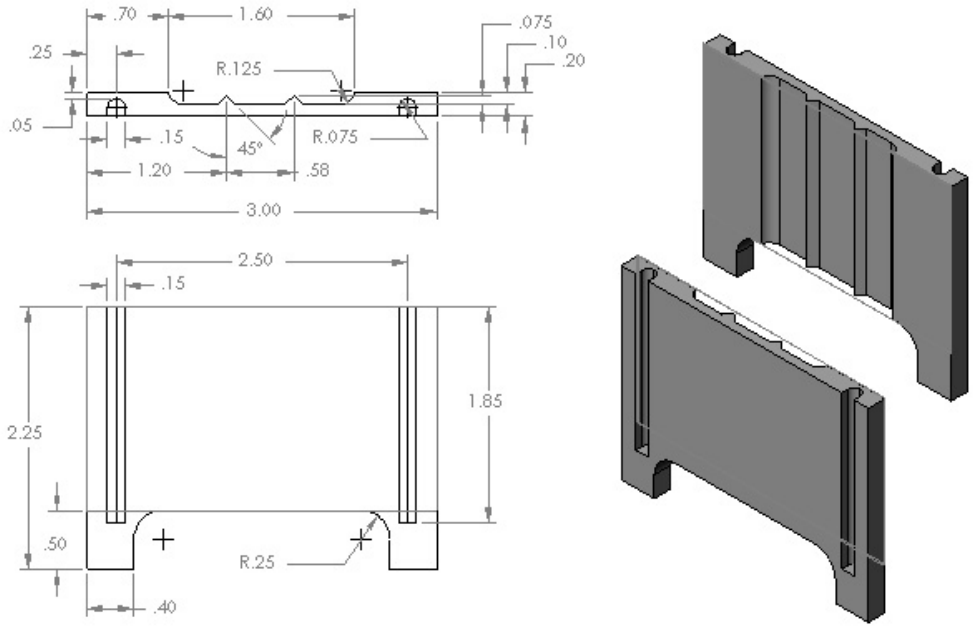

Figure 2.15: Extension plates for ARL fixture

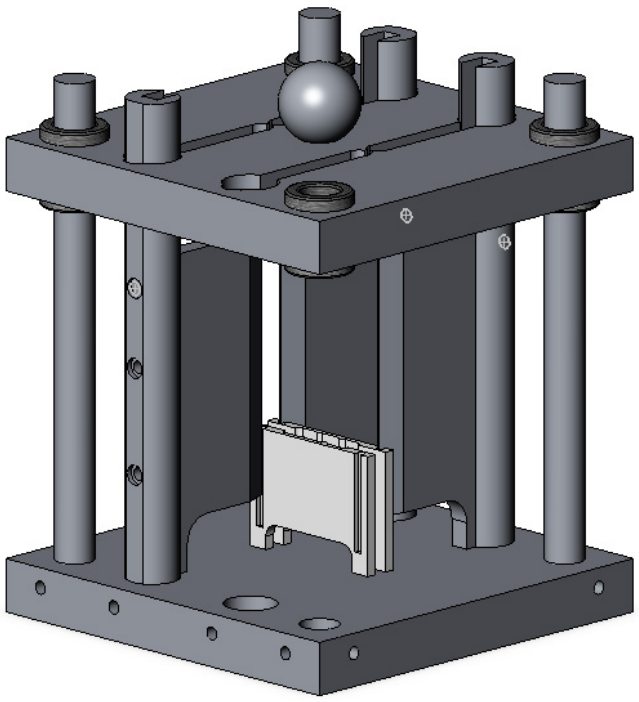

Figure 2.16: ARL-like fixture with supporting plates for narrow specimens

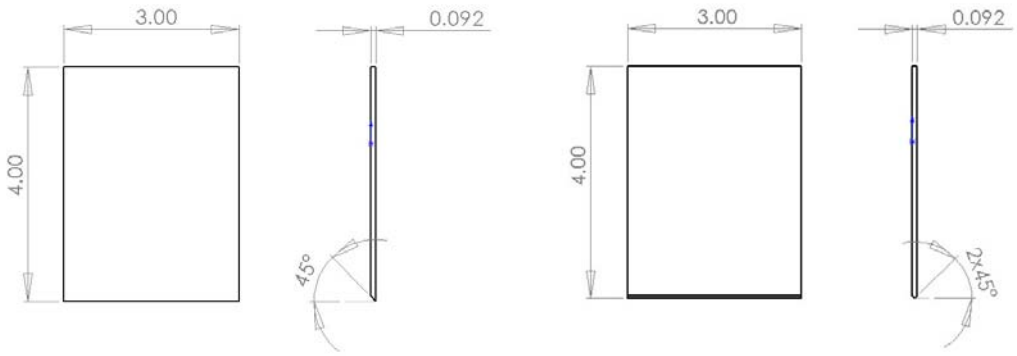

(a) Chamfer trigger (b) Steeple trigger

Figure 2.17: Specimen triggers

The unsupported length (h) of the specimen varies from 0 to 1.5 in. Besides the configuration of the test with the specimen constrained between the two pairs of knife-edges, as shown in figure 2.13, two new configurations were tested substituting one side of knife-edges with particular block-ends:

- *flat block*: a simple parallelepiped made of steel (figure 2.18) that prevent the specimen to open symmetrically in two fronds;
- *radius block*: a parallelepiped made of steel with a radius of 0.25 in on a side of its bottom (see figure 2.19); the radius is supposed to provide a kind of external trigger to the specimen, therefore in this configuration only the specimen without trigger was tested.

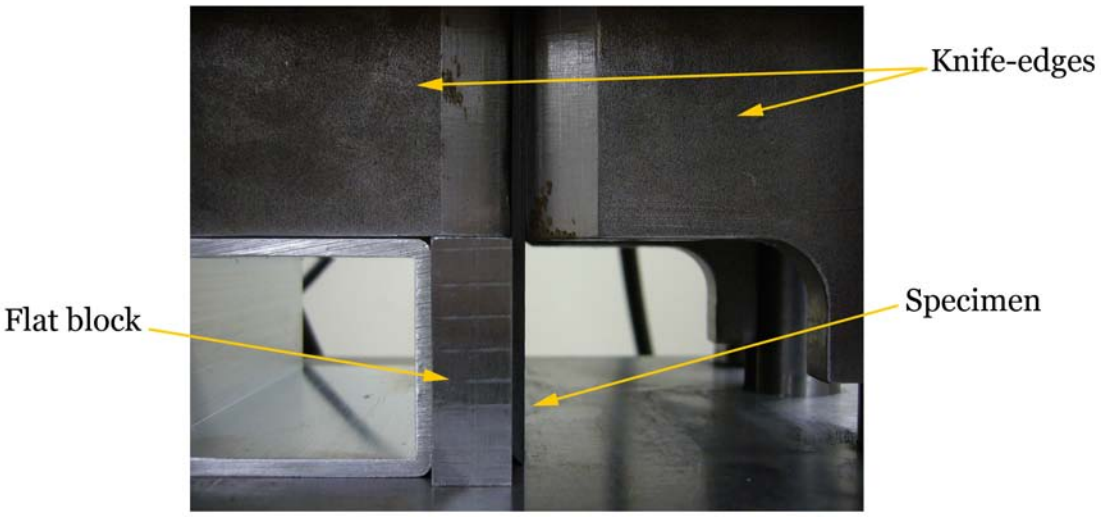

Figure 2.18: Setup with flat block

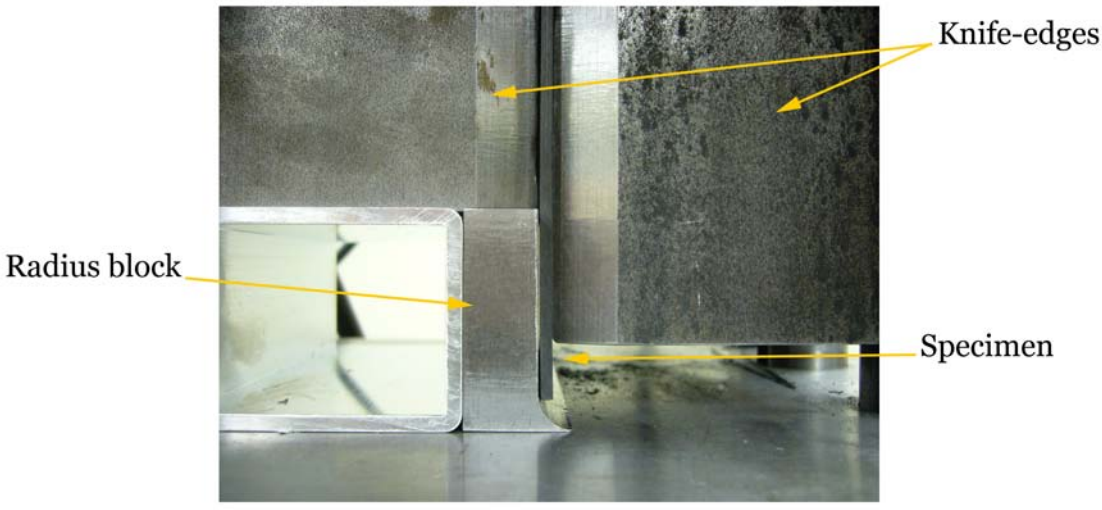

Figure 2.19: Setup with radius block

A general procedure to perform the test was defined. It consists in positioning the specimen between the anti-buckling supports, then tightening them up against the specimen; the specimen has to be firmly constrained, but at the same time the knife-edges should not engrave its surface. Afterwards, the fixture with the specimen is placed on the top of the movable head of a hydraulic press where the test is performed (figure 2.20).

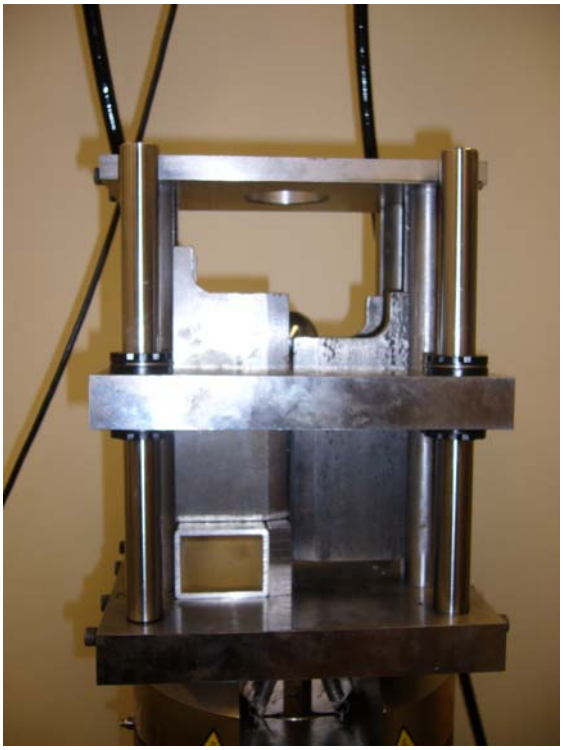

Figure 2.20: Fixture with specimen (flat block configuration) on the movable head of the hydraulic press

For each tested specimen, the load and the displacement of the movable head were recorded. When plotted, the force-displacement history shows important information about the efficiency and quality of the test. According to Cauchi Savona and Hogg [8], in a typical plot of the load-displacement history of a test (figure 2.21a), four features can be identified:

1. first peak resulting from the collapse of the trigger;

2. second peak resulting from formation of the two fronds;

3. drop in stress, the magnitude of which is determined by the distance that the split extends into the laminate;

4. region of sustained crushing.

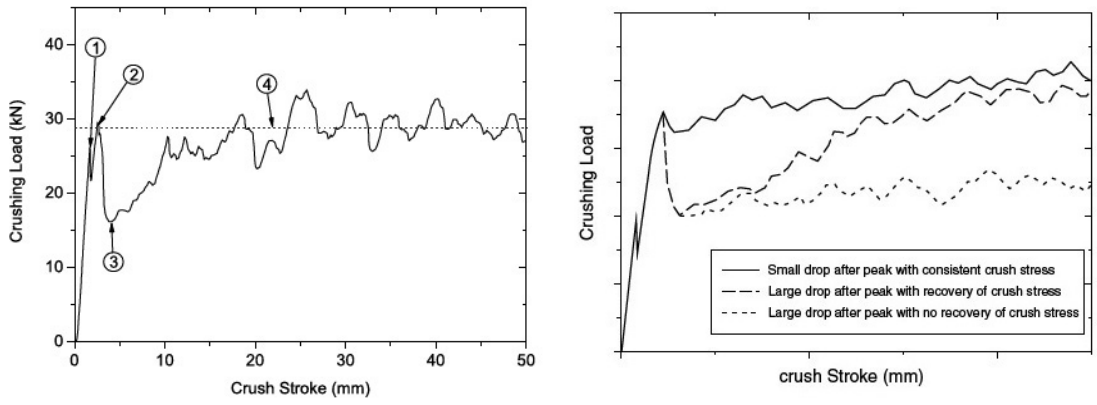

(a) (b)

Figure 2.21: (a) Typical load-displacement plot; (b) Schematic of the typical modes of crushing for a composite specimen [8]

From the load-displacement plot it was therefore possible to observe multiple aspects of specimen response to the crush.

First, the peak tells if the trigger mechanism is efficient: the higher the peak, the less efficient the trigger is.

The second significant aspect is the drop of the load that is related to the matrix strength. Considering that the fronds form through the splaying mode, which controlling mechanism is the matrix strength, the stronger the matrix the lower the drop.

Finally, the sustained load: three different behaviors can be identified during a test (figure 2.21b):

plain line small drop (or no drop at all) in load, after which the load recovers and remains consistent throughout the crushing stroke;

dashed line large drop in load which rises to a consistent crushing load after a certain crush stroke;

dotted line large drop of the load that does not recover over the remainder of the stroke.

Ideally, the preferable behavior of the test is the one described with the plain line; the dotted line represents the test of a material with poor energy-absorption properties.

During the performance of the test the development of the load-displacement history can be followed on the screen of the computer associated with the hydraulic press and therefore it is immediately possible to evaluate if the test is worthy to be carried to the end or not.

When the test is over, the fixture is removed from the hydraulic press. The top plate is taken off from the guiding rods and at least two knife-edges with their supporting rods have to be removed to extract the specimen.

In the end, the values of SEA associated to each test are easily calculated from the load-displacement data applying the equations (1.1) and (1.2). The data of the specimen necessary for the calculation of the SEA (width and thickness) are collected before the beginning of the test.

The summaries of the configurations tested in this session are in tables 2.3 and 2.4 for regular and narrow specimens respectively.

ID	Trigger	v [in/min]	h [in]
1	Arrow	1.5	0
2		0.5	0.5
3		1.85*	0.5
4		0.5	1.5
5	Chamfer	0.5	0.5
6		0.5	flat
7	None	0.5	r.25
8	Sawtooth	1.5	0.5
9	Steeple	0.5	0.5
10		0.5	flat

Table 2.3: Flat specimen tests part II - Regular specimens tests summary
*in/sec; flat refers to the configuration with flat block;
r.25 refers to the configuration with radius block.

ID	Trigger[1]	v [in/sec]	h [in]
1	C	0.5	0.5
2	ST	0.5	0.5

Table 2.4: Flat specimen tests part II - Narrow specimens tests summary
Trigger: C - chamfer; ST - steeple

[1] Arrow and sawtooth triggers were not tested with narrow specimens because the first trigger takes away a consistent portion of the specimen while the second requires a machining process not suitable with the specimen dimensions.

For each configuration at least one test is performed. The objective of the tests of this session is the evaluation of the overall behavior of the test setup: if the configuration does not lead to an appropriate crush (plain line behavior in figure 2.21b), there is no interest into further tests.

From the direct observation of the tests and their load-displacement histories, the following considerations can be made.

In figure 2.22 it is possibile to see the four different load-displacement histories of different specimens all tested in the same conditions (v=0.5 in/min and knife-edges h at 0.5 in). The only parameter that varies among the specimens is the trigger.

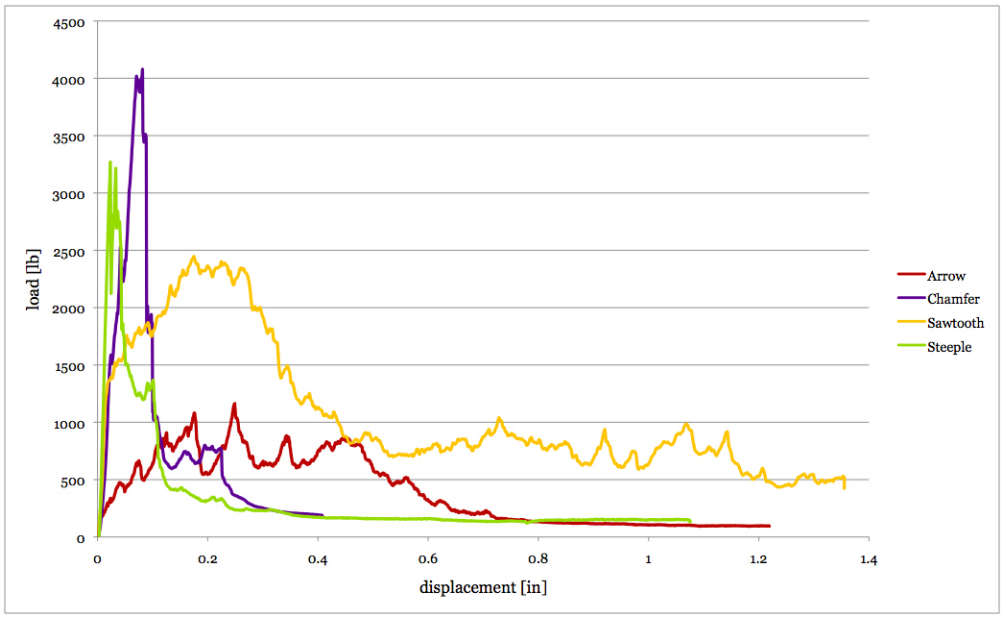

Figure 2.22: Comparison between load-displacement histories of four different specimens tested at 0.5 in/min (sawtooth at 1.5 in/min) between knife-edges at 0.5 in

Both the arrow trigger (red) and the sawtooth trigger (yellow) let the load to rise smoothly and they seem to allow a sustained crash until phenomena of splaying show up, then the sustained load drops (for the arrow trigger, to an inconsistent level). The chamfer (purple) and steeple (green) triggers show similar behaviors, even if the steeple trigger, with its symmetric shape, helps the crushing initiation more than the chamfer; the steeple trigger, in fact, produces a lower peak in load during the crush event. The same behavior between chamfer and steeple trigger mechanisms is shown also in the tests with narrow specimens (figure 2.23).

Both with regular specimens and narrow specimens, though, as soon as the trigger exhausts its function the load drops asymptotically to an unacceptable

value. The low level of sustained load has different reasons according to the nature of the trigger mechanism and consequently of the fracture mechanism.

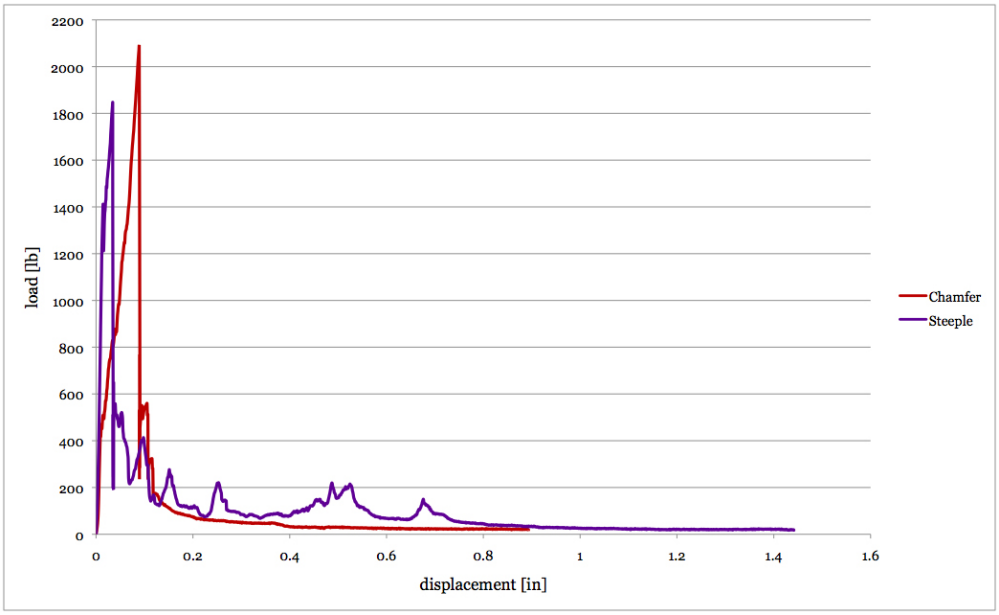

Figure 2.23: Comparison between load-displacement histories of narrow specimens tested at 0.5 in/min between knife-edges at 0.5 in

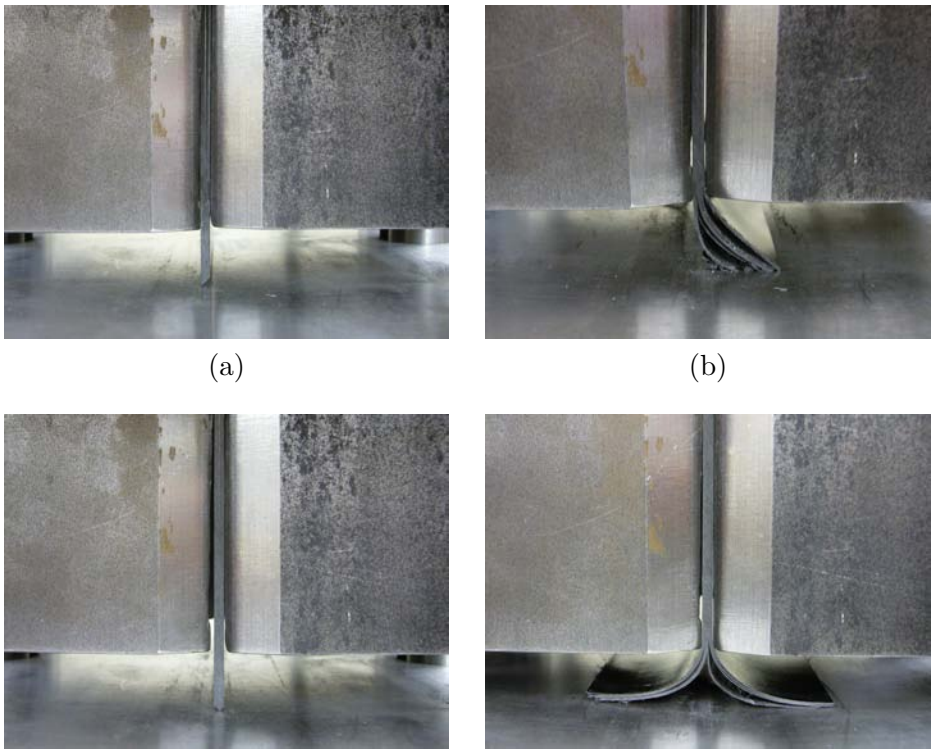

(a) (b)

(c) (d)

Figure 2.24: Trigger mechanisms comparison:
(a), (b) chamfer trigger; (c), (d) steeple trigger

The chamfer trigger (figure 2.24a) easily slides on a side (figure 2.24b) due to the asymmetry of the transmitted load; the sustained load is therefore very close to zero because the only resistance is opposed by the specimen that bends. The steeple trigger (figure 2.24c) on the other side, with its symmetric pointed end, is preferable to the chamfer, but it produces only delamination (figure 2.24d) that does not allow the sustained crush and the relative energy absorption.

The results in terms of SEA are summarized in tables 2.5 and 2.6 for regular specimens and narrow specimens respectively and in figure 2.25. Where more than one test has been performed, an average value of the SEA is reported.

ID	Trigger	v [in/min]	h [in]	SEA [J/g]
1	Arrow	1.5	0	79.348
2		0.5	0.5	12.714
3		1.85*	0.5	23.955
4		0.5	1.5	18.366
5	Chamfer	0.5	0.5	14.343
6		0.5	flat	7.193
7	None	0.5	r.25	4.054
8	Sawtooth	1.5	0.5	13.579
9	Steeple	0.5	0.5	5.421
10		0.5	flat	7.628

Table 2.5: Flat specimen tests part II - Regular specimens tests results
*in/sec; flat refers to the configuration with flat block;
r.25 refers to the configuration with radius block.

ID	Trigger	v [in/sec]	h [in]	SEA[J/g]
1	C	0.5	0.5	7.389
2	ST	0.5	0.5	5.324

Table 2.6: Flat specimen tests part II - Narrow specimens tests results
Trigger: C - chamfer; ST - steeple

Referring to figure 2.25, it is possible to note that the higher value of SEA is for $h = 0$ in, that is to say that the specimen is totally constrained between the knife-edges. This particular result was already found during the first session of tests on

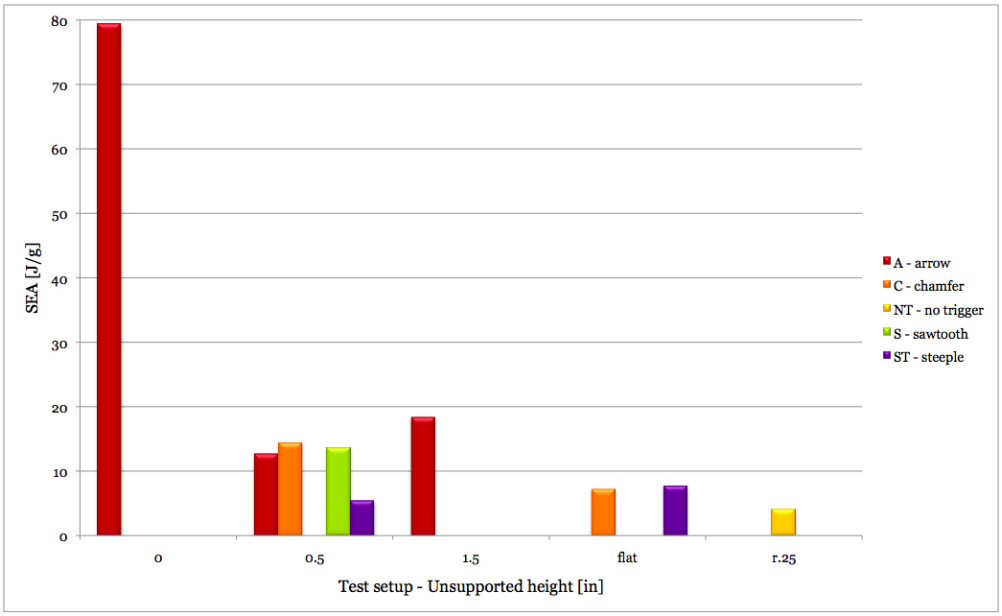

Figure 2.25: Flat specimen tests part II - Regular specimens test results

flat specimens: it suggests therefore that the unsupported height can affect the energy absorption of the specimen. Moreover, it seems that a large amount of the energy is absorbed by the fixture through the phenomena related to the closure force of the knife-edges and fronds tearing.

In conclusion to this test session it can be stated that:

- there are external parameters that affect the test introduced through the fixture (knife-edges closure force, unsupported height of the speciemen);
- in-plane triggers, arrow and sawtooth, allow a smooth crack initiation, while chamfer and steeple lead to very high peaks in initial load;
- in-plane trigger seems to be more reliable than chamfer or steeple, but arrow trigger cuts a considerably big portion of the specimen while sawtooth trigger is particularly expensive to realize because it requires water machine cutting;
- chamfer trigger is not suitable for flat specimens because it produces an asymmetric load that leads the coupon to slide on a side;
- steeple trigger, preferred to chamfer, produces only delamination in the specimen that does not allow the sustained crush and an adequate amount of energy absorbed.

2.3.3 Self-supporting specimens part I

From the flat specimens tests sessions a fact is pointed out: the fixture interferes with the performance of the test and affects its results, therefore the need of a test that is insensitive to the external factors rises. A coupon size test with self-supporting specimens is supposed to be unaffected by all the external influences introduced through the fixture.

Moreover, the utilization of self-supporting specimens simplifies the setup procedures: the flat specimens tests, in fact, required quite a long time for the positioning of the specimen and the tightening of the knife-edges. With self-supporting specimens instead, the setup time is drastically reduced because positioning the specimen on the center of the crushing plate is enough.

The self-supporting specimens were realized combining the hint given by the alternative shape of DLR specimens (figure 2.9) of a mandrel-free manufacturing with the stability of a periodic shape like the sine-wave beam of figure 2.8. The result of this union is a set of six specimens with three different shapes easily cut out from a corrugated plate made in a dedicated mold.

The dedicated mold for the production of corrugated plates used in this test session was developed at the Aeronautics and Astronautics dept. of the University of Washington, Seattle, WA (USA) (figure 2.26).

The mold comes from a single piece of aluminum of 8 in x 8 in x 1 in that was cut with wire EDM technology to create the particular sinusoidal profile; each half of the mold therefore measures 8 in x 8 in x 0.5 in.

The mold is designed to be used with prepreg material systems. It can host up to 12 plies of unidirectional (UD) tape, which nominal thickness is about 0.0058 - 0.0062 in, or 8 plies of plain weave material, with a nominal thickness of 0.0083 - 0.0089 in per ply (all the thicknesses refers to a single cured ply). In figure 2.27 the mold with the corrugated plate is represented.

A mold release agent is needed to uncouple the plate from the mold. Two release system were tested: teflon and wax.

Teflon was used as a thin sheet put at the interface between the mold and the stack of prepreg plies, but it made the stacking process very difficult because of its slippery surface; another effect related to the use of the teflon was that the surface of the specimens was not perfectly smooth, but during the curing process the texture of the teflon was engraved on the external layers of the plate.

Wax substituted teflon as mold release agent: it is a specific solid wax that has to be spread on the mold surface. Wax was very efficient and during the curing process it melted preventing the composite material to stick on the mold surface; on the other hand, the spreading process took one hour and a half for each plate, because at least three layers of wax are required and each layer takes thirty minutes to dry.

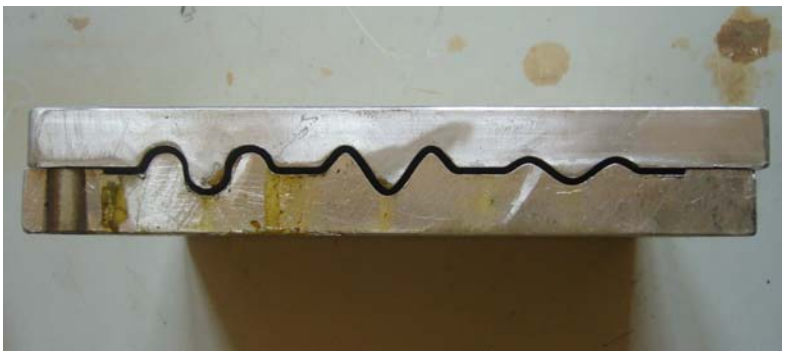

(a) Closed mold

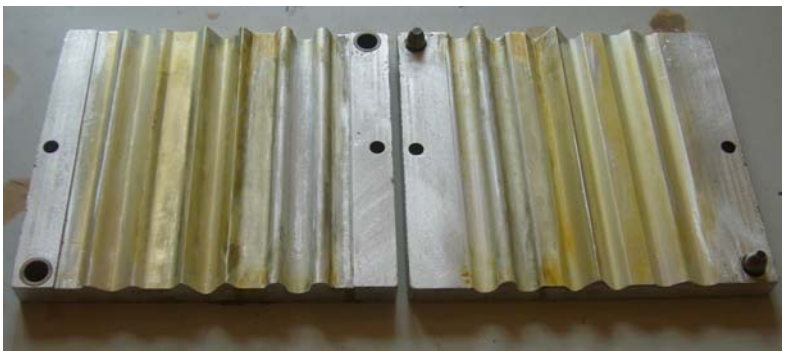

(b) Open mold

Figure 2.26: Mold for the production of corrugated plates developed at University of Washington

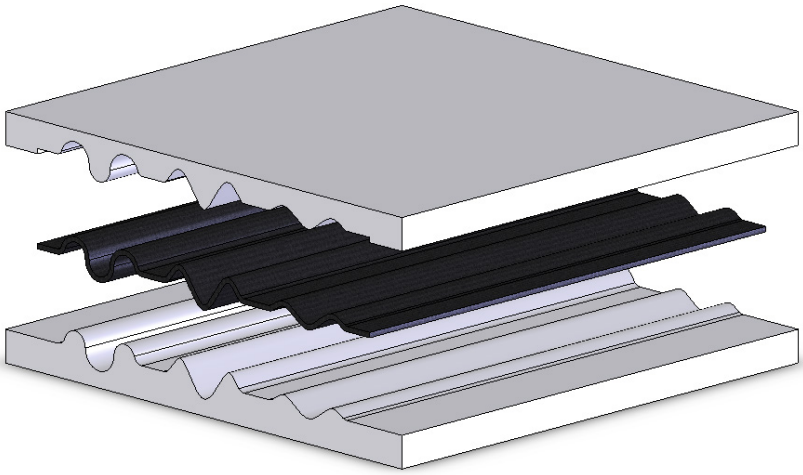

Figure 2.27: A schematic representation of mold and plate

The corrugated plate measures 8 in x 6.70 in and from it six specimens 3 in x 2 in are cut, two for each kind of sine-wave. Three different shapes are tested in this session: low sine (LS – figure 2.28a), deep sine (DS – figure 2.28b) and half circle (HC – figure 2.28c).

The choice of the shapes comes from examples found in literature: both the sinusoidal web and the half circle web are very common features in helicopters subfloors.

All the specimens were triggered with a simple chamfer trigger, because it is the easiest trigger to realize. If for flat specimens this kind of trigger is not appropriate, it works on self supporting specimens because of their self stabilizing shapes.

Four different material systems were tested:

- the generic material already used for flat specimen tests;
- Toray "Agate" unidirectional tape (T700GC 12K/2510);
- Boeing 787 material by Toray;
- Toray "Agate" plain weave fabric (T700SC-12K/2510).

All the material systems are carbon fiber reinforced plastics (epoxy).

The Toray Agate unidirectional tape prepreg (T700GC 12K/2510) is a material for general purpose structural applications. The fibers are continuous, no-twist carbon filaments, surface treated to improve handling and structural properties. The matrix is an epoxy resin manufactured by Toray Composites (America) and when the prepreg is cured the resin content is about 32 - 38% [14].

The Toray Agate plain weave fabric (T700SC 12K/2510) is a general purpose structural applications material as well. It has the same fibers and matrix of the unidirectional tape but once cured its resin content varies from 39 to 45% [14, 15].

The mechanical properties of the materials are summarized in table 2.7; the properties of the Boeing material are confidential and cannot be published.

To perform the tests, the existent fixture for flat specimen tests was used with a major change: all the knife-edges with their support rods were removed because with self-supporting specimens there is no need for anti-buckling supports. The specimen was positioned at the center of the plates (figure 2.29), in line with the load sphere and therefore the load direction.

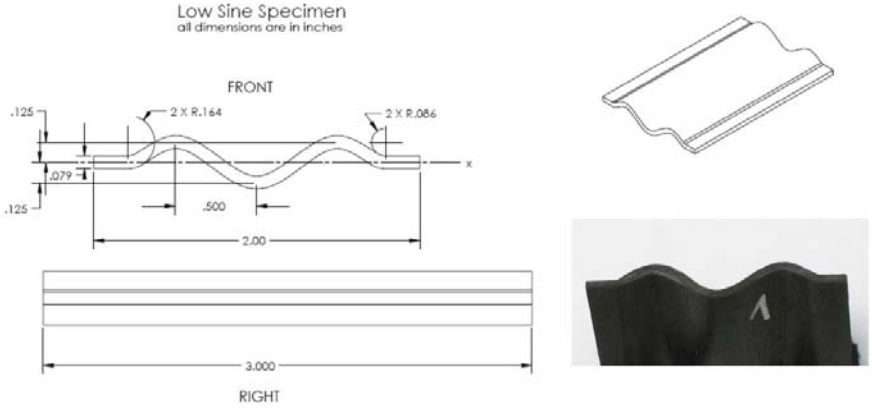

(a) Low sine specimen

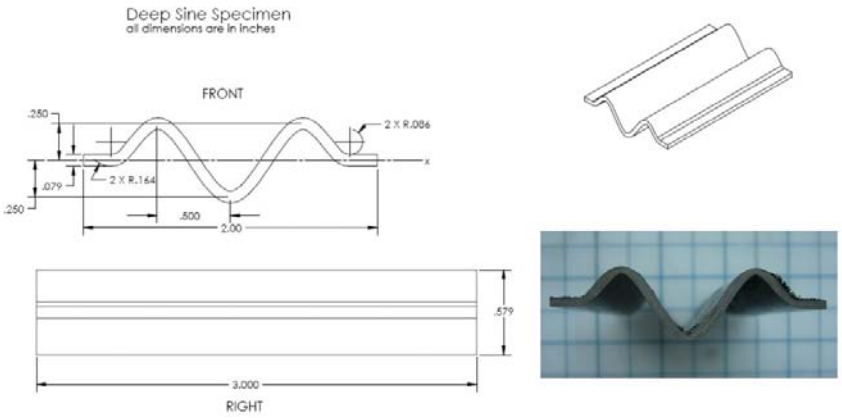

(b) Deep sine specimen

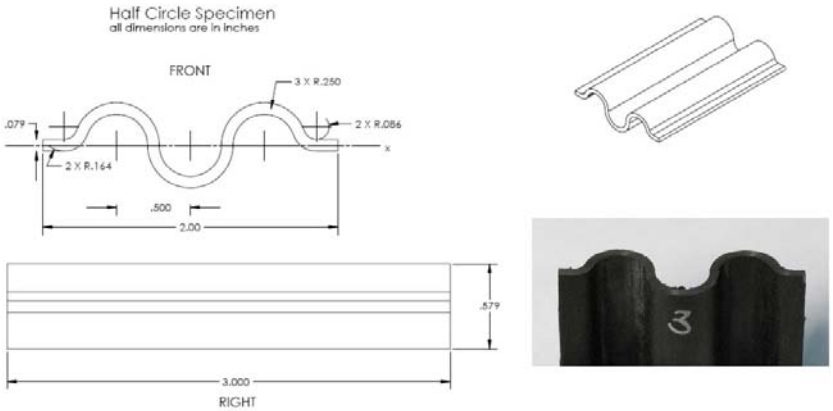

(c) Half circle specimen

Figure 2.28: Self-supporting specimens

	Generic	Agate	Boeing	PW
ρ [g/cm^3]	1.55	1.55	1.58	1.60
E_1 [MPa]		$126.86 \cdot 10^3$		$56.275 \cdot 10^3$
E_{1c} [MPa]		$113.76 \cdot 10^3$		$55.744 \cdot 10^3$
E_2 [MPa]		$8.41 \cdot 10^3$		$54.868 \cdot 10^3$
E_{2c} [MPa]		$10.135 \cdot 10^3$		$53.556 \cdot 10^3$
G_{12} [MPa]		$4.205 \cdot 10^3$		$4.213 \cdot 10^3$
ν_{12}		0.309		0.042
σ_{u1t} [MPa]		$2.199 \cdot 10^3$		917.596
σ_{u1c} [MPa]		$1.469 \cdot 10^3$		708.871
σ_{u2t} [MPa]		50.263		775.384
σ_{u2c} [MPa]		198.569		702.976
σ_{u12} [MPa]		154.443		132.572

Table 2.7: Material properties: generic – unclassified cfrp; Agate – Toray T700GC 12K/2510 unidirectional tape; Boeing – unidirectional tape; PW – Toray T700SC 12K/2510 plain weave fabric

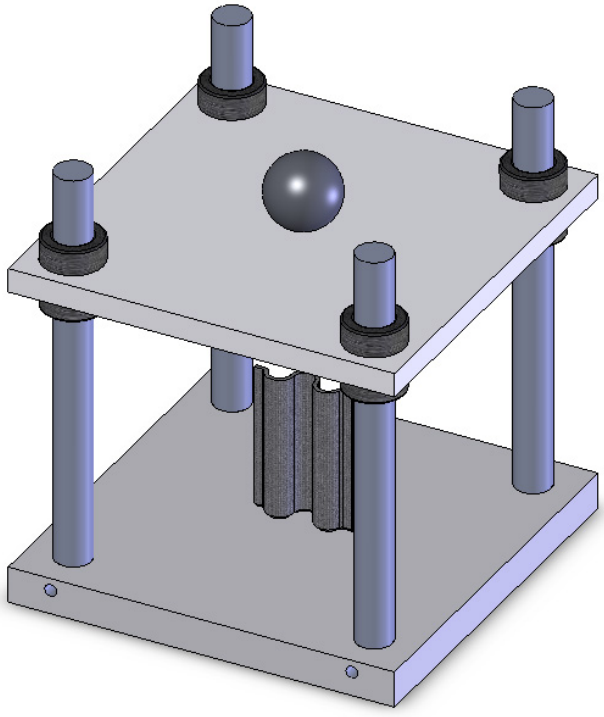

Figure 2.29: Schematic setup for self-supporting specimens tests

Before proceeding with the test, each specimen was measured in width with a flexible rule and in thickness with a caliper in seven different points of its corrugated section, so that the average thickness was calculated. The test procedure was the same as for flat tests: once the specimen was correctly positioned between the plates of the fixture, the whole thing was placed on the top of the hydraulic press movable head. For each specimen, the load and displacement of the movable head were recorded. Applying the equations (1.1) and (1.2), the value of the SEA for each specimen is obtained.

Tests were performed at different speeds, both quasi static and dynamic; the dynamic tests were performed at General Motors facilities in Detroit, MI (USA). All the quasi static tests were performed at 2 in/min while the dynamic tests speeds were of 0.5, 1 and 2 in/sec.

During this test session, different setup configurations were tested. The parameters that varied were:

- specimen layup;
- mold release;
- curing cycle;
- friction at the interface between specimen and crushing surface.

The tested specimens layup were four, three with the unidirectional tape and one with the plain weave. The layups with the unidirectional material were:

- $[0/90]_{3s}$
- $[0/45/\text{-}45]_{2s}$
- $[45/\text{-}45]_{3s}$

while with plain weave the specimens were made of 8 plies stacks, with the fibers oriented 0-90 compared to the load direction.

As previously discussed, two mold release systems were tested: teflon and wax.

The curing cycle for the unidirectional prepreg, according to the instructions from the supplier, is one hour at 250 °F for the generic and the Agate material and one hour at 350 °F for the Boeing material, both under a pressure of 90 psi/in^2. Few plates of the generic material were erroneously cured according at 350 °F for one hour and they were tested anyway to see the influence of the over-cure to the energy absorption capability of the material. For the plain weave fabric, the specimens were produced directly at the factory, so the parameters of the curing cycle are unavailable.

The last parameter evaluated during the test session was the effect of the friction at the interface between the fronds of the specimen and the crushing surface. A group of specimens were tested spreading some grease on the surface of the bottom plate of the fixture to record the influence of an alternative friction condition.

The quasi-static test configurations ($v = 2$ in/min) for the unidirectional tape are summarized in table 2.8. All the three shapes are tested in each test group. The plain weave fabric was tested in only half circle specimens, directly produced at Toray facilities.

Group	Material	Layup	Mold release	Curing cycle	Lubricant
A	generic	$[0/90]_{3s}$	wax	regular	no
B	generic	$[0/90]_{3s}$	teflon	regular	no
C	generic	$[0/45/\text{-}45]_{3s}$	wax	regular	no
D	generic	$[0/45/\text{-}45]_{3s}$	wax	over-cured	no
E	generic	$[45/\text{-}45]_{3s}$	wax	regular	no
F	agate	$[0/90]_{3s}$	wax	regular	no
G	agate	$[0/90]_{3s}$	wax	regular	yes
H	boeing	$[0/90]_{3s}$	wax	regular	no

Table 2.8: Unidirectional tape tests summary

In table 2.9 the dynamic tests performed at General Motors facilities are summarized. Only half circular specimens were used, with the base layup of $[0/90]_{3s}$; the materials tested were Agate and Boeing.

Group	Material	v [in/sec]
A1	Agate	0.5
A2		1
A3		2
B1	Boeing	0.5
B2		1
B3		2

Table 2.9: Dynamic tests summary

For each configuration of both quasi static and dynamic tests, at least two specimens were tested and their average behavior and results are reported.

The typical load-displacement histories for each shape are illustrated in figure 2.30.

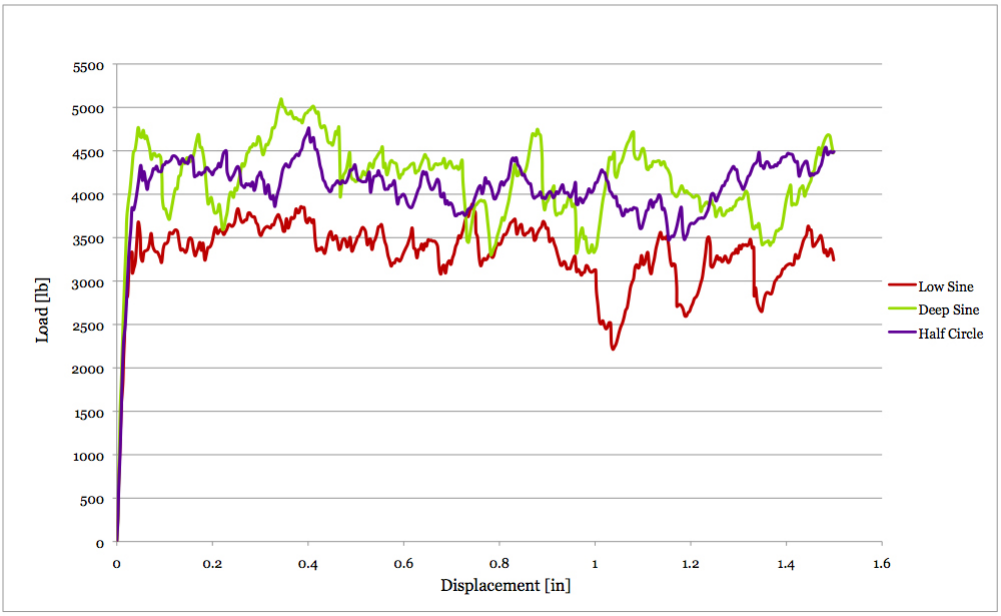

Figure 2.30: Typical load-displacement histories for self supporting specimens

For all the shapes it can be noticed that there is not a high peak as it happened with flat specimens; the chamfer trigger works perfectly, initiating the crushing smoothly up to an almost steady level of sustained load. The second peak is absent and this is due to the way the specimens crush: as shown in figure 2.31, during the crushing process there is not the formation and propagation of single central intralaminar crack, but the particular three dimensional shape of the specimen forces it to open radially. In self supporting specimens, besides a macroscopic behavior of splaying, the main fracture mechanism involved is the fragmentation mode that, with the fracture of lamina bundles, absorbs a high amount of energy (figure 2.32 and 2.33).

(a) Top view (b) Bottom view

Figure 2.31: Example of a crushed self supporting specimen

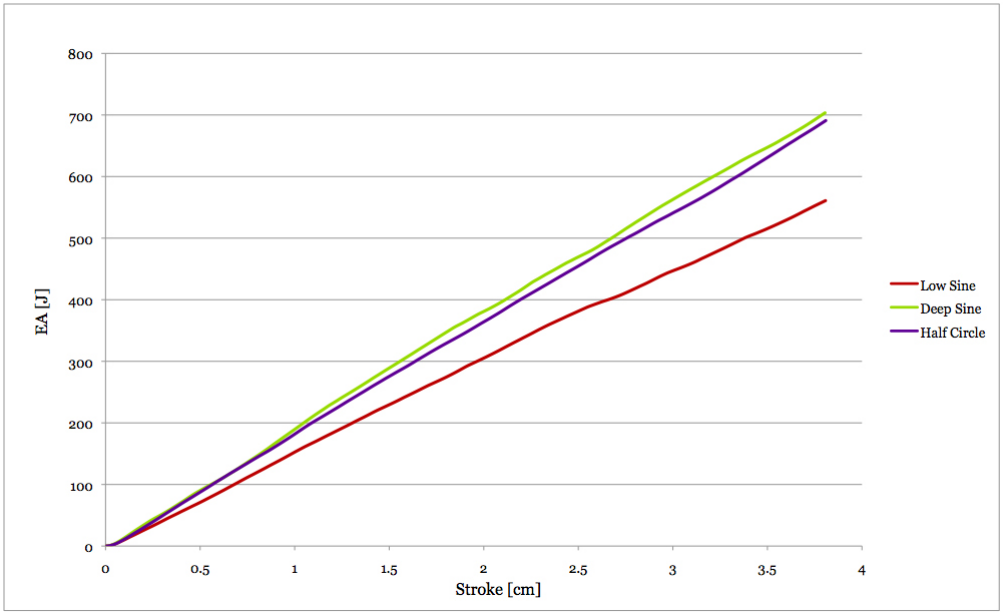

Figure 2.32: Typical EA-stroke histories for self supporting specimens

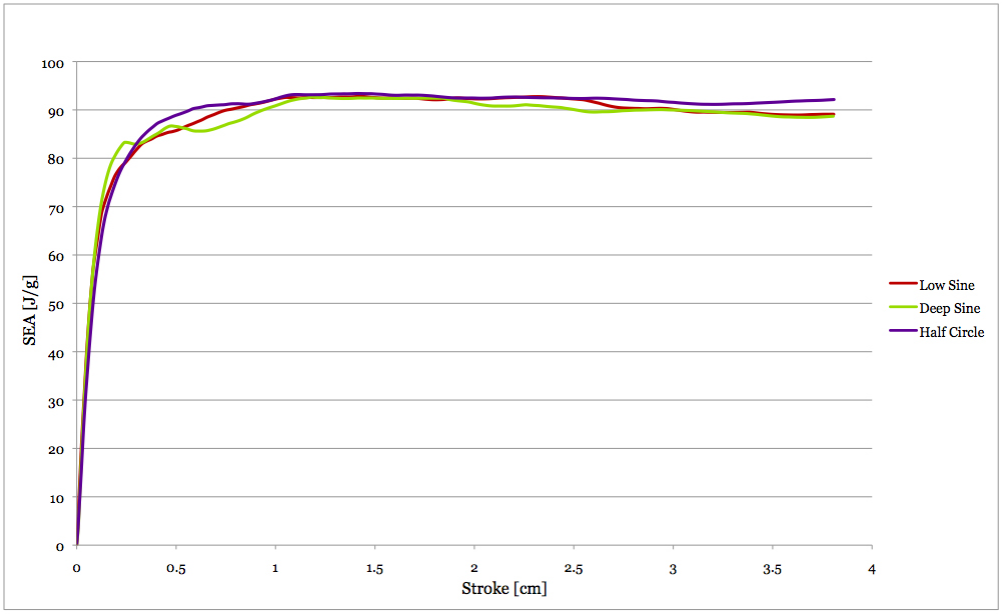

Figure 2.33: Typical SEA-stroke histories for self supporting specimens

Referring to figure 2.30, it is evident that the deep sine and half circular shapes are able to sustain a higher load than the low sine shape, but when the behaviors of the relative specific energy absorption are compared, the low sine shape reaches the same level of the other two shapes. Due to the smaller cross-sectional area of the specimen that faces the load, the low sine shape is weaker than the deep sine and half circle shapes and this is reflected also in the lower steepness of its EA curve.

The SEA is therefore the referring parameter for a comparison between the different specimens configurations.

The first comparison between SEAs refers to the different layup and test conditions with the generic material. In figure 2.34 the test groups A – E are represented, arranged by the shape of the specimens.

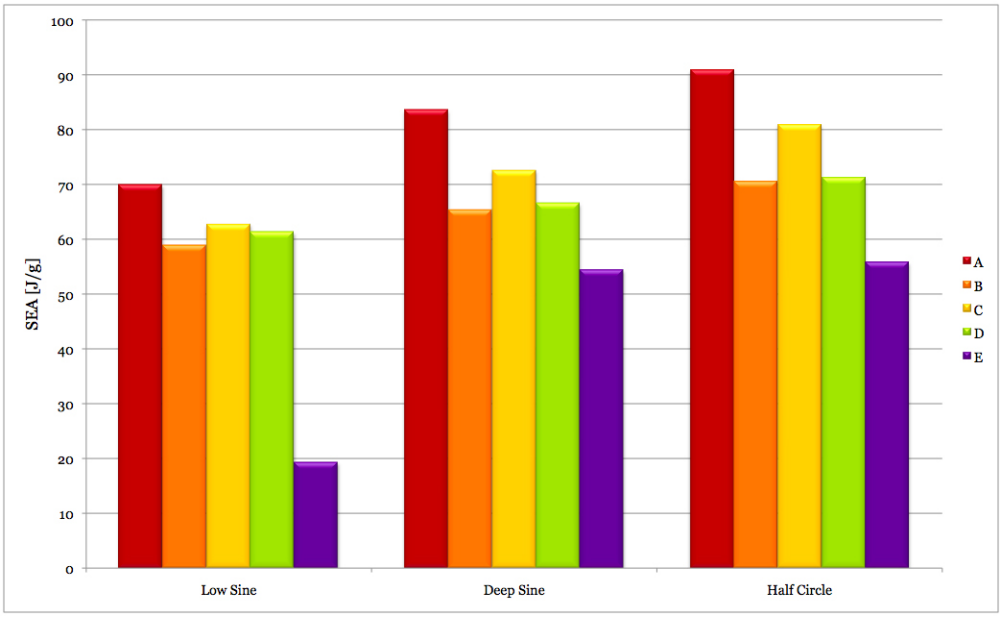

Figure 2.34: SEA of different test configurations and specimens layup with generic carbon/eopxy material

Group A (red) is the baseline configuration: layup $[0/90]_3 s$, wax as mold release agent, regular curing cycle and no lubricant on the surface of the bottom plate of the fixture.

All the other test setups have lower values of SEA compared to the baseline configuration:

- group B (orange), that differs only for the mold release agent (teflon), has a lower value of the SEA due probably to defects introduced through the pattern of the teflon fabric engraved on the specimen;

- groups C – E contain layers oriented at 45°, that weaken the specimen generating phenomena of fiber sliding (figure 2.35);
- the presence in groups C (yellow) and D (green) of 0° layers helps the specimen to sustain a higher load than the pure $[45/\text{-}45]_{3s}$ specimens (group E - purple);
- the very low value of SEA for the low sine specimen with $[45/\text{-}45]_{3s}$ layup (purple) is due mainly to instability (buckling) effects.

(a) $[0/90]_{3s}$

(b) $[0/45/\text{-}45]_{2s}$

(c) $[45/\text{-}45]_{3s}$

Figure 2.35: Influence of the 45° layers on the crushing behavior

About the effect of over-curing (group D, green, in figure 2.34), it is more evident as the specimen shape changes from low sine to half circle, due to the

progressively major role that the matrix has into the crushing mechanisms. In fact, deep sine and half circle specimens involves mechanisms of fragmentation more than low sine specimens, therefore the role of the matrix is significant: a more efficient matrix contrasts more the fracture mechanism, requiring a higher load to be broken. The over-curing process degrades the matrix properties: the matrix is less efficient than the one regularly cured and the effect is a crush at lower load than in regular conditions.

From figure 2.34 another aspect is evidenced: the influence of the shape of the specimen on the energy absorption.

Referring to the research of Jacob et al. [3], they evaluated the influence of a large number of parameters on the specific energy absorption and one of the parameters was the specimen geometry. Their research studied the behavior of thin-walled tubes with different cross sections and they concluded that the specific energy absorption follows the order circular > square > rectangular. The worse behavior of rectangular and square tubes compared to the circular ones is due mainly to three reasons:

- the main fracture mechanisms of sides of the square and rectangular tubes are bending and splaying;
- in square and rectangular tubes the only areas where the fracture of fibers occurs are the corners, so the main contribution to energy absorption is the corner splitting;
- circular tubes tend to open radially, so along the whole lateral surface the fibers break contributing to a steady and continuous energy absorption.

Getting back to the different corrugated specimens tested in this session, the specific energy absorption increases along the path low sine – deep sine – half circle. This is explainable with the following considerations:

- the low sine specimen tends to behave similarly to a flat specimen: splaying is the main fracture mechanism and the gentle curvature of the surface does not help the radial splitting of the layers;
- the low sine specimen is not stable enough under compressive loads and phenomena of buckling occur;
- the deep sine specimen and the half circle specimens do not suffer of buckling instability;
- the energy absorptions of the deep sine and half circle specimens are similar, but the acute angle of the sine shape leads to phenomena of corner splitting and the sides of the sine wave act like little flat panels;
- deep sine specimens have often showed highly variable thicknesses in the corrugated section: the layers in the peak of the sine were more packed than

on the straight sides and it introduces defects like damage of the fibers and zones with higher concentration of resin;

- half circle specimens do not show significative constrictions in the cross-section;
- the semicircular modulus of the half circle specimens behaves like a circular tube, fragmentation mode occurs and the lamina bundles break absorbing energy.

The second comparison derivable from this test session is about the influence of the material on the energy absorption. In figure 2.36 the four different material systems employed are compared. The specimen configuration is the one defined as the baseline: $[0/90]_{3s}$ layup, wax as mold release, regular curing cycle and no lubricant.

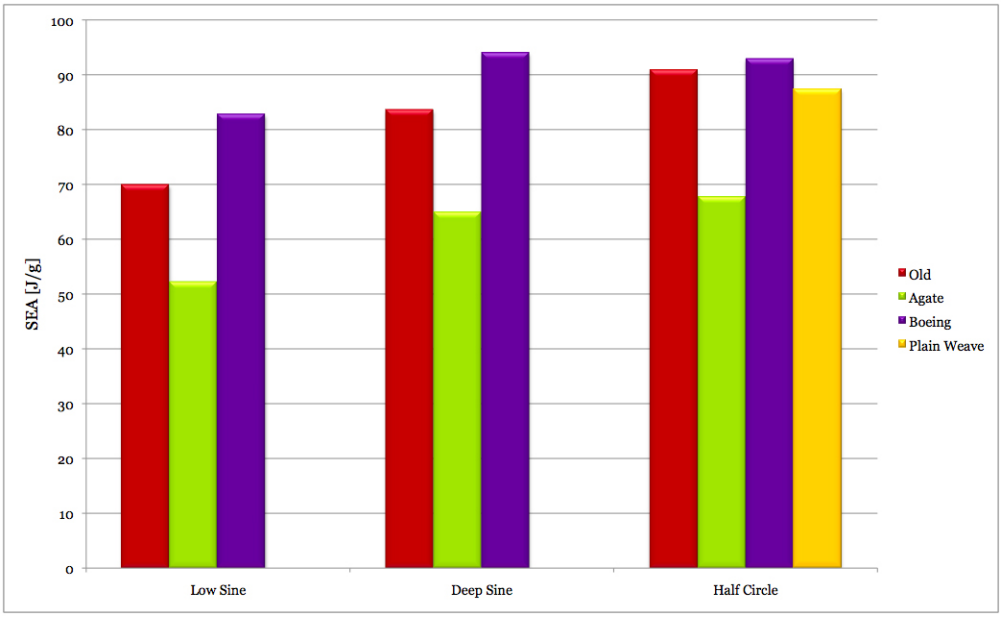

Figure 2.36: Influence of the material system on the energy absorption

Among the unidirectional tapes, the Boeing material shows the better performance in terms of energy absorption. Unfortunately, the lack of information about its mechanical properties, as well as the ones of the generic material, does not make possible the formulation of considerations about the materials behavior.

The only possible comparison is between the Agate material in form of unidirectional tape and plain weave fabric. The unidirectional tape shows very high elastic modulus in the fibers direction while the properties in the perpendicular direction are essentially the properties of the matrix (see table 2.7). The alternate symmetric $[0/90]_{3s}$ layup balances the lamina properties in the laminate. On

the other hand, the plain weave fabric has fibers in both directions, balanced and symmetric, and the mechanical properties reflect a quasi orthotropic behavior. Specimens made of the plain weave material are a stack of eight plies with the fibers parallel/perpendicular to the load direction.

The mechanical properties of the specimens (Young's moduli and Poisson's ratios) are equivalent in those two layups, but the higher amount of energy absorbed with the plain weave material suggests that there is something else that contributes to the energy absorption. The difference between the materials is the way the fabric is. In the specimen made with the unidirectional tape, the load is carried in half of the plies by the fibers (0° laminae) and in the other half by the matrix (90° laminae). During the crushing process, the 0° laminae are stronger because they oppose the fiber resistance to the load and tend to open with interlaminar cracks parallel to the fiber, while the 90° laminae simply fold because the matrix has not high resistance. But the laminae are not isolated during the crush: the 0° lamina helps the nearby 90° one providing support to its natural folding behavior and, at the same time, the 90° layer constrains the 0° fibers to split. With the plain weave fabric this mutual help behavior becomes more marked because the fibers are woven together in weft and warp, so the load necessary to break these bonds is higher.

Also in this comparison, the trend of the higher energy absorption for half circle specimens and lower for low sine specimens is confirmed.

Another data comparison for this test session is between the results of groups F and G: same material system (Agate), same $[0/90]_{3s}$ layup, same mold release agent (wax) and regular curing cycle, but presence of grease on the crushing plate for the specimens of group G.

According to Brimhall [16], friction is the reason for most of the energy is absorbed during a crushing process, so the presence of some substance act to reduce the sliding friction between the specimen (or, in this case, its fronds) and the crushing surface, would have reduced the energy absorption.

To verify the influence of friction in the energy absorption process, some grease was spread on the crushing surface of the fixture. The effect obtained was actually the contrary to the one supposed: the grease did not help the fronds to slide over the surface but it held all the debris made during the crushing, increasing the friction between the fronds and the plate surface.

The role of the friction is still evaluated though: an increase of the sliding friction led to an increase of specific energy absorption (figure 2.37).

Once again, the relation between the energy absorption and the specimens shape is shown: the low sine shape absorbs less energy than the half circle shape and the deep sine is in-between.

The results summary of quasi-static tests is presented in table 2.10.

The last batch of specimens is the one tested in dynamic conditions at General Motors facilities in Detroit, MI (USA). The tested specimens were only half circle

Group	Material	Layup	Mold release	Curing cycle	Lubricant	Shape	SEA [J/g]
A	generic	$[0/90]_{3s}$	wax	regular	no	LS DS HC	69.875 83.537 90.789
B	generic	$[0/90]_{3s}$	teflon	regular	no	LS DS HC	58.102 65.233 70.427
C	generic	$[0/45/\text{-}45]_{3s}$	wax	regular	no	LS DS HC	62.725 72.543 80.908
D	generic	$[0/45/\text{-}45]_{3s}$	wax	over-cured	no	LS DS HC	61.302 66.531 71.188
E	generic	$[45/\text{-}45]_{3s}$	wax	regular	no	LS DS HC	19.326 54.400 55.810
F	agate	$[0/90]_{3s}$	wax	regular	no	LS DS HC	52.135 64.831 67.614
G	agate	$[0/90]_{3s}$	wax	regular	yes	LS DS HC	64.120 74.583 82.516
H	boeing	$[0/90]_{3s}$	wax	regular	no	LS DS HC	82.730 93.949 92.819
PW	plain weave	8 plies	n/a	factory	no	HC	87.316

Table 2.10: Quasi static tests summary – Specimens shape:
LS - Low Sine; DS - Deep Sine; HC - Half Circle

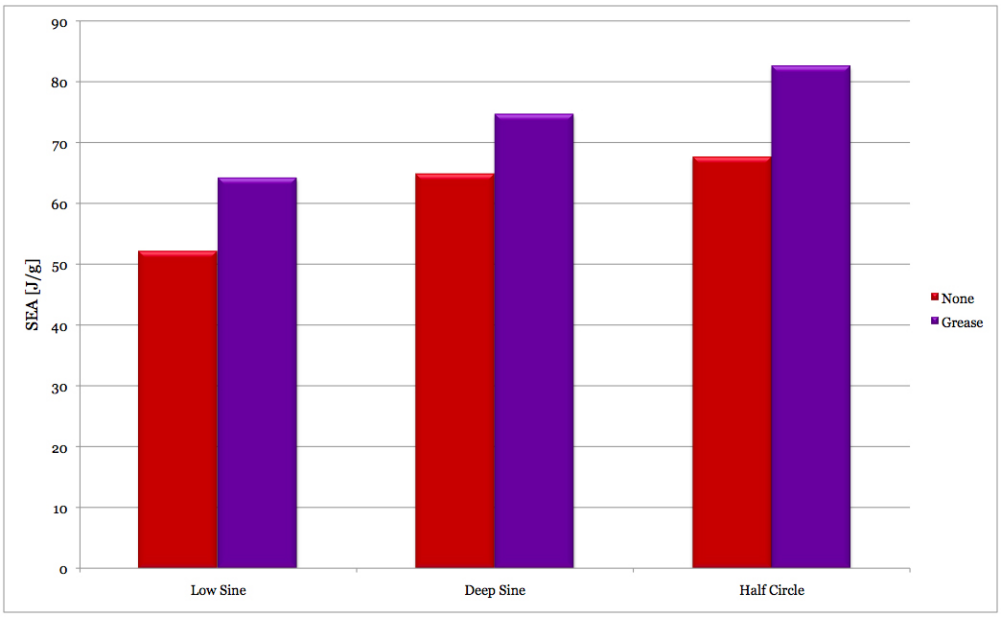

Figure 2.37: Influence of the friction on the energy absorption

ones, with $[0/90]_{3s}$ layup, made of both Agate and Boeing material. The specimens were tested at three different speeds of 0.5, 1 and 2 in/sec (see table 2.9).

The results are shown in figure 2.38 and summarized in table 2.11.

Group	Material	v [in/sec]	SEA [J/g]
A1		0.5	64.524
A2	Agate	1	62.494
A3		2	66.512
B1		0.5	88.879
B2	Boeing	1	81.671
B3		2	88.251

Table 2.11: Dynamic tests results summary

Comparing the results of the dynamic tests, it is possible to state that there is not a significative dependency of the SEA from the crushing speed. The orange line in figure 2.38 represents the level of specific energy absorption reached in quasi static tests and it is evident that there is not any considerable difference between them and the dynamic ones.

At this stage of the behavioral analysis of specific energy absorption capability of composite materials it is therefore a useless complication (and a waste of money

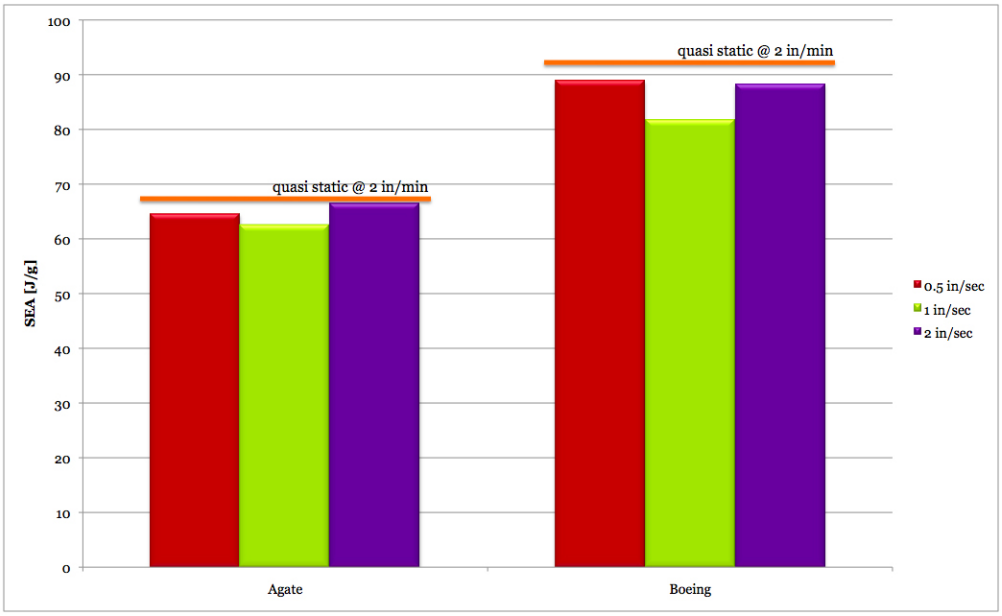

Figure 2.38: Dynamic tests on half circle specimens

in expensive equipment) performing dynamic tests instead of quasi static ones. Different conclusions can be made at a higher level of test, involving complex structures where their structural dynamics can affect the crushing mechanisms.

In conclusion to this test session, the following considerations can be formulated:

- the shape of the specimen influences the energy absorption, in particular the half circle shape has a better behavior than both low and deep sine shape;
- in the case of pure compressive load, layups with fibers oriented at 45° do not improve the energy absorption capability of the specimen;
- over-cured materials are weaker than ones regularly cured according to suppliers instructions because the matrix properties are degraded;
- among the materials tested, Boeing material is the one with the best energy absorption capability;
- plain weave fabric has better energy absorption capability than the corresponding version as unidirectional tape, because the load is sustained by fibers woven together and not only bounded through the matrix as it happens in the tape;
- sliding friction between the fronds and the crushing plate affects the energy absorption: the higher the friction, the higher the energy absorbed;

- speed does not affect significantly the specific energy absorption capability of materials (in relation to coupon size tests).

2.3.4 Flat specimen part III

While performing the self supporting specimens test session, a new concept of anti-buckling fixture for flat specimens was designed and realized to provide a more handling tool than the ARL-inspired fixture and an easier and quicker setup procedure for the test.

The new fixture (figure 2.39), developed at the laboratories of the University of Washington, takes the main frame structure from the existent ARL-inspired fixture, while the anti-buckling supports are an improvement of the University of London fixture (figure 2.2).

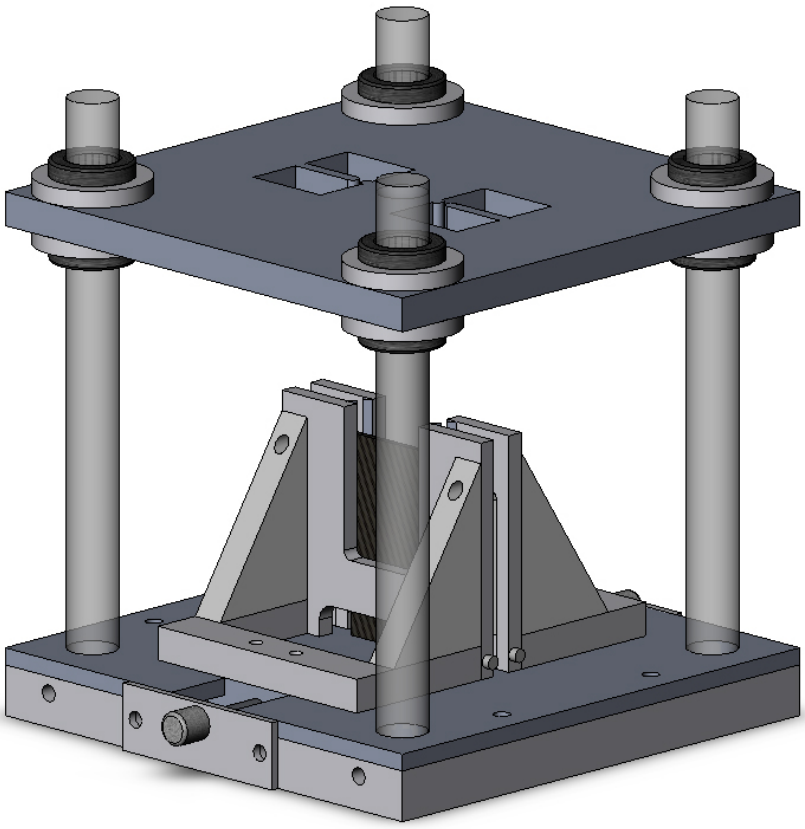

Figure 2.39: Innovative fixture for flat specimens test

The bottom plate is part in aluminum and the crushing surface is in steel as well as the top plate, reducing the weight of the main frame compared to the old fixture and increasing its handiness. The innovation of the fixture is the mechanism that supports the knife-edges: they are not inserted in support rods, but they are machined on a plate like the support plates for narrow specimens of the previous

fixture (figure 2.15). The plates are then fixed on a rigid support that slides along a channel guide, regulated through an endless screw; this mechanism let the test operator to perform a quicker setup and to regulate more precisely the closing force of the anti-buckling supports towards the specimen. The fixture has six different sets of knife-edges plates, that allow the unsupported height of the specimen vary from 0 in to 1 in at discrete intervals.

The main objective of this test session is to determine the influence of the unsupported height on the specific energy absorption. Also, it is possible to make a comparison between two material systems, two different trigger mechanisms and the influence of sliding friction during the test.

For each knife-edges set, an extensive range of specimens was tested. The specimens behavior was evaluated at six different values of unsupported height h:

- 0 in;
- 0.125 in;
- 0.25 in;
- 0.5 in;
- 0.75;
- 1 in.

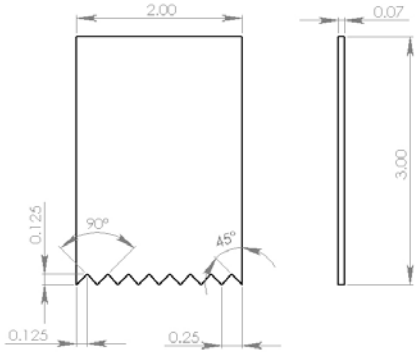

Figure 2.40: Notch trigger

The specimens dimensions for this test session were 2 in x 3 in, all with a $[0/90]_{3s}$ layup. Two different trigger mechanisms were machined on the specimens: steeple (figure 2.17b) and notch (figure 2.40). The material systems used to produce the specimens were Agate and Boeing.

In this session, another attempt to determine the influence of the sliding friction on the energy absorption was made. Two lubricants were employed: grease, as in part I of self supporting specimens session, and a spray of dry powder of zinc stearate as it was suggested by Brimhall [16]. The grease was spread only on the crushing surface of the fixture, while the zinc stearate was sprayed both on the specimen surface (to ideally reduce the friction between specimen and knife-edges) and on the crushing surface.

All the tests were performed at the quasi-static speed of 2 in/min.

The tests performed are summarized in table 2.12.

Material	Trigger	Lubricant	h [in]
Agate	Steeple	none	0
			0.125
		Zn	0.25
	Notch		0.5
		grease	0.75
			1
Boeing	Steeple	none	0
			0.125
			0.25
	Notch	Zn	0.5
			0.75
			1

Table 2.12: Flat specimens tests part III - Test summary

The first aspect studied during this test session is the influence of the unsupported height h of the specimen. From the previous test sessions on flat specimens, it is evident that when the specimen is totally constrained between the knife-edges the specific energy absorption reaches very high values, while as soon as the knife-edges rise, the SEA drops to very inconsistent values.

The same behavior is evidenced and confirmed in this dedicated study, in particular it is extremely representative for the Agate material as shown in figure 2.41a.

The specimen tested at $h = 0$ in (red) is the one closer to the expected behavior of a steep rise of the specific energy absorption during the crushing of the trigger, then reaches almost an asymptotic value even if with ample fluctuations. The high values of SEA reached in this configuration can be explained with the phenomenon of fronds tearing that appears when the specimens are constrained along their full length (figure 2.42a).

All the other tests, with $h > 0$ in, show a different behavior compared to the $h = 0$ in test: the initial peak, relative to the crushing of the trigger and the formation of the central interlaminar crack, reaches a value of SEA comparable to the one of the 0 in test, but after the transient state, the specific energy absorptions converge towards a very low value (between 3 and 6 J/g). This behavior, with this test setup, suggests that splaying (see specimens in figure 2.42b) is not an efficient fracture mode to reach a consistent level of energy absorption.

It is more difficult to formulate the same considerations referring to the results obtained with Boeing material, shown in figure 2.41b.

The $h = 0$ in test (red) presents a peak value in the absorbed energy, but

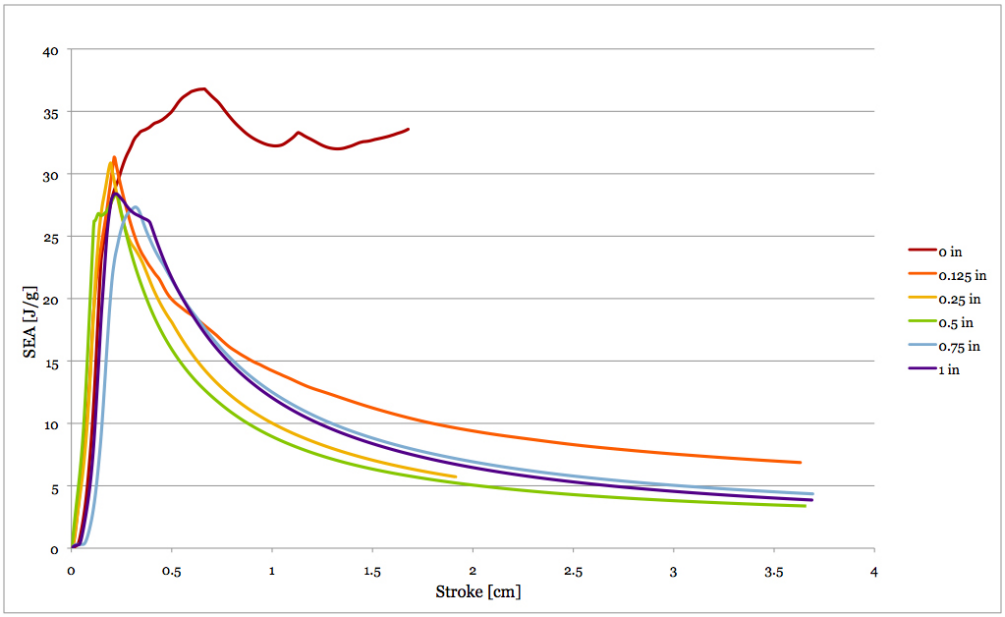

(a) Agate material

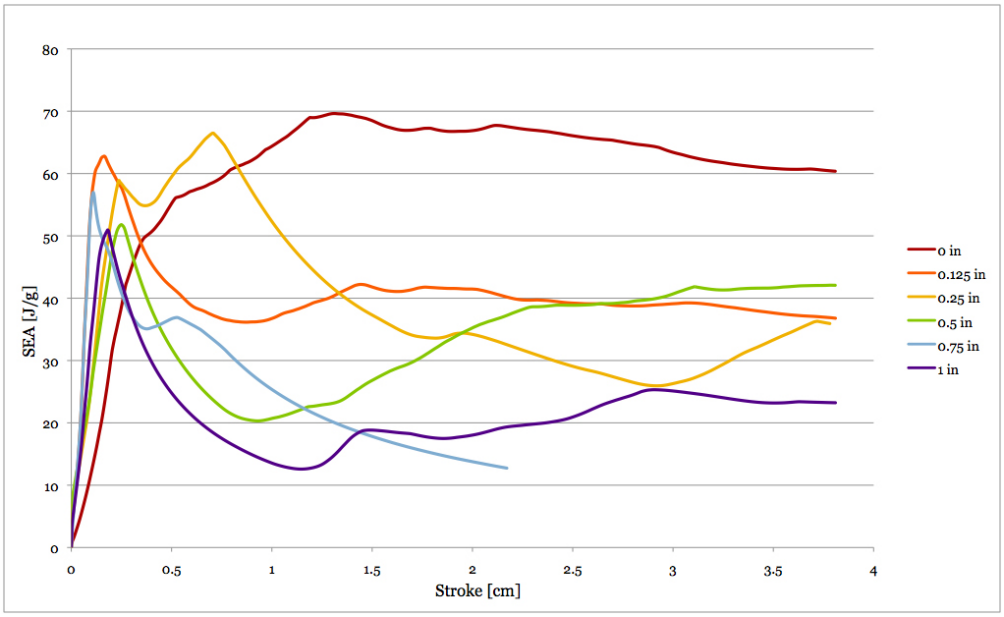

(b) Boeing material

Figure 2.41: Effect of the unsupported height h on the specific energy absorption for (a) Agate and (b) Boeing material

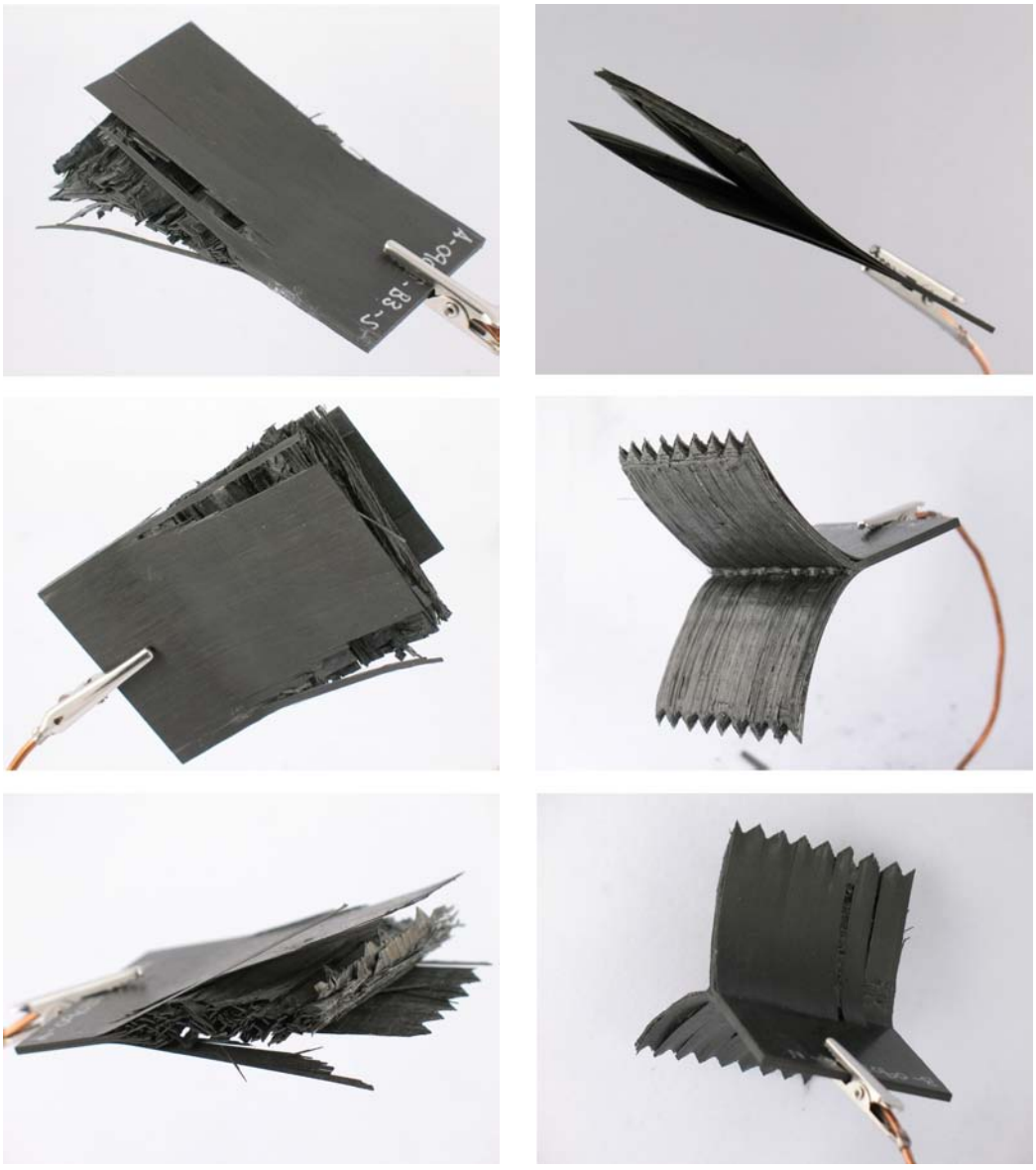

(a) $h = 0$ (b) $h \neq 0$

Figure 2.42: Crushed specimens (a) totally constrained by the anti buckling supports ($h = 0$) and (b) with an unsupported height $h \neq 0$

too late in relation to the small portion of the specimen influenced by the trigger mechanism: the peak relative to the crush of the trigger is in fact located at a stroke of about 2 mm; afterwards, the absorbed energy smoothly decreases without stabilizing around an asymptotic value. This behavior of the 0 in test, comparable to the one observed during the tests with Agate material, confirms that the fronds tearing phenomenon has some influence on the SEA, leading to an overestimation of it.

All the other tests performed with a variable $h > 0$ in tend to behave similarly to the relative ones performed with specimens made of Agate material, even if on different magnitude scale: in fact, they show a high peak at the very beginning of the test, around the stroke length of the crushing of the trigger, then decrease toward a relatively low level of energy absorbed (between 10 and 40 J/g).

In this test session it is confirmed that the choice of the material influences the specific energy absorption. In figure 2.43 the average values of SEA for Agate and Boeing materials are reported, referring to specimens triggered with steeple and without lubricant on the crushing surface. The Boeing material (purple) has a better energy absorption capability than the Agate (red), but they both follow the trend of a significant decrease of the specific energy absorbed with the increasing of the unsupported height of the specimen.

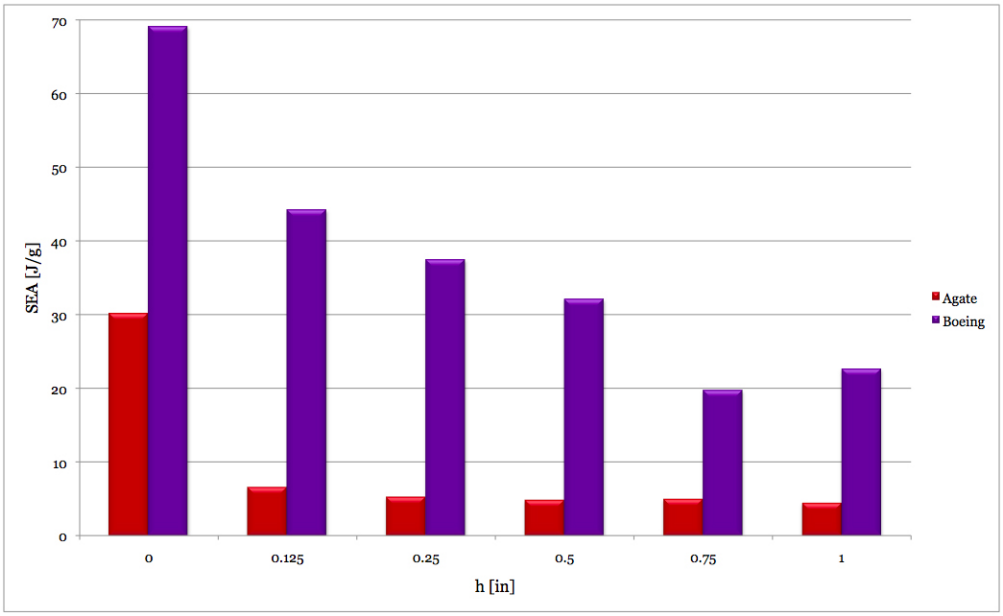

Figure 2.43: Material performance in terms of SEA varying the unsupported height of the specimen h

The third parameter considered in this session is the trigger mechanism: an in-plane trigger (notch, figure 2.40) and a trigger machined on the thickness (steeple, figure 2.17b) are compared in terms of influence on the load-displacement history

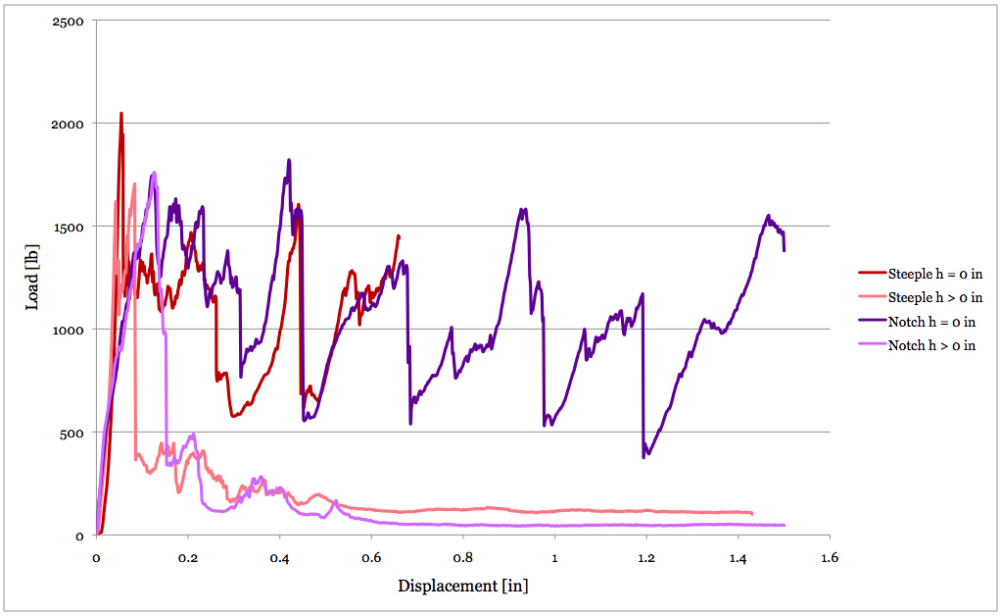

(a) Influence of the trigger in the load-displacement progress

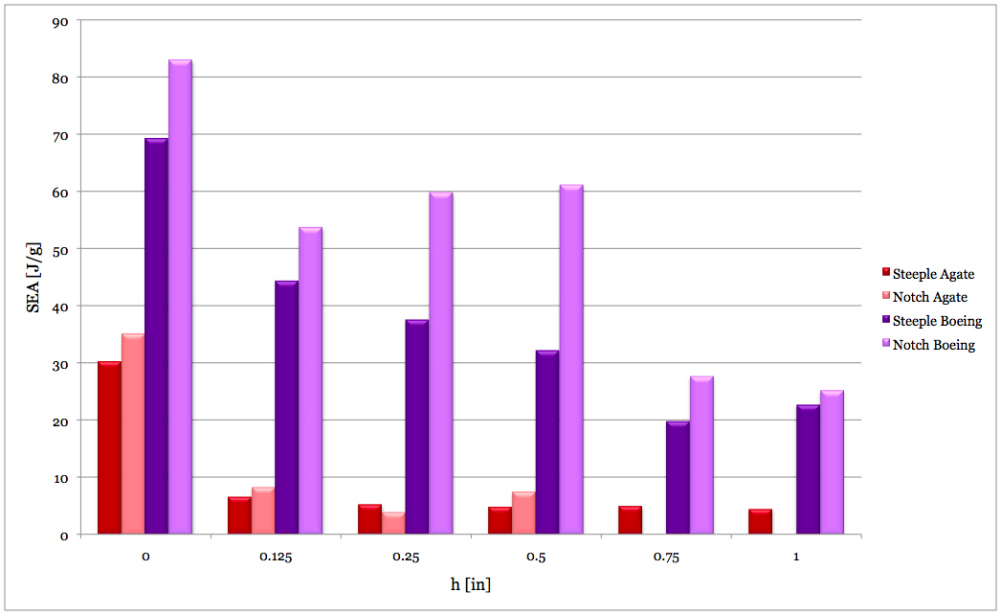

(b) SEA in function of the trigger

Figure 2.44: Effect of the trigger mechanism on the load (a) and on the specific energy absorption (b)

of the test (figure 2.44a) and on the specific energy absorption (figure 2.44b).

For both the trigger mechanisms two test cases are considered:

1. $h = 0$ in, specimen fully constrained between anti-buckling supports (dark shade);

2. $h > 0$ in, a certain amount of the specimen height is unsupported (light shade).

Both the cases are referred to a specimen made of Agate material.

Referring to figure 2.44a, the steeple trigger (red) leads the load to a very high peak compared to the development of the test, in particular for the 0 in test; in the $h > 0$ case (light red), in fact, the peak is still very steep, but reaches a lower value of load, comparable to the peak reached with the notch trigger (purple and light purple). The notch trigger, on the other hand, has a slightly smoother ramp before reaching the initial peak in the load-displacement history, due to its longer extension. The difference between the two slopes is due to the trigger heights: steeple trigger is high half of the thickness of the specimen and it exhausts its influence in about 1 mm from the beginning of the crushing test, while the notch trigger is high one twentieth of the width of the specimen, that means that it influences the load-displacement history of the test for about 2.5 mm.

Moreover, the trigger influences the SEA, as it is possible to see in figure 2.44b. Independently from the material used to make the specimens, with the notch trigger a higher level of SEA is reached than with the steeple trigger. The reason for this result is in the geometry of the trigger: while the steeple mechanism works essentially as a wedge that induces the splaying of the specimen in two fronds and helps the formation and propagation of a long interlaminar central crack (fig. 2.42b, first picture from the top), the notch trigger helps the specimen to open progressively, without the long central crack (fig. 2.42b, central picture); furthermore its in-plane geometry introduces a preferential path for cracks on planes different from the middle one (fig. 2.42b, central picture).

The last parameter evaluated in this part of flat specimens test is the influence of the sliding friction between the crushing surface and the fronds of the specimens.

During the previous test session with self supporting specimens, the influence of friction was evaluated using grease as lubricant, but instead of reducing the friction, the grease held the debris and increased the friction with a relative increase of specific energy absorption.

In this test session two lubricants were evaluated: grease, again, and zing stearate (dry powder in form of spray). Both the lubricants were tested with specimens made of Agate material, while with Boeing material only the zinc stearate was used.

Theoretically, according to the result found that there is a direct link between the friction and the specific energy absorption, the expected result is that the SEA decreases according to the order grease > no lubricant > zinc stearate. In figure

2.45 the results are reported: red and pink shades are for Agate specimens while purple and its lighter shade are for Boeing specimens.

The results confirm the supposed trend for Agate material with zinc stearate (pink), which SEA is always lower than the case of the specimen without any lubricant (red). As for the use of grease with Agate specimens (light pink), the hypothesized trend is verified only for the specimens totally constrained between the anti buckling supports. In all the other cases with grease, when the unsupported height h is greater than zero, the SEA is lower than the referring value without lubricant. This phenomenon can be explained with the low load applied to the specimen during the test and with the fact that the specimen simply opens in two fronds without the formation of a significative amount of debris; as a matter of fact, without the debris mixed with grease and with low loads, the specimen slides on the crushing surface without seeing an effective increase in the friction as it was for self supporting specimens.

With Boeing material, up to an unsupported height of 0.25 in the specific energy absorption with zinc stearate is even higher than the one without lubricant; the reason for this behavior can be found in the high loads reached during the tests, loads that, when transmitted from the crushing surface to the fronds of the specimen, let the fronds scrape off the layer of lubricant from the surface of the bottom plate of the fixture. From $h = 0.25$ in the relation between specimens lubed with zinc stearate and specimens without lubricant goes back to what expected: the zinc stearate is not scraped away from the crushing fronds and the lubed specimens absorb less energy than the ones with no lubricant.

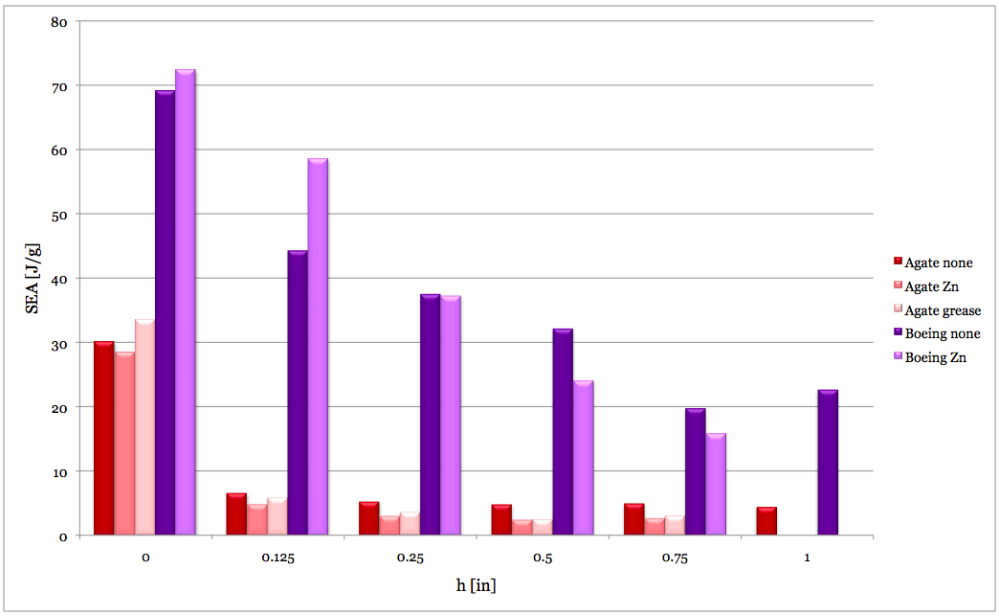

Figure 2.45: Influence of the friction on the SEA evaluated introducing different lubricant agents in the test setup

In table 2.13 the average values of specific energy absorption obtained are summarized.

Material	Trigger	Lubricant	h [in]					
			0	0.125	0.25	0.5	0.75	1
Agate	Steeple	None	30.121	6.579	5.254	4.83	4.968	4.434
		Zn stearate	28.369	4.820	3.017	2.431	2.684	
		Grease	33.473	5.876	3.655	2.514	3.106	
	Notch	None	34.980	8.242	3.888	7.465		
Boeing	Steeple	None	69.116	44.254	37.490	32.131	19.761	22.646
		Zn stearate	72.381	58.566	37.264	24.081	15.896	
	Notch	None	82.873	53.646	59.738	61.056	27.637	25.182

Table 2.13: Flat specimens tests part III - Test results summary

In conclusion, in this test session the influence of the following parameters was evaluated:

- h, unsupported length of the specimen;
- material;
- trigger mechanism;
- sliding friction.

The results obtained lead to the following conclusions:

- the unsupported length of the specimen has a relevant role in the amount of energy absorbed during the test;
- when the specimen is totally constrained between the anti-buckling supports ($h = 0$ in) the highest values of SEA are reached because of fronds tearing phenomenon, that means that part of the energy is absorbed by the fixture;
- for h greater than zero the specimens tend to open in two fronds and in the most of the cases a long central interlaminar crack forms (splaying mode), leading to a very low level of sustained load;
- the material influences the answer of the test in terms of energy absorption scaling the SEA in accordance to the better or worse material properties;
- the trigger mechanism influences the steepness of the initial peak in load;

- in-plane trigger mechanism (notch) helps a better crushing process than triggers machined in the thickness (steeple);
- steeple trigger helps the formation of the central interlaminar crack in the specimen that leads to splaying crushing mode;
- there is a proportional relation between friction and specific energy absorption (higher friction coefficient means larger amount of absorbed energy).

2.3.5 Self-supporting specimens part II

The last and most recent test session focuses the attention on half circular self supporting specimens and investigates the effects of different material systems, layups and number of repetition of the semicircular modulus.

To realize the specimens, a new dedicated mold was designed and realized in the MaSTeR Lab facilities at the Second Faculty of Engineering of the University of Bologna in Forlí.

The new mold is machined from two aluminum plates and measures, once closed, 280 mm x 180 mm x 30 mm; each half is 15 mm thick (figure 2.46).

Figure 2.46: Mold for half circle self supporting specimens realized at MaSTeR Lab, University of Bologna

As the mold used at the University of Washington, also this mold is designed to be used with prepreg material systems; it can host up to 12 plies of unidirectional

prepreg or 8 plies of plain weave fabric. In figure 2.47 the open mold with a cured plate of unidirectional material is shown.

The composite plate measures 210 mm x 180 mm x 1.8 mm approximately and it is cut into six specimens: four with three repetitions of the half circular modulus (60 mm x 80 mm, figure 2.48a) and two with five repetitions (80 mm x 80 mm, figure 2.48b).

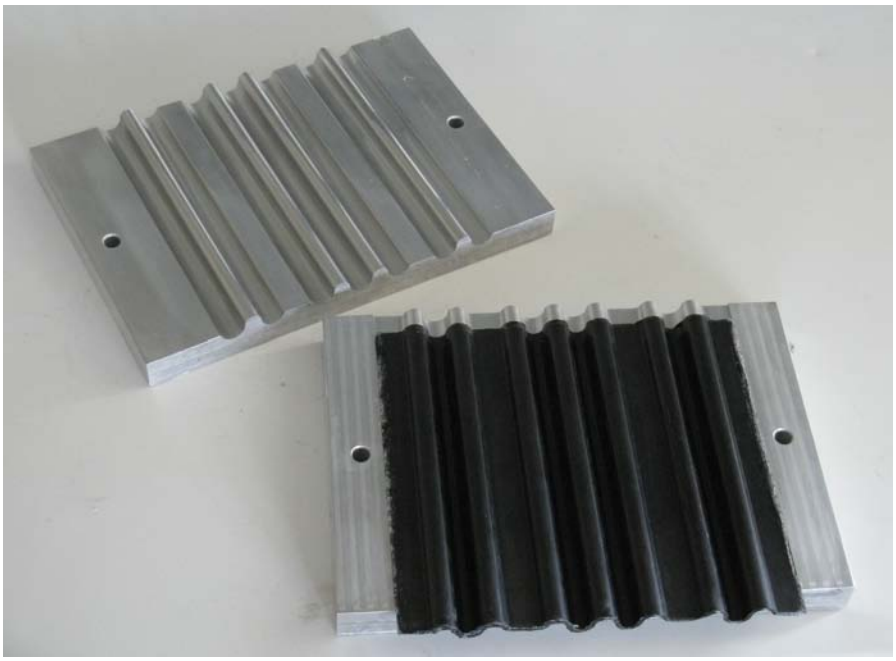

Figure 2.47: Mold with cured plate of composite material

(a) HC3 (b) HC5

Figure 2.48: Similar specimens with (a) three repetitions and (b) five repetitions of the half circular modulus

The mold released used was different from the previous session: it is a liquid mold release (Frekote 770NC) and it has to be gently brushed on the surface in a thin film and it takes only few minutes to dry, so the process was quicker than with wax.

Two material systems were tested:

- ACG unidirectional tape (T700 24k/MTM57);
- custom plain weave material by Angeloni (GG200P/IMP530R).

All the material systems are carbon fiber reinforced plastics (epoxy). Both materials are custom made from the suppliers according to requirements of a general purpose material for structural applications.

The ACG unidirectional tape prepreg (T700 24k/MTM57) is a high strength carbon fiber material. The T700 material is the same as Toray materials: the fibers are continuous, no-twist carbon filaments. The matrix is an epoxy resin produced by ACG, that exhibits excellent toughness; when the prepreg is cured the resin content is around 35%.

The material by Angeloni is a custom combination of a 200 g/m^2 plain weave carbon fabric with a resin (IMP530R) by Impregnatex Compositi. The resin is designed specifically for automotive applications and has high surface finishing qualities. Once the material is cured, the resin content is nominally 42%.

Both materials were cured in autoclave, according to the supplier indications for the correct cycle.

The mechanical properties of the unidirectional tape are reported in table 2.14. The supplier of the plain weave material did not disclose the material datasheet; the only declared property about the fabric is that the carbon fibers are HR (high resistance).

The density of the plain weave material has been calculated: 1.65 g/cm^3.

	UD
ρ [g/cm^3]	1.52
E_1 [GPa]	128
E_{1c} [GPa]	118
E_2 [GPa]	7.9
E_{2c} [GPa]	–
G_{12} [GPa]	3.0
ν_{12}	0.3
σ_{u1t} [MPa]	2481
σ_{u1c} [MPa]	1296
σ_{u2t} [MPa]	52.9
σ_{u2c} [MPa]	–
σ_{u12} [MPa]	91.3

Table 2.14: Material properties according to the datasheets supplied by the factory; UD – ACG unidirectional tape T700/MTM57

The test procedure was the same as the first self supporting specimens test session: the specimen, measured in width and thickness, was positioned at the center of the crushing fixture, then the applied load and the displacement of the movable head of the hydraulic press were recorded.

The test speed was set at 0.83 mm/s, that is the equivalent of 2 in/min of the previous self supporting session.

Four different layups were tested, three with a conventional chamfer trigger and one with a particular layup that works as an auto-trigger. The conventional layups are:

- $[0/90]_{3s}$;
- 8 plies PW 0°;
- 8 plies PW 45°;

where the directions of the plain weave fabric plies are referred to the load direction (0°).

The innovative auto-trigger layup consists in a stack of 12 unidirectional plies $[0/90^*]_{3s}$ where the 90* ply is shorter than the height of the 0° layers: when the specimens were cut from the plate, at one end of them there was a weaker section of about 1 cm with only 6 plies oriented along the load direction (figure 2.49). The thickness of the specimens on the weaker side was not sensibly reduced because, even if there were only six plies instead of twelve, the squeezing action of the constant section of the mold helped the excess of resin flow from the thickest section to the thinnest one, filling the voids between the plies.

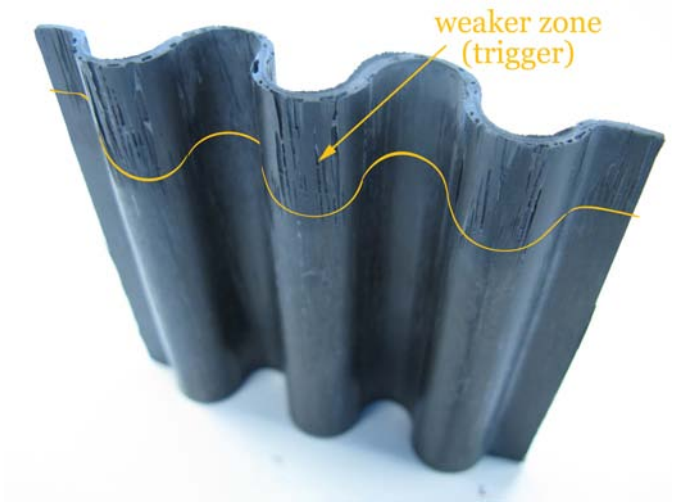

Figure 2.49: Auto triggered specimen: the weaker zone presents voids and fibers distortion due to the lack of plies but not sensible contraction in the thickness

The tests performed are summarized in table 2.15.

Test ID	Material	Layup
UD	UD	$[0/90]_{3s}$
PW0	PW	8 plies 0°
PW45	PW	8 plies 45°
ATF	UD	$[0/90^*]_{3s}$

Table 2.15: Self supporting specimens part II – Test summary
UD – ACG unidirectional tape T700/MTM57;
PW – Angeloni plain weave fabric GG200P/IMP530R

An extensive number of specimens was tested for each configuration and the results refer to their average values.

The first result obtained from this test session is that the number of half circular periods of the specimen does not influence significantly the specific energy absorption; this means that the energy absorption capability is an intrinsic property of the material.

In figures 2.50 and 2.51 it is evident how the crushing load and the energy absorption depend on the kind of specimen: the smaller specimen (HC3 – three half circle repetitions) sustains a lower load and the relative energy absorption is lower than the one of the specimen with five half circle periods (HC5). This difference is no longer seen in figure 2.52, where the energy absorbed is divided for the material density and the cross sectional area.

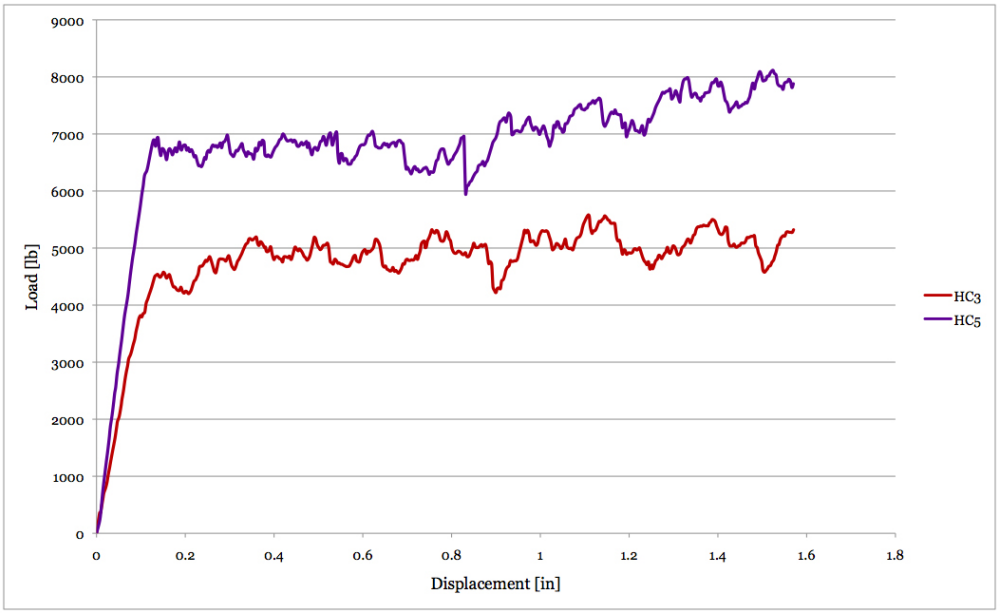

Figure 2.50: Load vs. displacement history for similar half circle specimens

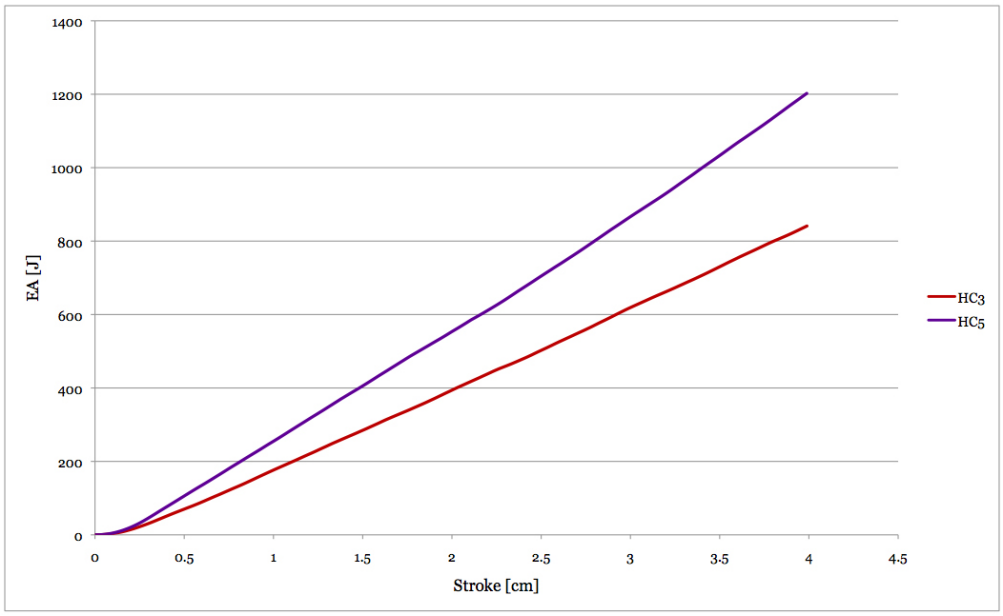

Figure 2.51: EA vs. stroke trend for three and five half circles specimens

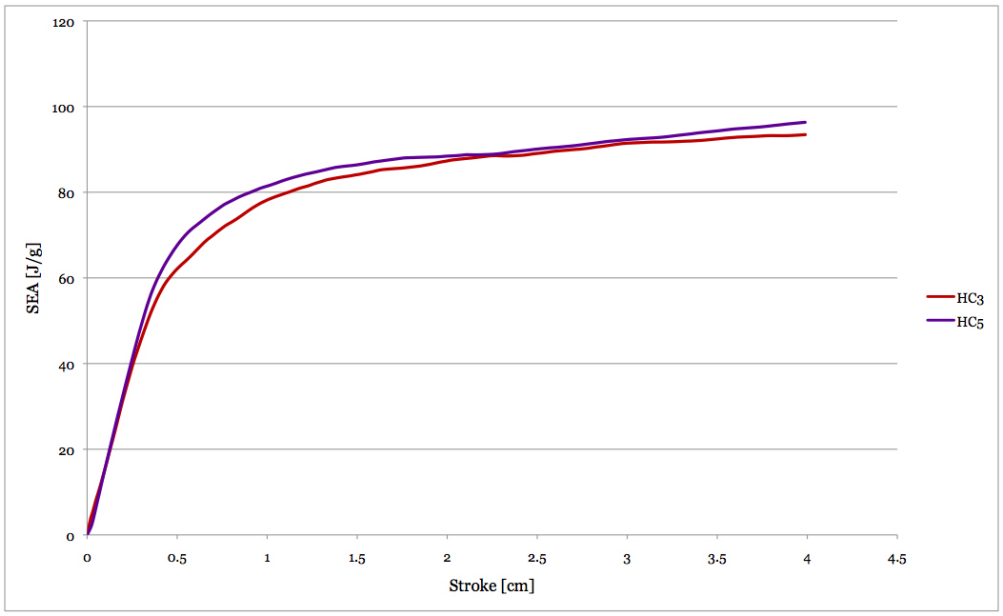

Figure 2.52: SEA vs. stroke behavior for specimens with three and five repetitions of the half circle modulus

In figure 2.53 the average values of SEA for the two kind of specimens are compared and the values are reported in table 2.16.

Except for the plain weave specimens with fibers at 45°, the difference between the specific energy absorptions is ±10%.

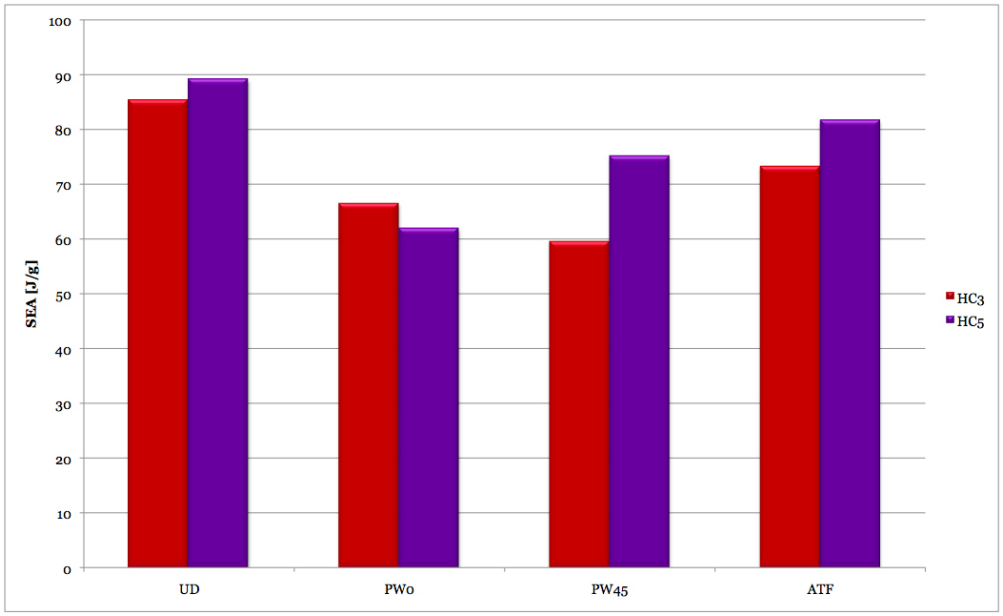

Figure 2.53: SEA comparison between specimens with different number of repetitions of the half circle modulus

Test ID	Material	Layup	Speciemen	SEA [J/g]
UD	UD	$[0/90]_{3s}$	HC3	85.399
			HC5	89.127
PW0	PW	8 plies 0°	HC3	66.495
			HC5	61.913
PW45	PW	8 plies 45°	HC3	59.544
			HC5	75.095
ATF	UD	$[0/90^*]_{3s}$	HC3	73.268
			HC5	81.629

Table 2.16: Self supporting specimens part II – Test results summary

Of the four configurations tested, the most coherent with the results expected is the one assumed as baseline: the $[0/90]_{3s}$ specimens made with unidirectional tape.

The two test cases with plain weave material showed an interesting crushing behavior during the performing of the test: the material literally crumbled (figure 2.54) under a relatively low applied load. It is not possible to formulate further considerations about this behavior because of the missing material properties of the plain weave fabric, but comparing the crush of those specimens made with HR carbon fibers with those tested in the previous session made with HS (high strength) carbon fibers, the employment of high strength fibers is preferable in compressive events.

(a) Specimen crushing during the test

(b) Crushed specimen

(c) Debris

Figure 2.54: Crushing behavior of plain weave fabric specimens (0°)

The same crushing behavior is shown also by the plain weave specimens with fibers at 45°. The interesting aspect of this behavior in the 45° specimens comes from the comparison with the similar specimens made with unidirectional tape and tested in the part I of the self supporting specimens tests: the plain weave fabric, in fact, helped to avoid the phenomenon of shear of the fibers already seen in figure 2.35c.

The last setup tested is the innovative auto-trigger specimen denoted as ATF. Their particular layup is designed to initiate the fracture on the side of the specimen where the 90° plies are shorter and therefore defects as voids, high concentration of resin and fibers distortion are present.

The specimen crushed as expected during the test and its SEA revealed a two-steps behavior if the specific energy absorption is calculated assuming constant density and cross sectional area through all the specimen. As shown in figure 2.55, the length of the weak section, that is to say the trigger, of the specimen is easily recognizable.

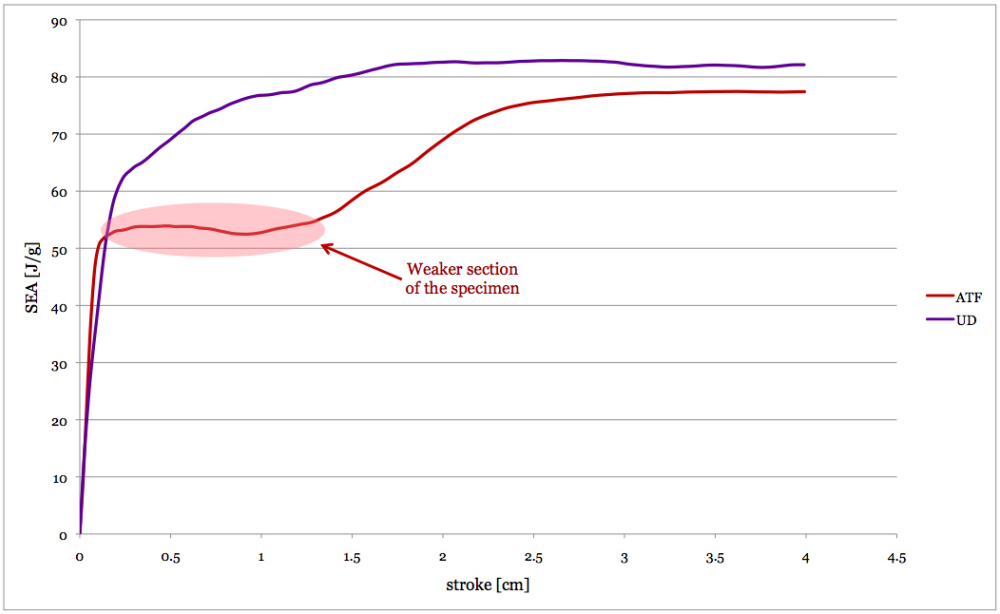

Figure 2.55: SEA comparison between auto trigger specimen (ATF) and the baseline unidirectional specimen (UD)

A more accurate calculation of the SEA can be performed imposing for the length of the trigger a different value of the density, assuming that the constant section of the mold forces the specimen to have almost the same thickness through all the height of the specimen, but this approach requires the exact knowledge of the exact extension of the weak zone in the specimen and its density, that is not constant but increases monotonically. The two-steps approach, on the other side, gives a conservative estimation of the specific energy absorbed and better reflects the different areas of the specimen.

In conclusion to this last test session the following considerations can be formulated:

- the number of repetitions of the half circular modulus of the specimen does not influence significantly the specific energy absorption;

- the plain weave specimens showed a peculiar crushing behavior, crumbling up during the performance of the test;
- due to the crumbling behavior, the comparison between the results obtained with a high strength plain weave material in the previous self supporting specimens test session and the values obtained with the high resistance material used in this session, suggests that high strength materials are preferable in crushing events;
- in specimens with fibers at 45°, the use of plain weave fabric contrasts the shear of the fibers during the compression helping the crushing process;
- the auto-trigger layup behaved as it was supposed to, opening the way to possible structures with calibrated weak sections able to initiate the crushing during an impact event, without manufacturing particular trigger mechanisms.

2.4 Experimental tests conclusions

During the five test sessions performed, two test methods were compared:

- the flat specimen test method;
- the self supporting specimen test method.

The comparison pointed out pros and cons of the two test methods.

The main pro of the flat specimens method is the production of the specimen itself: the specimens, in fact, are easy to produce because they are simply cut from a flat plate. They are also quick to prepare for the test: except for the realization of notch trigger that requires the use of a water machine, the triggers are easily machined on a flat surface and the determination of the cross sectional area of the specimen needs only two measures.

On the other hand, the cons for this test method are many:

- the test setup is complicated and takes a lot of time;
- a dedicated fixture is required to support the specimens in vertical position;
- the fixture introduces in the test external factors, like the variable unsupported length of the specimen or the closing force of the anti-buckling supports.

The self supporting specimens test method has advantages where the flat specimens one fails and it has minor issues where the flat specimens method presents its major benefits.

The most relevant features of the self supporting specimens test method are two:

- it does not need any anti-buckling fixture;
- the test is not sensitive to external factors.

The minor issues of this test method are referred to the specimens production: they need a dedicated mold to be manufactured, though it is a simplification and an improvement compared to the internal mandrel used in the production of tubes; in the preparation phase, the specimen has to be carefully triggered by hand and multiple measurements have to be performed because of possible little variations in the thickness.

The two test methods differ also in terms of fracture mechanisms involved in the crushing of the specimens as shown in figures 2.42 and 2.31.

Figure 2.42 shows different flat specimens crushed both fully constrained between the anti-buckling supports and with unsupported length: in all cases the main fracture mechanism is splaying. In the case of the specimens totally constrained (fig. 2.42a), the internal plies show some phenomena of fragmentation, but it is due only to the boundary conditions imposed by the fixture, therefore the load and the relative energy absorption results are corrupted. Fracture of lamina bundles (figure 2.31b) is instead the main fracture mechanism of self supporting specimens.

The difference between the fracture mechanisms involved reflects in different specific energy absorption behaviors.[1]

In figure 2.56 the progress of the specific energy absorption of a flat Agate $[0/90]_{3s}$ specimen (red) is compared with its analogous self supporting one (purple): the flat specimen crushes with splaying mode, which main energy absorption mechanism is the matrix crack growth. This mechanism does not involve the fibers of the plies, that remain slightly bended but integer at the end of the test (2.42b, first picture from the top). On the other hand, the higher amount of energy absorbed showed by the self supporting specimen is due exactly to the fracture of lamina bundles, that is the main absorption mechanism for the fragmentation mode.

The specific energy absorption trends of flat and self supporting test methods, still on analogous specimens, are further compared in figure 2.57. In the figure the average values of flat specimen tests are reported in function of the unsupported

[1]The results used for the discussion from now on refers to the tests presented in sections 2.3.4 and 2.3.5 because the same materials, curing cycles and mold release are used during the test sessions, but they can be generalized for all the others configurations.

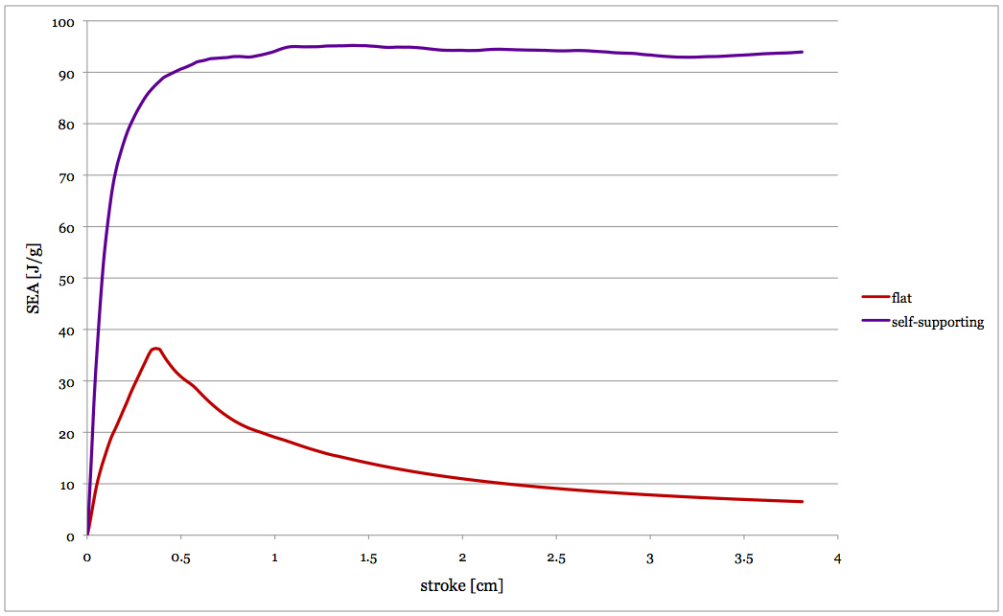

Figure 2.56: Comparison between typical behaviors of SEA obtained with flat and self supporting tests

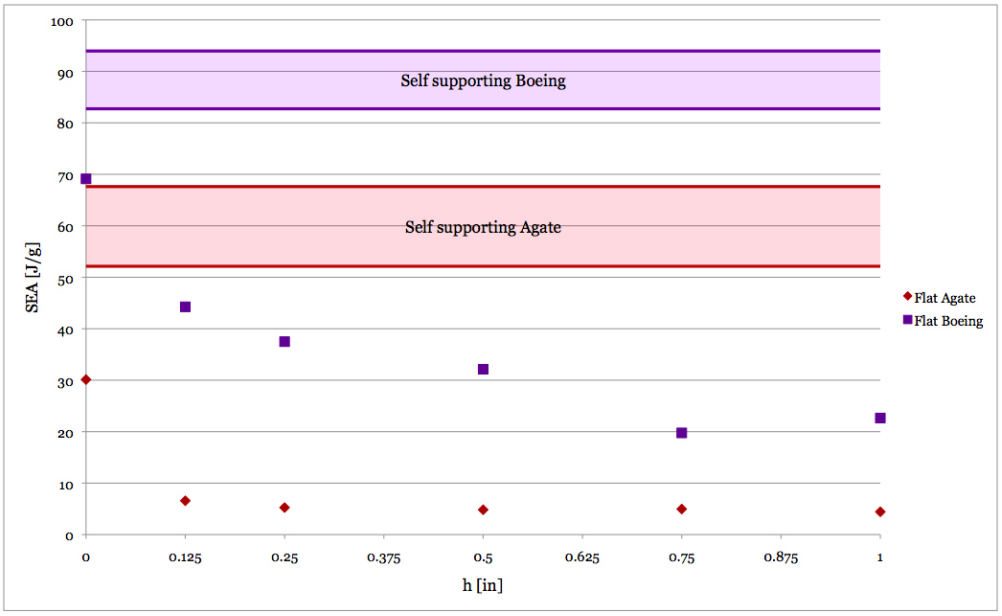

Figure 2.57: SEA as a function of unsupported height h and comparison with results of correspondent self supporting specimen

length of the specimen (red and purple markers) and they are compared with the zone where self supporting specimens collocate their SEA. The same comparison is made for both Agate (red) and Boeing (purple) material specimens. Once again, it can be pointed out that self supporting specimens perform better than flat specimens, even than those totally constrained in which phenomena of fracturing of lamina bundles appear.

During the test sessions presented in this chapter an extensive number of configurations for each test method was tested.

The flat specimen test method denoted a lack of reliability due to the influence of the fixture on the test execution, while the self supporting specimen test method showed repeatable results in all the configurations tested; therefore, the guidelines for a standard test procedure based on the use of self supporting specimens can be formulated for the determination of the specific energy absorption.

- The suggested test method requires the use of a half circle self supporting specimen with three repetitions of the semicircular modulus.
- The specimen has to be measured accurately in width and in thickness; for the thickness, at least seven measurements have to be performed to take into account the variations due to the curvature of the mold.
- A minimum thickness of 1.8 mm is required; according to the thickness of the specific material, the appropriate number of plies will be determined.
- For unidirectional tapes a symmetric and balanced layup $[0/90]_{ns}$ is recommended; for plain weave or other fabrics, the orientation of the fibers at 0° is recommended; fibers at 45° should be avoided.
- The trigger mechanism is a simple chamfer on one of the two corrugated sides.
- Once measured and triggered, the specimen is positioned in the center of two iron plates that slide along four rods; the alignment of the top plate is guaranteed by four linear bearings that fit the rods.
- Assuming that the crash speed does not affect the specific energy absorption capability of the material (figure 2.38), a quasi static test is preferable to an impact one because it is cheaper, therefore the speed can be set at a value of 2 in/min or 1 mm/sec.
- During the test, the displacement of the movable head of the hydraulic press where the test is performed and the applied load to the specimen are recorded.
- From the displacement and load data, applying the equations (1.1) and (1.2), the specific energy absorption of the material can be calculated.

The test as defined above is the starting point for the numerical model implemented in the next chapter of this thesis, that will complete the first stage of the building block approach for the characterization of complex structures.

The collected experimental results will help the validation of the finite element model.

Chapter 3

Numerical model

If at first you don't succeed,
call it version 1.0.

ANONYMOUS

3.1 Introduction

The achievement of the numerical model implemented in this work is to provide a quick tool to simulate the macroscopic behavior of a structure designed for crashworthiness.

The aim of the model is therefore not to simulate what happens in every single layer of the composite structure or at the interface between the plies, but to give a global feeling of how the structure behaves and of the approximate amount of energy it is capable to absorb.

As previously mentioned, this work is based on the building block approach (BBA) method, a sequence of steps in which the complexity of the structure increases from the lowest level of tests on specimen to the top level of the test on the complete structure, stepping through intermediate levels subcomponents and components. Graphically represented, this approach is a pyramid, where at the bottom the largest number of tests is performed to reduce it to few, significative ones going up towards the complete structure; figure 3.1 helps the visualization with an exemplar case of a wing structure for airplane [2].

Building block approach ensures that cost and performance objectives are met by testing greater numbers of smaller and less expensive specimens and building on the knowledge acquired at a given level of structural complexity before progressing to a level of more complexity [17].

There is a close relation between experimental tests and numerical simulations: the experimental tests described in chapter 2 are used to define a reliable test procedure and this test procedure is reproduced numerically in a finite element environment.

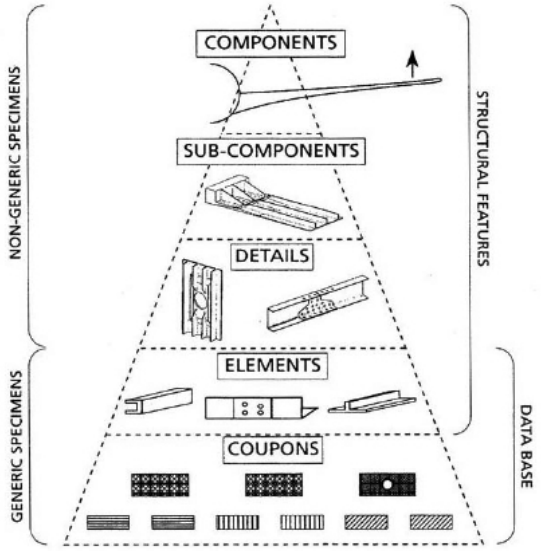

Figure 3.1: Representation of the pyramidal structure of the building block approach [2]

The implementation of a finite element model has the advantage, once calibrated on the particular material or layup of the specific case, of reducing the number of experimental tests of the stage the model refers to. Considering the case of the first level at the bottom of the pyramid, the one that refers to coupons, if a numerical model of the generic test with the coupon exists, there will be only the need to perform a limited number of experimental tests to get the minimum amount of data necessary to calibrate the numerical model. Moreover, the calibrated numerical model, if applied to the more complex elements of the second step, can give a rough prediction of their behavior and let the designer limit the investigation field.

Building block approach programs can achieve significant cost reductions by seeking a synergy between testing and analysis. The more the development relies on analysis, the less expensive it becomes [18].

To accomplish the objective of completing the first step of the design process, this chapter focuses on the simulation with finite elements of a self supporting test defined as baseline.

According to the crashworthiness requirements, the objectives of the numerical model are:

- the reproduction of the macroscopic behavior of the specimen;
- giving an estimation of the specific energy absorption, approximating its progress during the time of the test.

The main feature that will determine the possibility of predicting the performance of the test specimen in the numerical environment is the numerical model

that describes the material behavior. In fact, the way the material is modeled, how its properties decay in function of the growth of the damage in the structure, determines the accuracy and reliability of the numerical simulation.

The finite element software used to model the progressive crush of the composite specimen is Abaqus, a commercial FEA (Finite Element Analysis) software very popular for its features dedicated to composite materials.

3.2 Something about progressive failure analysis

The need of a progressive damage model rises with the increasing use of composite materials in structures: besides the advantages that the use of composite materials brings, such as the possibility to tailor the stiffness and strength to specific design loads, their intrinsic nature based on a heterogeneous combination of fibers and matrix leads to the development of local failures or they can exhibit local damages such as matrix cracks, fiber breakage, fiber-matrix debonding or delamination that may contribute to the failure of the structure under normal operative loads.

A typical methodology for a progressive failure (or damage) analysis is illustrated in figure 3.2 [19].

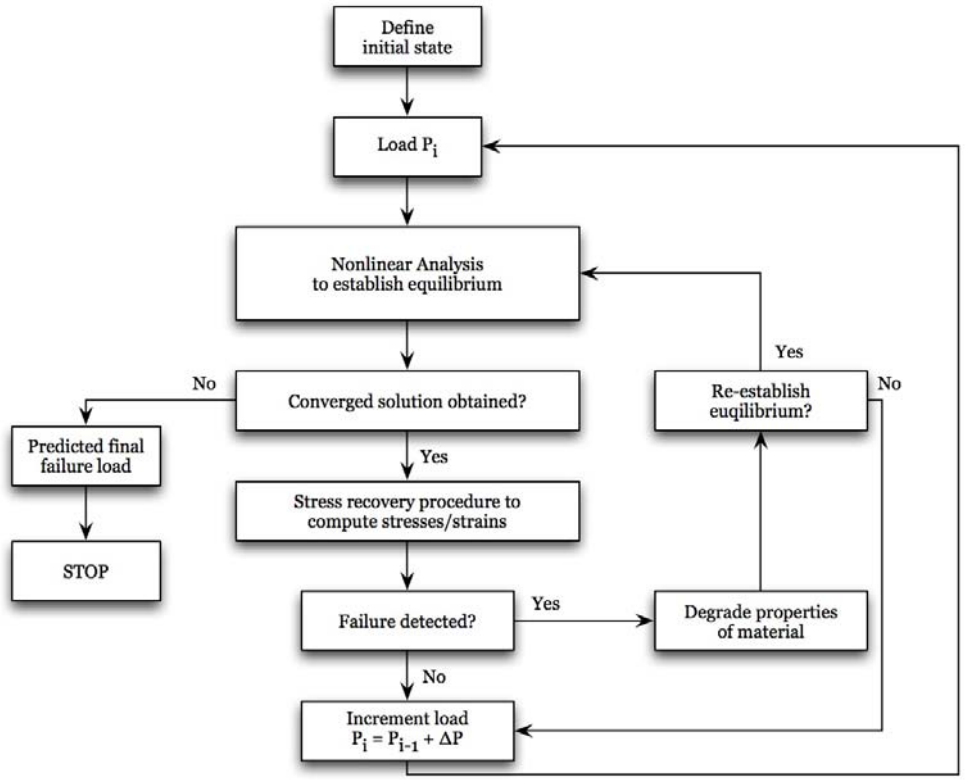

Figure 3.2: Typical progressive failure analysis methodology

At each load step, a nonlinear analysis is performed until a converged solution is obtained assuming no changes in the material model. Referring to this equilibrium state, the stresses within each lamina are computed and then compared with material allowables and used to determine failure according to the specific failure criteria imposed. If lamina failure is detected, the lamina properties are modified according to a particular degradation model. Since the initial nonlinear solution no longer corresponds to an equilibrium state, equilibrium of the structure needs to be re-established utilizing the modified lamina properties for the failed lamina while maintaining the current load level. This iterative process is continued until no additional lamina failure is detected. The load step is then incremented until the structure completely fails.

Typical progressive failure analysis method involves five key features:

1. the nonlinear analysis capability used to establish the equilibrium;
2. the stress recovery procedure, that establishes the local lamina stress state;
3. the failure criteria;
4. the material degradation damage model;
5. the procedure to re-establish equilibrium after modifying local lamina properties.

Composite laminates typically behave in a linear elastic manner until local structural failures develop. After material degradation and local failures within the laminate, the global structural stiffness changes. Globally, the structure fails due to the propagation or accumulation of local damage as the load increases; initial failure of a layer within the composite structure can be predicted by applying an appropriate failure criterion.

Laminated composites may fail by fiber breakage, matrix cracking or by delamination of the layers and the mode of failure depends from multiple factors like the applied load, the stacking sequence and the specimen geometry.

Failure criteria are used in the model to predict macroscopic failures in the composite laminate in function of the stress state of the individual lamina. When the failure criterion is exceeded in a given layer, the material constants corresponding to the particular mode of failure are reduced depending on the material degradation model.

Failure criteria for composite materials are generally classified into two groups:

1. non-interactive failure criteria;
2. interactive failure criteria.

The non-interactive failure criteria are also known as independent failure criteria, because they have no interaction between the stress or strain components. They are based on the comparison between the individual stress or strain components with the corresponding material allowable strength value. The criteria that belong to this category are:

- maximum stress;
- maximum strain.

The failure surface for these criteria is rectangular in stress and strain space, respectively.

Interactive failure criteria, on the other hand, involve interactions between stress and strain components and can be divided into three categories:

1. polynomial theories, that use polynomial functions of the material strengths to describe the failure surface;
2. direct-mode determining theories, usually polynomial equations based on the material strengths and using separate equations to describe each mode of failure;
3. strain energy theories, based on local strain energy levels determined during the non-linear analysis.

The most popular interactive criteria are:

- Tsai-Wu (polynomial);
- Tsai-Hill (polynomial);
- Hashin (direct).

When failure is detected according to the particular failure criterion used in the analysis, the properties of the lamina must be adjusted in agreement with the material property degradation model. The material degradation models are generally divided into three categories (figure 3.3):

1. instantaneous unloading, the material property is degraded instantly to zero;
2. gradual unloading, the material property is degraded gradually until it reaches zero;
3. constant stress at ply failure, the material properties are degraded such that the material cannot sustain additional load.

The degradation methods can also be divided in two other categories according to the function the stress has in the degradation of the stiffness property:

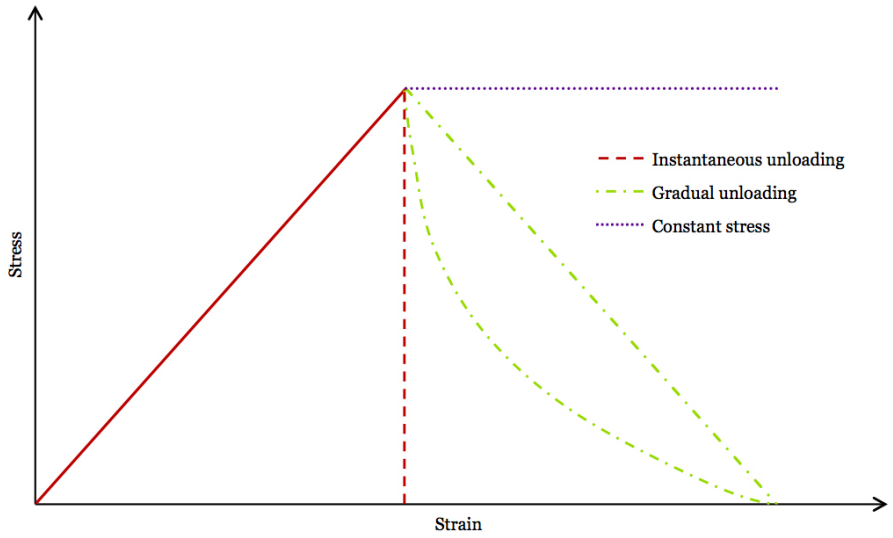

Figure 3.3: Material degradation models

- independent, if each stress only contributes to the degradation of the corresponding stiffness property;
- interactive, if coupling is assumed between the normal and shear stiffness lamina properties.

Of the five key features that are involved in a typical progressive failure analysis, the nonlinear analysis and the calculations for the determination of the stress state of the structure are commonly implemented in finite elements softwares. The choice of an appropriate failure criterion and of a reliable material degradation damage model, instead, is still a challenge for programmers and designers.

3.3 Progressive failure implementation in Abaqus

Although several models of progressive failure analysis have been implemented through the years and also successfully included in commercial finite elements softwares [20–25], they are mainly designed for the modeling of the composite structure layer by layer with cohesive elements at the interface between plies.

Recently, Simulia developed and introduced into its FEA software (Abaqus) the so-called "composite package", a feature that lets the designer create custom sections layups, defining only the mechanical properties of the single lamina. With this helpful tool, the designer is able to perform a first macroscopic analysis of the composite structure without modeling the composite material section ply by ply or applying the laminate theory to calculate the values of the mechanical properties of the whole stack.

Moreover, starting from release 6.8, Abaqus included into its features a new function for the simulation of progressive damage that previously was a VUMAT (a routine that describes a custom material model in Abaqus/Explicit) for fabric reinforced composites.

Using those two features, a virtual model of the experimental test has been realized and then implemented.

3.3.1 Virtual model of the experimental test

The virtual model of the experimental test reproduces in Abaqus environment the test in its whole configuration, steel plates included (figure 3.4).

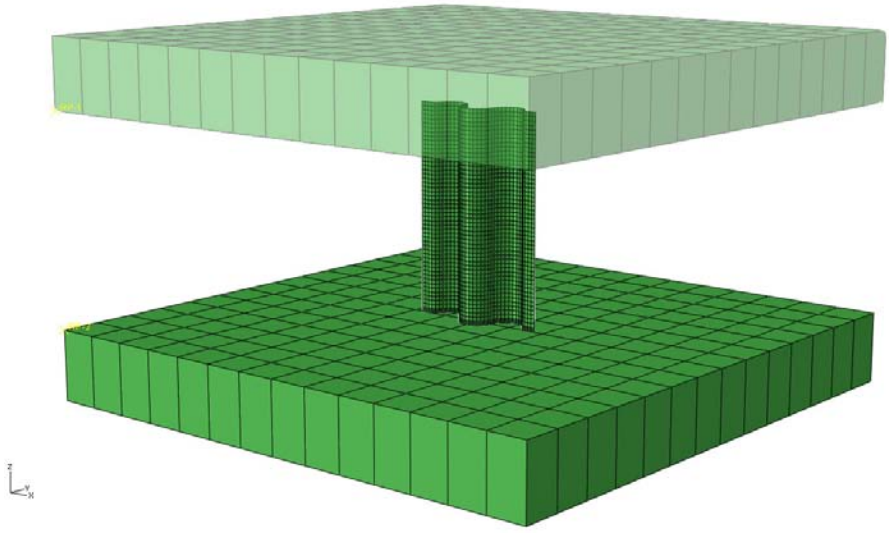

Figure 3.4: Experimental test modeled in Abaqus/Explicit

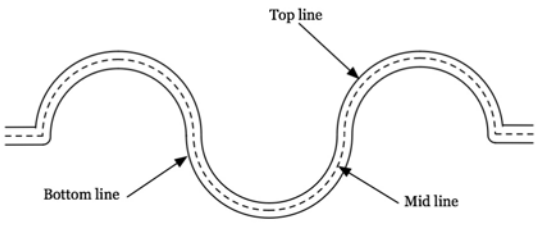

Figure 3.5: Specimen section with surfaces generatrices

Considering the peculiar geometry of the specimen, the tools for creating parts inside Abaqus are not adequate; therefore, the specimen, and also the plates, are separately designed with a CAD commercial software, in particular SolidWorks. The specimen is designed as a single surface that follows the bottom line (figure 3.5) of the corrugated profile, while the plates are two solid parallelepipeds. The three parts are then imported in Abaqus as a single assembly, so the relative positions are imposed.

Inside Abaqus, the specimen and the plates are meshed and modeled with appropriate elements.

The two steel plates are modeled as rigid bodies, so they do not interfere with the specimen crush, but their presence simplifies the definitions of boundary conditions and loads on the specimen.

The specimen is modeled with shell elements of type S4R: 4-node, doubly curved shell with reduced integration, hourglass control and finite membrane strains [26].

The stratification of composite material is realized using the composite layup feature of Abaqus. The usefulness of the composite layup tool is precisely the fact that only one surface discretized with shell elements is required to model custom stacking sequences instead of as many surfaces as the number of layers that constitutes the real stack.

In the composite layup modulus, for each set of elements corresponding to specific zones of the specimen it is possible to define:

- the number of plies;
- the material that constitutes the ply;
- the orientation of the fibers, with the possibility to refer it either to the global reference system or to a local one;
- individual ply thicknesses.

In this model, the specimen has four different sections that can be grouped into two zones (figure 3.6 as it really is: the trigger (three sections) and the full section (one section).

The full section is modeled with 12 plies $[0/90]_{3s}$, each ply has the nominal thickness of 0.15 mm for a total of 1.8 mm, the theoretical thickness of the specimen. The stratification of the shell elements (figure 3.7) can be set referring to the part surface: the surface can act as top, middle or bottom reference surface of the stack; in this case the part surface is set to be the bottom of the stack.

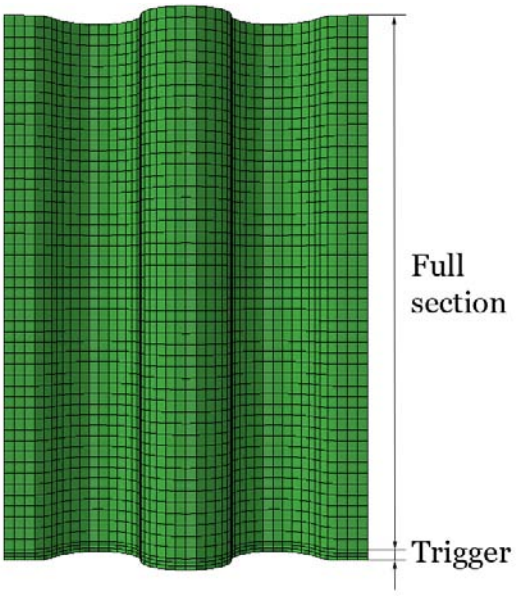

Figure 3.6: Main zones of the specimen

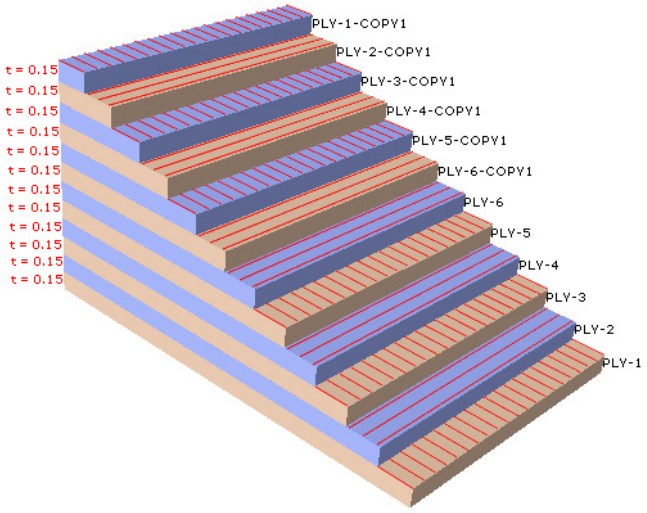

Figure 3.7: Full section stacking sequence – $[0/90]_{3s}$

The trigger itself is further divided into three sections, with a decreasing number of plies, to simulate the 45° chamfer (figure 3.8). The length of the trigger is equal to the thickness of the specimen and each section is equal to a third of the thickness.

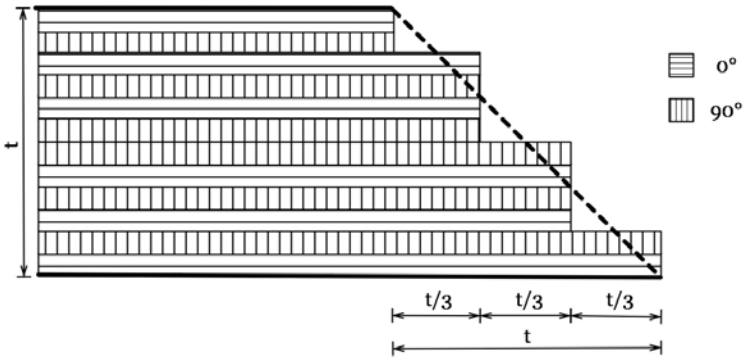

Figure 3.8: Trigger approximation – Stacking sequences

The carbon fiber reinforced plastics of which it is supposed to be made the specimen is described as a homogeneous orthotropic elastic-plastic material. The material properties assigned to the stack plies are those of Agate material, unidirectional tape, listed in table 2.7.

Besides the material properties, for each section the values for the transverse shear of the section are also required, defined [26] as

$$K_{11}, K_{22} = \frac{1}{6}\left(D_{11} + D_{22}\right) + \frac{1}{3}D_{33} \qquad K_{12} = 0 \tag{3.1}$$

where D_{11}, D_{22} and D_{33} are the elements of the stiffness matrix $\mathbf{D}$ of the laminate [27]. The calculated values for the four sections are reported in table 3.1.

Section	Layup	Number of plies	Transverse shear $K_{11},\ K_{22}$ [MPa·mm]
Main	$[0/90]_{3s}$	12	$4.336{\cdot}10^4$
Trigger 3	$[(0/90)/(0/90)_{2s}]$	10	$3.614{\cdot}10^4$
Trigger 2	$[0/90]_3$	6	$2.168{\cdot}10^4$
Trigger 1	$[0/90]$	2	$7.227{\cdot}10^3$

Table 3.1: Transverse shear values

Abaqus requires the definition of both boundary conditions and interactions for the assembly and its instances.

In order to reproduce faithfully the experimental test, to the top plate a condition of encastre is applied, while to the bottom plate the in-plane displacements and all the rotations are constricted, that is to say that it is free to move only in the vertical direction.

The specimen interacts with the plates through two tie constraints. The tie condition constraints each node of the slave surface (or, in this case, set of nodes) to have the same motion of the master surface to which it is closer.

These three conditions assure that the virtual model respects the real conditions applied to the experimental tests.

The last necessary condition to complete the finite elements model of the test is the definition of the load. While the experimental test develops under a condition of imposed displacement (1.5 in at 2 in/min or 37.5 mm at 0.83mm/sec), Abaqus requires a step time and gives ample choice of loading conditions except imposing pure displacement. The loading condition, therefore, is imposed through a predefined field of vertical velocity equal to 0.83 mm/sec in a step that lasts 45 sec.

3.3.2 Abaqus progressive damage model

As long as the model described in the previous section is not associated to a material model that describes the points 3 and 4 of the progressive analysis method, this model will essentially remain an empty vessel, a structure with which only linear elastic analysis can be performed.

As today, the progressive damage model for fabric reinforced plastics of Abaqus is still a hidden feature that activates giving a specific name to the material.

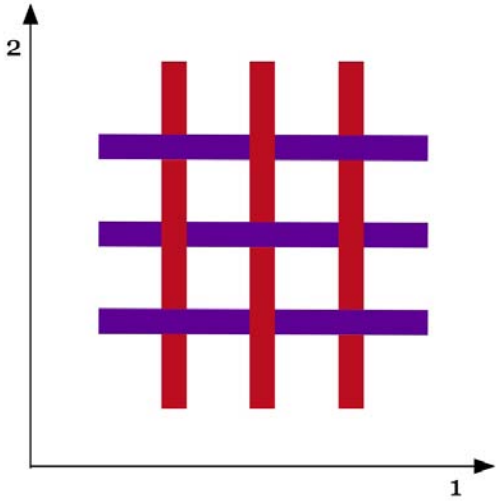

Figure 3.9: Schematic representation of a woven fabric with local system oriented along fibers direction

The fabric reinforced ply is modeled as a homogeneous orthotropic elastic-plastic material, which properties are degraded due to fiber/matrix cracking. Referring to the local coordinate system aligned with the fibers direction as in figure 3.9, the properties degradation is realized through the introduction of damage parameters into the elastic compliance matrix $\mathbf{S}$ in its general form [28]:

$$\mathbf{S} = \begin{pmatrix} \frac{1}{E_1(1-d_1)} & -\frac{\nu_{12}}{E_1} & 0 \\ -\frac{\nu_{12}}{E_1} & \frac{1}{E_2(1-d_2)} & 0 \\ 0 & 0 & \frac{1}{G_{12}(1-d_{12})} \end{pmatrix} \tag{3.2}$$

The three scalar parameters d_1, d_2 and d_{12} represent the damage evolution: d_1 and d_2 are associated to fiber damage or failure, while d_{12} is related to matrix micro-cracking due to shear deformation. The damage parameters have value $0 \leq d_i \leq 1$ and are monotonically increasing quantities. In figure 3.10 the qualitative evolutions of a generic material property (purple) and its related damage (red) are represented: the damage is constant set to 0 while the material reaches its elastic

limit; when the elastic limit is reached, the damage increases from 0 to 1 and at the same time the material property decreases to 0.

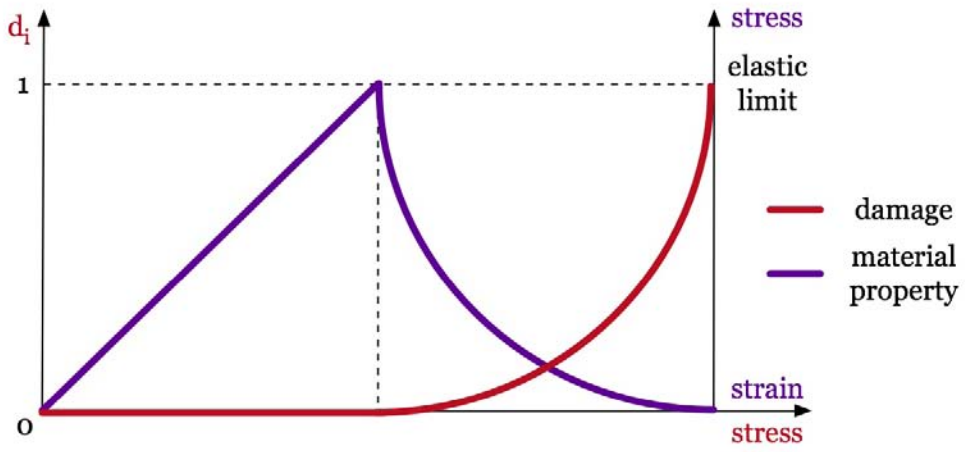

Figure 3.10: Qualitative behavior of a mechanical property in relation to the damage evolution

The model distinguishes the cases of tension and compression, activating the corresponding damage variable according to the stress state on the fiber direction. Also the initial (undamaged) values of E_1, E_2 and ν_{12} are assumed to take their tensile or compressive values depending on the sign of $tr(\varepsilon) = \varepsilon_{11} + \varepsilon_{22}$.

The evolution of the damage variables is a function of the corresponding damage thresholds and the fracture energy per unit area under tensile/compressive loading G_f^α, $\alpha = 1(\text{t/c}), 2(\text{t/c})$.

The values of G_f^α are determined experimentally with a procedure described by Pinho et al. [29].

The test procedure to determine the fracture toughness of the tensile and compressive fiber failure modes in laminated composites described in the paper, uses compact tension (CT) and compact compression (CC) tests respectively and is divided in two different parts:

1. a finite elements simulation of the experimental test with the application of the one-step VCCT (virtual crack closure technique), that provides the value of the normalized energy release rate $f(a)$ for different values of the crack length a;

2. a tensile/compressive test that provides data of load, displacement and position of the crack tip (using specific photogrammetry equipment).

From the finite elements simulation, the value of the J-integral around the crack tip can be determined; from the J-integral J, the value of the normalized energy release rate $f(a)$ is obtained through the definition

$$f(a) = J \cdot \left(\frac{1 \text{ mm}}{1 \text{ N}} \right)^2 \tag{3.3}$$

Once the value of $f(a)$ is known, it is possible to calculate the value of $G_{Ic}|_{lam}$ as

$$G_{Ic}|_{lam} = \left(\frac{P}{h} \right)^2 \cdot f(a) \tag{3.4}$$

where P is the load registered during the test for that exact value of a to which the calculation of $f(a)$ is referred and h is the specimen thickness.

With the value of the critical energy release rate for the laminate, it is now possible to find the critical energy release rate corresponding to the fiber tensile failure or fiber kinking simply subtracting the term corresponding to matrix cracking registered in the 90° layers. Matrix cracking in the 90° layers is assumed to occur as a single crack in mode I for the CT tests and in mode II for CC tests, therefore:

$$G_{Ic}|_{fiber\ tensile} = G_{Ic}|_{lam\ tensile} - G_{Ic}|_{matrix\ Intra} \tag{3.5}$$

$$G_{Ic}|_{fiber\ kinking} = G_{Ic}|_{lam\ compr} - G_{IIc}|_{matrix\ Intra} \tag{3.6}$$

but in carbon/epoxy systems, the matrix failure mode toughness is much lower than the fiber failure toughness, so the terms in the equations (3.5) and (3.6) associated to matrix can be omitted without a significant loss in accuracy.

The progressive failure model provides also options for the deletion of the elements when either the tensile or compressive damage variable along the fiber directions reaches a maximum specified value $d_\alpha = d_{\max}$, or when the plastic strain due to shear deformation reaches a maximum specified value $\bar{\varepsilon}^{pl} = \bar{\varepsilon}^{pl}_{\max}$.[1]

The material model requires twenty-five input values for material properties, that can be divided in four groups:

1. mechanical properties of the material;
2. damage evolution coefficients;
3. shear plasticity coefficients;
4. controls for material point failure.

[1]It is not possible to disclose further details of the mathematical model because of the confidential nature of the relative documentation

The mechanical properties of the material (table 3.2) are evaluated through standard tests:

- ASTM D3039 [30] for the determination of tensile properties;
- ASTM D695 [31] for compressive properties;
- ASTM D7078 [32] for the determination of in-plane shear properties.

Mechanical properties of the material	
E_1, E_2	Tensile Young's moduli in directions 1 and 2
E_{1c}, E_{2c}	Compressive Young's moduli in directions 1 and 2
ν_{12}, ν_{12c}	Poisson's ratios, tensile and compressive
G_{12}	In-plane shear modulus
$\sigma_{u1t}, \sigma_{u2t}$	Ultimate tensile stresses in directions 1 and 2
$\sigma_{u1c}, \sigma_{u2c}$	Ultimate compressive stresses in directions 1 and 2
σ_{u12}	Ultimate shear stress

Table 3.2: Model input – Mechanical properties of the material

The damage evolution coefficients (table 3.3) G_f^{α} (fracture energies per unit area) are determined with the experimental procedure described by Pinho et al. [29]; α_{12} is set as a standard value for carbon/epoxy systems at 0.22 and $d_{12\ \max}$ is imposed as a maximum value allowable for the damage parameter d_{12}.

Damage evolution coefficients	
G_f^{1t}, G_f^{1c}	Tensile and compressive fracture energies
G_f^{2t}, G_f^{2c}	per unit area in directions 1 and 2
α_{12}	Parameter for shear damage evolution
$d_{12\ \max}$	Maximum shear damage

Table 3.3: Model input – Damage evolution coefficients

Of the shear plasticity coefficients (table 3.4), the ones of the hardening curve C and p are calculated using a polynomial model by Ramberg-Osgood that uses the mechanical characteristics of the matrix G_{12}, τ_u and γ_u, respectively the shear modulus, ultimate shear stress and ultimate shear strain obtained from the resin data sheet; the initial yield value $\tilde{\sigma}_{y0}$ is set as the 0.2% of the residual yield stress.

Shear plasticity coefficients	
$\tilde{\sigma}_{y0}$	Initial yield
C	Hardening coefficient
p	Hardening power

Table 3.4: Model input – Shear plasticity coefficients

The last three input values are the controls for the material point failure (table 3.5). `lDelFlag` is the element deletion flag and it can be set only to 0 or 1; if set to 1, the element deletion is active; $d_{\max}$ is the maximum value the damage variable can reach before the element deletion is activated and similarly the parameter $\bar{\varepsilon}^{pl}_{\max}$ is the maximum value allowed for equivalent plastic strain element deletion criterion. If $\bar{\varepsilon}^{pl}_{\max}$ is set to zero, the criterion is inactive.

Controls for material point failure	
`lDelFlag`	Element deletion flag
$d_{\max}$	Maximum value of damage variable allowed
$\bar{\varepsilon}^{pl}_{\max}$	Maximum value of equivalent plastic strain allowed

Table 3.5: Model input – Controls for material point failure

While the determination of the most of the parameters listed above is possible with standard experimental tests or through calculations, the energies per fracture area G_f^α require very expensive equipment for their determination, not available at university facilities. The determination of the values of G_f^α, therefore, required an extensive work of tuning of the numerical model.

The calibration of the values of the fracture energies per unit area started with a first set of simulations to evaluate the influence of each G_f^α on the model response and their interactions, using an explorative constant value of 100 J/mm^2.

This first DoE (table 3.6) showed that in the particular case of a stack of plies of unidirectional tape with the fibers oriented with direction 1, referring to figure 3.11, G_f^{1t} has no influence on the specific energy absorption (1) and that G_f^{1c} controls the peak amplitude of the SEA (2) in different measures when coupled with G_f^{2t} and G_f^{2c}.

Focusing the attention on the influence of G_f^{1c} on the energy absorption behavior, another set of simulations was performed. Different values of G_f^{1c} were used and the relative peak value of the SEA was recorded; a polynomial interpolation

ID	G_f^{1t}	G_f^{1c}	G_f^{2t}	G_f^{2c}
1	0	0	0	0
2	100	0	0	0
3	0	100	0	0
4	0	0	100	0
5	0	0	0	100
6	100	100	0	0
7	100	0	100	0
8	0	100	100	0
9	100	0	0	100
10	0	100	0	100
11	0	0	100	100
12	0	100	100	100
13	100	0	100	100
14	100	100	0	100
15	100	100	100	0
16	100	100	100	100

Table 3.6: Explorative DoE for fracture energies per unit area G_f^{α}

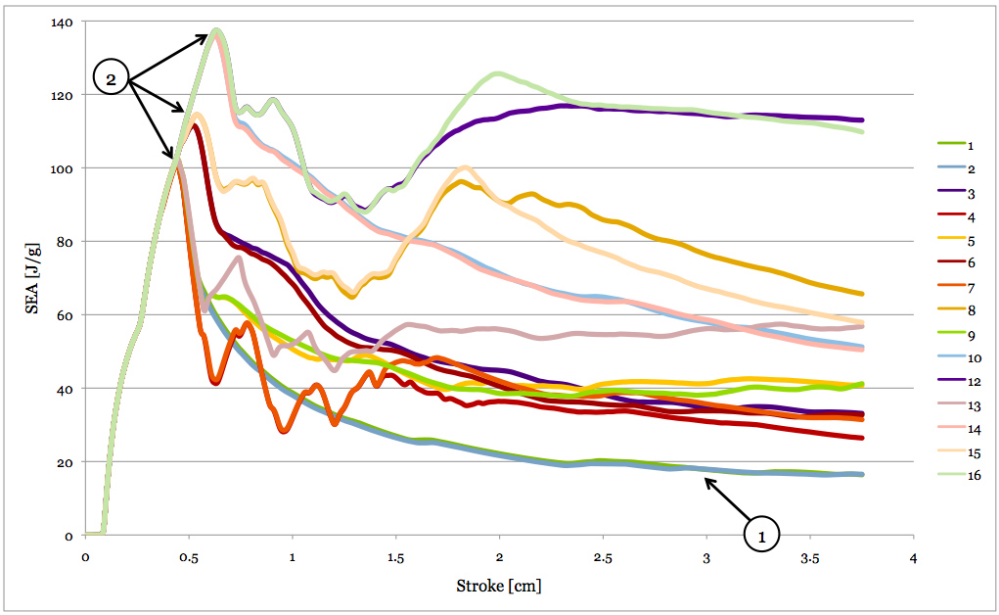

Figure 3.11: Influence of an explorative value of G_f^{α} on the SEA

of the data helped the determination of the value of G_f^{1c} corresponding to a realistic peak value for the SEA. Consequently, the values for G_f^{1t}, G_f^{2t} and G_f^{2c} were iteratively defined to complete the set of required input data.

The numerical analysis has to provide two relevant results in terms of macroscopical reproduction of the experimental test: they are the deformed shape of the assembly at the end of the simulation and the specific energy absorption behavior.

In figure 3.12 the deformed shape of the assembly is shown. The red elements are still active elements while the blue ones are dead. Macroscopically, it can be stated that the numerical model looks like the experimental test, except that it disintegrates progressively as the bottom plate moves towards the top one; this behavior is as expected, considering that the specimen is constituted by only one layer of shell elements and that delamination phenomena are not visualizable with the actual modeling of the composite layup.

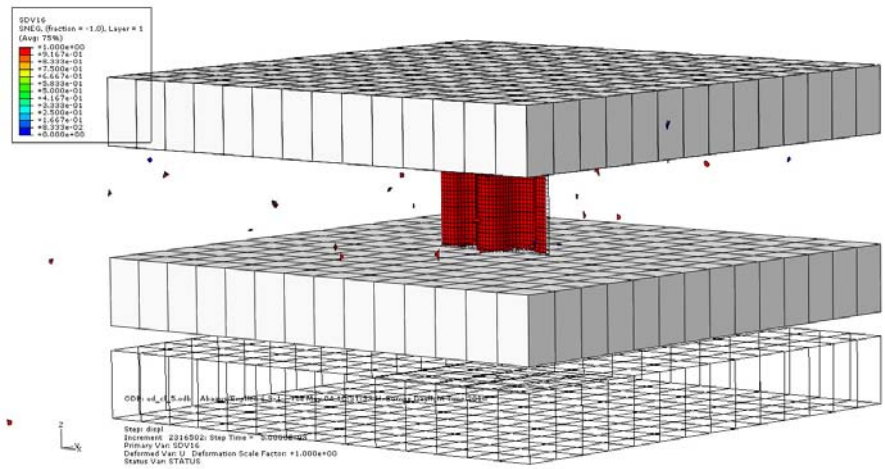

Figure 3.12: Undeformed and deformed shape of the assembly at the end of the simulation

During the crushing simulation, though, there is not a progression of the damage level inside the elements: as it is possible to see in figure 3.13, the damage parameters d_1 (red) and d_2 (green) for a randomly picked dead element pass instantaneously from 0 to 0.9999, the value set for $d_{\max}$; in this case the damage parameter referred to shear d_{12} (purple) does not contribute to element failure. Their behavior, therefore, lead to the case of instantaneous unloading represented in figure 3.3.

As for the experimental test, a force-displacement history is obtained, referring to the reaction force in the displacement direction recorded on the top plate (as rigid body, the position of the point where the force is evaluated does not affect the force value) and considering the displacement of the bottom plate. From the data collected, applying the equations (1.1) and (1.2), the evolution of the SEA

in function of the bottom plate displacement, as reported in figure 3.14, can be determined.

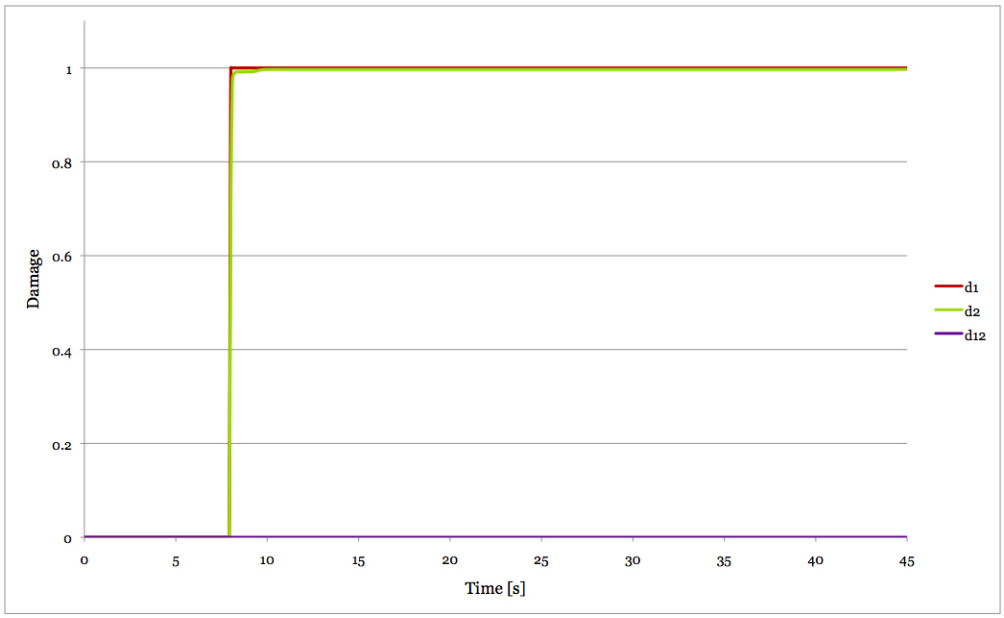

Figure 3.13: Damage evolution for a failed element

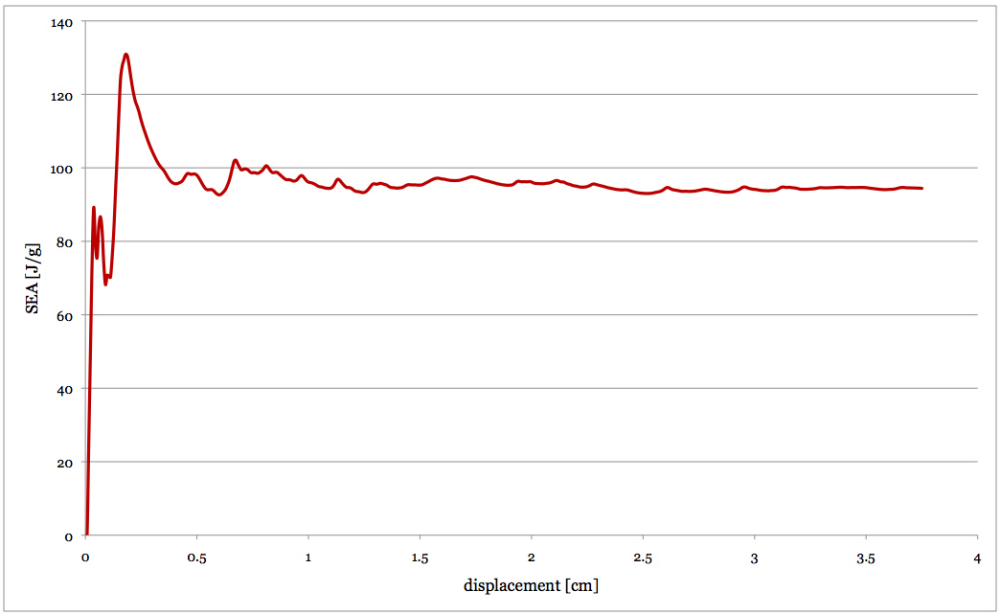

Figure 3.14: Specific energy absorption obtained with numerical simulation

Although the results obtained with this model of progressive damage for fabric reinforced materials accomplish to the requirements of macroscopical reproduction

of the deformed shape of the specimen with a relative constant value for specific energy absorption (the comparison with experimental results will be discussed in chapter 4), the model setup presents several issues.

The main difficulty is the high number of the input parameters required for the definition of the material characteristics. In fact, besides properties easily obtainable with standard test methods [30–32], the determination of a group of material properties extremely relevant for this model (G_f^{α}, fracture energies per unit area) requires a complex procedure and expensive equipment [29] or, in alternative, a long tuning procedure focused on the particular material system used in the analysis. This aspect, therefore, interferes with the expectations of a quick and economic tool to speed up the building block approach process.

Another aspect that should be improved in this model is the progression of the damage level at least into discrete steps. Even though the instantaneous passage of the damage parameters from 0 to $d_{\max}$ is the most common degradation method for the material properties of a lamina [19], it not appropriate to simulate the failure of a laminate, because of the load redistribution that happens in a laminate when one of the plies fails.

3.3.3 Alternative VUMAT for progressive damage

The idea of a new progressive damage model arose inspired by the two needs of:

- a material model with a simpler set of input values than the one integrated in Abaqus;
- a more realistic progressive damage, suitable for a model based on stratified shell elements that should simulate a laminate and not a single lamina.

As previously mentioned, the progressive damage model included in Abaqus was originally a VUMAT, a Fortran code that implements a custom user material model.

Starting from that particular VUMAT for fabric reinforced composites, a new VUMAT has been developed implementing a different failure criterion and a different damage parameters evolution than the existent Abaqus routine. The general scheme of the VUMAT is illustrated in figure 3.15. The new VUMAT is applied to the same finite element model of the experimental test described in 3.3.1.

As failure criterion, the new VUMAT described in this section uses the Tsai-Wu criterion because with just one equation it is possible to define if the material fails; moreover, with a limited number of mechanical properties of the material the criterion equation is defined.

The Tsai-Wu criterion is a polynomial criterion and it assumes the existence of a failure surface in the stress space that has the form

$$f_i\sigma_i + f_{ij}\sigma_i\sigma_j = 1 \qquad i,j = 1,2,\ldots,6 \tag{3.7}$$

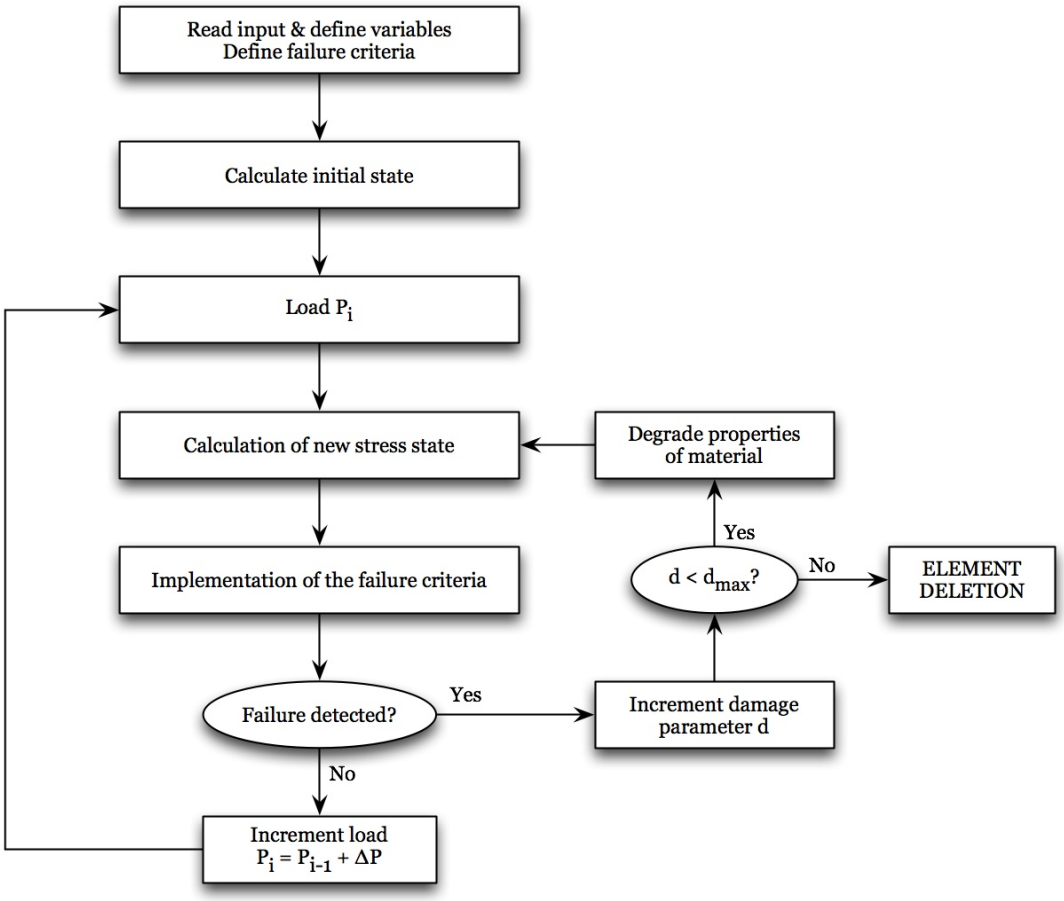

Figure 3.15: Scheme of a VUMAT routine for progressive damage

where f_i and f_{ij} are the components of the lamina strength tensors in principal material axes.
Assuming a plane stress condition, the explicit form of the criterion is

$$f_1\sigma_1 + f_2\sigma_2 + f_3\sigma_{12} + f_1 1{\sigma_1}^2 + f_{22}\sigma_2^2 + f_{33}\sigma_{12}^2 + 2f_{12}\sigma_1\sigma_2 + 2f_{13}\sigma_1\sigma_{12} + 2f_{23}\sigma_2\sigma_{12} = 1 \tag{3.8}$$

However, if a pure shear stress is applied along the principal axes of the material, the material strength should not be influenced by the sign of σ_{12}, therefore

$$f_3 = f_{13} = f_{23} = 0$$

and the criterion assumes its simplified form

$$f_1\sigma_1 + f_2\sigma_2 + f_1 1{\sigma_1}^2 + f_{22}\sigma_2^2 + f_{33}\sigma_{12}^2 + 2f_{12}\sigma_1\sigma_2 = 1 \tag{3.9}$$

The linear terms of the expression above distinguish the stress between tension and compression, while the term f_{12} takes into account the interaction of the stresses in the two principal directions.

To define the coefficients of the Tsai-Wu failure criterion (3.9), the input data required are ultimate strengths of the material, obtainable with ASTM standard tests [30–32]. The coefficients are defined as

$$f_1 = \frac{1}{\sigma_{u1t}} - \frac{1}{\sigma_{u1c}} \qquad f_{11} = \frac{1}{\sigma_{u1t}\ \sigma_{u1c}} \tag{3.10}$$

$$f_2 = \frac{1}{\sigma_{u2t}} - \frac{1}{\sigma_{u2c}} \qquad f_{22} = \frac{1}{\sigma_{u2t}\ \sigma_{u2c}} \tag{3.11}$$

$$f_{33} = \frac{1}{\sigma_{u12}} \tag{3.12}$$

$$f_{12} \approx -0.5\sqrt{f_{11} \cdot f_{22}} \tag{3.13}$$

and the qualitative shape of the failure surface, assuming the case of $\sigma_{12} = 0$, is represented in figure 3.16; in three-dimensions, the failure surface is an ellipsoid, symmetric in σ_{12} direction (orthogonal axis to the σ_1-σ_2 plane) and the failure surface of figure 3.16 is the particular case of its equatorial plane (figure 3.17).

The failure criterion as it is defined, determines the failure of the material when the stress condition satisfies the equation

$$\mathrm{TW} = f_1\sigma_1 + f_2\sigma_2 + f_1 1{\sigma_1}^2 + f_{22}\sigma_2^2 + f_{33}\sigma_{12}^2 + 2f_{12}\sigma_1\sigma_2 \geq 1$$

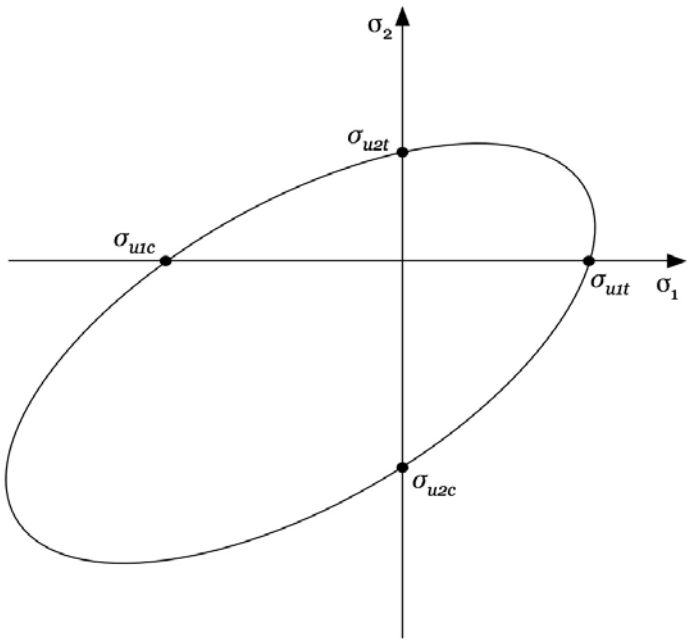

Figure 3.16: Qualitative representation for the failure surface of the Tsai-Wu failure criterion

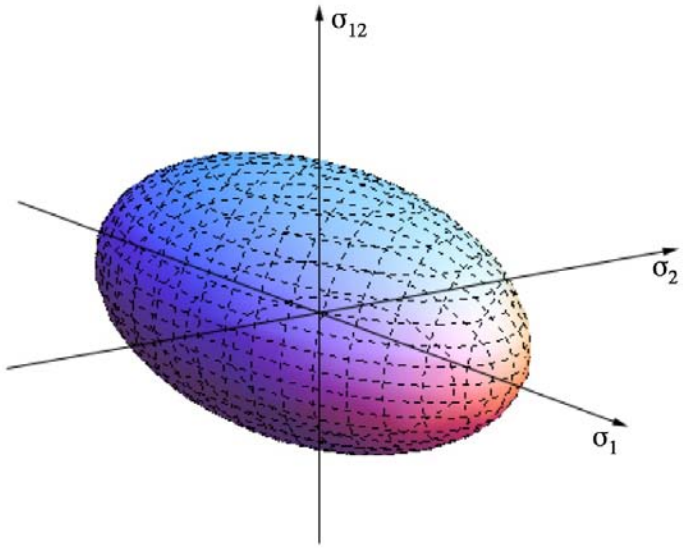

Figure 3.17: 3D qualitative representation of the Tsai-Wu ellipsoid

Assuming a damage parameter d related to the failure criteria (3.9) and

$$d = 1 \qquad \text{when} \qquad \text{TW} = 1 \tag{3.14}$$

a discrete number of damage levels d_i, with $0 < d_i < 1$ can be defined. In this model, the damage parameter d_i assumes the values

$$d_i = \{0.1, 0.25, 0.5, 0.75, 0.99\} \qquad i = 1, 2, \ldots, 5 \tag{3.15}$$

The damage levels are a family of ellipsoids: each d_i ellipsoid contains the smaller d_{i-1} ellipsoid and, referring to their symmetry plane σ_1-σ_2, their centers are positioned progressively on the segment $\overline{OC}$ (figure 3.18), where $O\,(0,0)$ is the origin of axes of the reference system and $C\,(x_c, y_c)$ is the center of the ellipsoid TW = 1. Tthe axes of the ellipsoid are proportionally scaled in accordance with the imposed value of the damage parameter d_i.

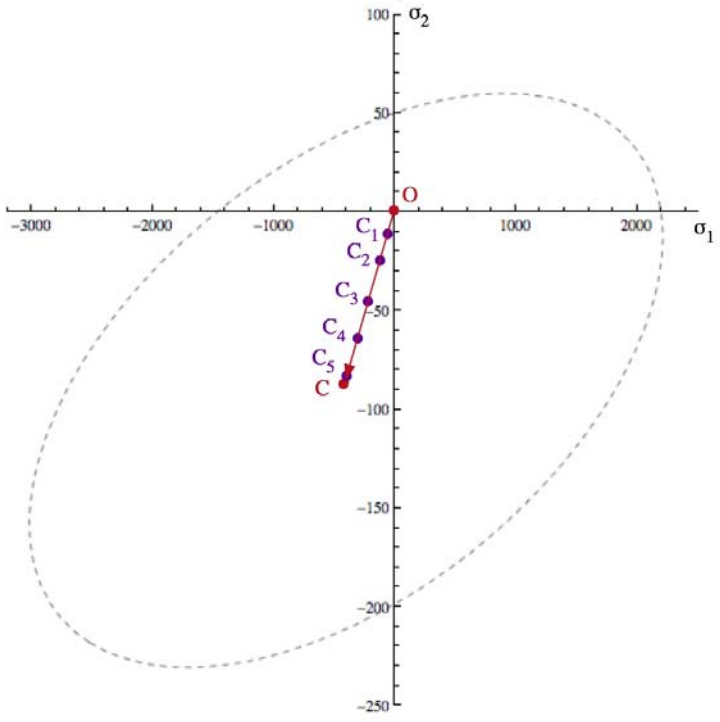

Figure 3.18: Position of the centers of the ellipsoids corresponding to intermediate damages

To define the ellipsoids corresponding to the intermediate damage levels, it is necessary to apply to the original ellipsoid two linear transformations, a rotation and a translation as showed in figure 3.19.

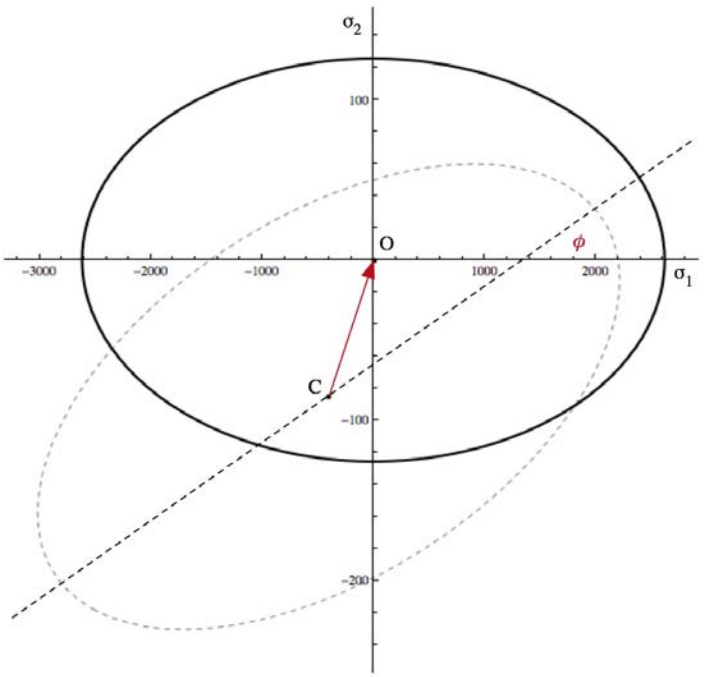

Figure 3.19: Rotation (ϕ) and translation transformations applied to the TW ellipse

For each damage level d_i, the ellipsoid equation is calculated with the new scaled axes and centered in the translated point C_i. The damage levels are therefore defined and visualized in figure 3.20.

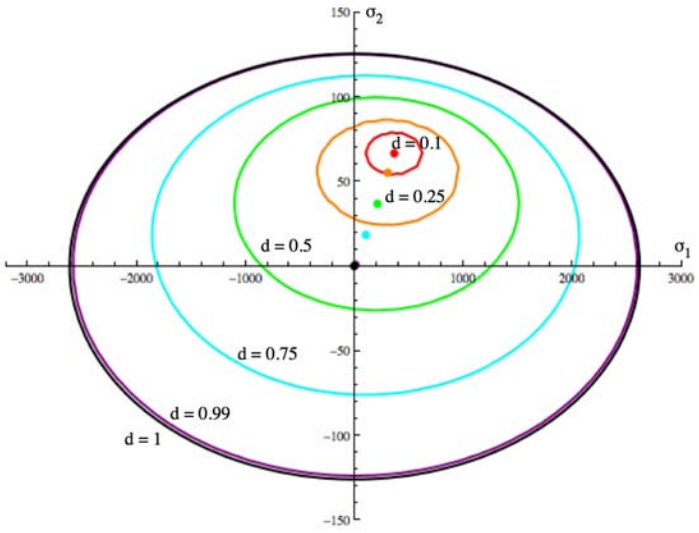

Figure 3.20: Damage levels visualization

In the VUMAT routine, for every iteration the linear transformations of rotation and translation are applied to the stress components of each element; the point $P\{\sigma_1, \sigma_2, \sigma_{12}\}$ that represents the element in the stress space is then univocally defined in the transformed space as $P'\{\sigma'_1, \sigma'_2, \sigma'_{12}\}$; then, according to its stress conditions, the damage level d_i of point P' is identified.

The damage level d_i so identified is the total damage of the element that degrades the material properties.

The material is modeled as homogeneous and orthotropic with damaged elastic stress-strain relations given by the compliance matrix

$$\mathbf{S} = \begin{pmatrix} \frac{1}{E_1(1-d_1)} & -\frac{\nu_{12}}{E_1} & 0 \\ -\frac{\nu_{12}}{E_1} & \frac{1}{E_2(1-d_2)} & 0 \\ 0 & 0 & \frac{1}{G_{12}(1-d_{12})} \end{pmatrix} \tag{3.16}$$

As in the Abaqus model, three damage parameters d_1, d_2 and d_{12} degrade the properties of the material: d_1 and d_2 are associated with the fiber fracture while d_{12} is related to the matrix micro-cracking due to shear deformation.

The three damage components are calculated as a percentage of the total damage d_i assigned to the element and identified in accordance with its effective stress state. $P'\{\sigma'_1, \sigma'_2, \sigma'_{12}\}$ is the point that identifies the element in the transformed stress state and to which the damage level d_i is assigned: the damage parameters d_1, d_2 and d_{12} that degrade the material properties are proportional to the element stresses according to the relations

$$\bar{d}_1 = \frac{\sigma'^2_1}{\sigma'^2_1 + \sigma'^2_2 + \sigma'^2_{12}} \qquad d_1 = \bar{d}_1 \cdot d_i \tag{3.17}$$

$$\bar{d}_2 = \frac{\sigma'^2_2}{\sigma'^2_1 + \sigma'^2_2 + \sigma'^2_{12}} \qquad d_2 = \bar{d}_2 \cdot d_i \tag{3.18}$$

$$\bar{d}_{12} = \frac{\sigma'^2_{12}}{\sigma'^2_1 + \sigma'^2_2 + \sigma'^2_{12}} \qquad d_{12} = \bar{d}_{12} \cdot d_i \tag{3.19}$$

Conditions of monotonic increase to the damage parameters are imposed; the element is deleted when the total damage is greater than $d_{\max}$.

The number of input values the new VUMAT needs is lower than the ones needed by the Abaqus progressive damage model: only 13 instead of 25 (table 3.7). The mechanical properties that describe the material are evaluated with standard ASTM tests: D3039 for tensile properties, D695 for compressive properties and D7078 for the in-plane shear properties. Of the input parameters that control the element failure, `lDelFlag` activates the element deletion when it is set equal to

one, while $d_{\max}$ is the maximum value allowed for the sum of the three damage parameters of the material matrix d_1, d_2 and d_{12}.

E_1, E_2	Tensile Young's moduli in directions 1 and 2
E_{1c}, E_{2c}	Compressive Young's moduli in directions 1 and 2
ν_{12}	Poisson's ratio
G_{12}	In-plane shear modulus
$\sigma_{u1t}, \sigma_{u2t}$	Ultimate tensile stresses in directions 1 and 2
$\sigma_{u1c}, \sigma_{u2c}$	Ultimate compressive stresses in directions 1 and 2
σ_{u12}	Ultimate shear stress
`lDelFlag`	Element deletion flag
$d_{\max}$	Maximum value of damage variable allowed

Table 3.7: Tsai-Wu VUMAT input

The results obtained with this new progressive damage model accomplish the requirement of an effective progression of the damage evolution during the simulation inside the element: as shown in figure 3.21, the total damage parameter d assumes progressively different values according to the damage level the element is in.

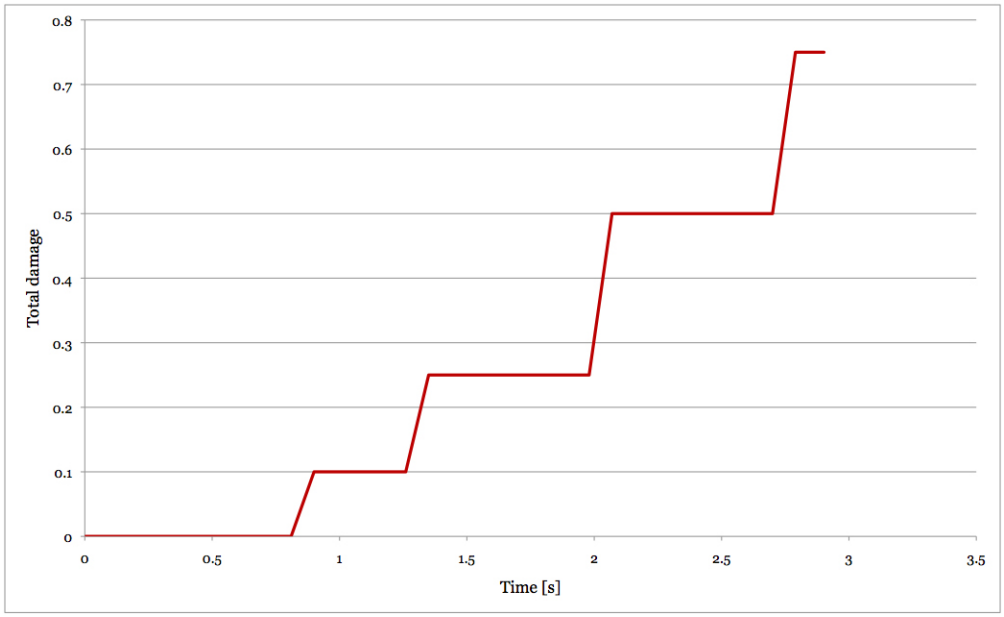

Figure 3.21: Damage parameter evolution during the simulation

Looking at the whole virtual model, the overall behavior reflects the progression of the damage levels (figure 3.22), concentrating the more damaged elements at the bottom of the specimen where the crushing load is applied.

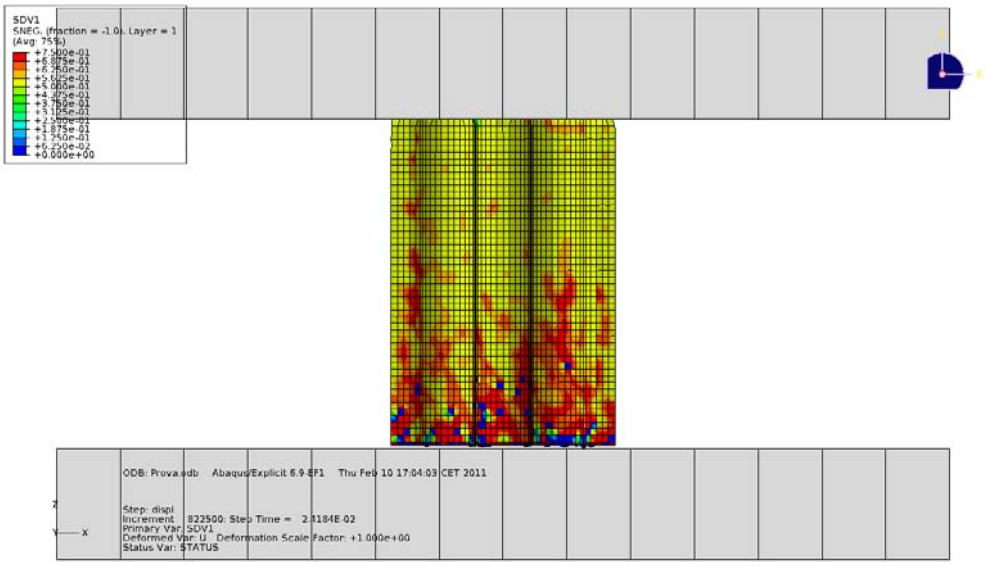

Figure 3.22: Damage evolution during the simulation

3.4 Numerical model conclusions

In this chapter, a numerical model for the simulation of the macroscopic behavior of a structure designed for crashworthiness will be presented.

The achievement of the numerical model is to provide a quick tool that can be used as an integration for the experimental tests during the first step of a building block approach program.

A virtual model of the experimental test was reproduced in Abaqus environment; with this model, two different progressive failure analysis were performed.

The first progressive failure model implemented is a native Abaqus model of progressive damage for composite materials.

The model is able to reproduce the macroscopical progressive crush of the specimen and provides an adequate level of energy absorbed, but it does not accomplish to the requirement of quickness: it requires a large amount of input data, some of them coming from complicate and expensive experimental tests. To override the experimental tests for the determination of those parameters, a long tuning procedure has to be performed, dedicated to the particular material system used

in the analysis. Moreover, the single elements do not fail progressively but instantaneously. This behavior is appropriate for the simulation of a single lamina, not for the simulation of a laminate which properties are supposed to degrade progressively during the analysis.

The second model for progressive failure is an improvement of the existent Abaqus one. The purpose of this model is to reduce the number of input values needed to define the model itself and provide an effective progression of the damage in the element during the analysis. The model is implemented in Abaqus through a VUMAT, an external routine that defines custom user materials.

The model is based on the Tsai-Wu failure criterion that for its definition requires only the mechanical properties of the material, which are obtainable with standard test methods. This new progressive failure routine is able to reproduce the damage progression in the element, but due to numerical issues dependent from the solver of Abaqus/Explicit, all the simulations interrupt before completing. The data collected are therefore only partial and at the moment it is not possible to show relevant results in terms of energy absorption for this progressive damage model.

Chapter 4

Results discussion

There is no such thing like failure.
There are only results.

A. Robbins

4.1 Introduction

In this chapter, the comparison between experimental and numerical results will be discussed.

The comparison between the experimental tests and the numerical simulations results focuses on two main points:

1. the macroscopical behavior of the real and the virtual specimen during the crushing process;
2. the capability of the numerical model of approximating the specific energy absorption progress of the experimental test.

The experimental tests results refer to those of self supporting specimens made of Agate unidirectional tape with $[0/90]_{3s}$ layup, because it is the configuration reproduced in the finite elements analysis.

4.2 Macroscopical crushing behavior

The macroscopical crushing behavior can be analyzed from two points of view:

1. the deformed shape of the virtual model;
2. the capability of the virtual model of simulating the progression of the damage.

The main aspect that can be noted from the comparison between the real crushed specimen (figure 2.31) and its virtual representations (figures 3.12, 3.22) is the absence of the two fronds in the latter.

The virtual model of the specimen, used with both the progressive damage models, is constituted by a single surface, composed of elements that simulate the composite layup according with the stacking sequence of the real specimen; this compact representation of the laminate is not able to reproduce the splaying mode and therefore the central intralaminar crack that forms in the reality. The absence of the fronds formation phenomenon does not affect the results in terms of energy absorption capability: the formation and propagation of the intralaminar crack involves mainly the material matrix, which contribution to the energy absorption is negligible.

More accurate results in terms of simulation of the deformed shape can be obtained by modeling each ply of the specimen as a single surface and then assigning cohesive elements at their interface, but this will increase the time of model definition and the computational cost, moving away from the requirement of easiness of modeling and quickness of setup.

Comparing the real specimen and the deformed shape of the virtual model obtained with the Abaqus progressive damage model, it can be stated that it accomplishes the requirement of macroscopic reproduction of the specimen crush, even if the damage parameter progression and the relative material properties degradation is of the instantaneous type (figure 3.3).

An improvement in this direction is proposed by an alternative progressive damage model implemented through an external VUMAT, as shown in figure 4.1.

Although numerical issues prevent the simulation with the custom VUMAT to complete, it is possible to see that the damages of two elements randomly picked in the same area of the specimen have different progressions. The damage parameter of the Abaqus model passes instantaneously from zero to one, degrading consequently the material properties of the element and the element is deleted; the damage parameter of the custom VUMAT, on the other hand, rises gradually towards its maximum value degrading progressively the material properties of the element it is refered. The difference between the damage progressions is reflected, consequently, also in the whole specimen, evidencing in the simulation with the VUMAT a progressive distribution of the damage, which value decreases from the bottom to the top (the elements are more damaged near the crushing surface and less damaged close to the top plate).

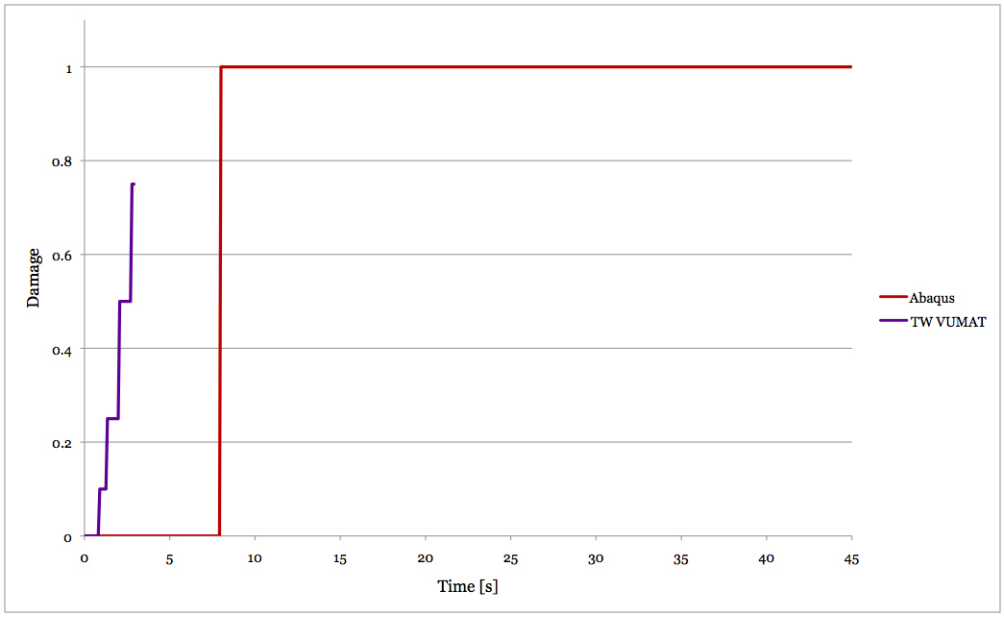

Figure 4.1: Damages progression during the simulation

4.3 Specific Energy Absorption approximation

The comparison of the specific energy absorptions takes place between the average of the experimental results and the numerical results obtained with the Abaqus progressive damage model and it is shown in figure 4.2.

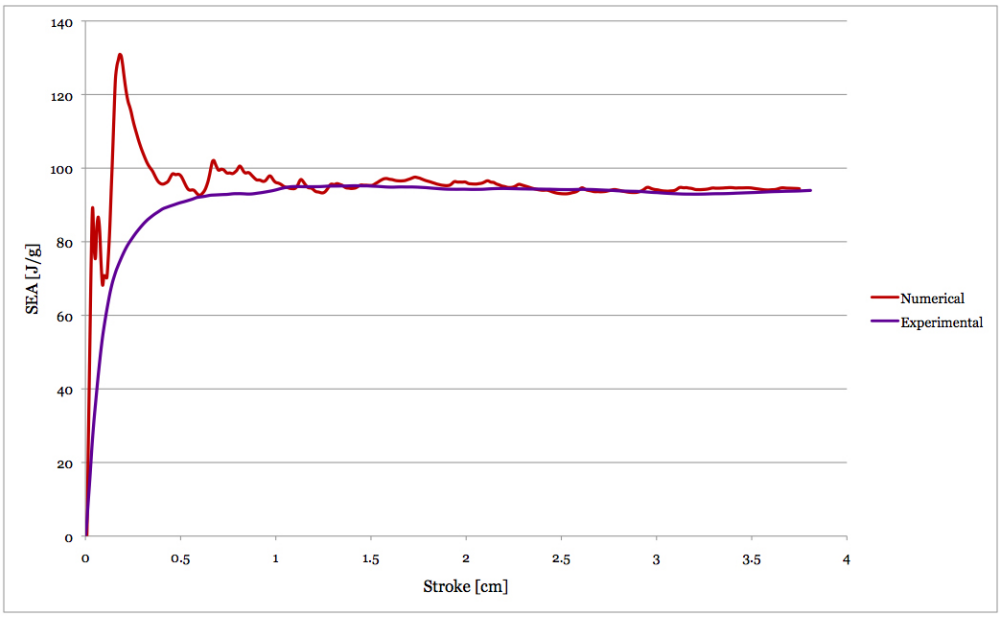

Figure 4.2: Damages progression during the simulation

The numerical result (red) differs for few aspects from the experimental result (purple), but at a first look it can be said that the overall behavior is similar and comparable.

The most remarkable difference is the presence of three peaks at the beginning of the crush. These three peaks represent the transient state, in fact the higher one corresponds exactly to a displacement value of 1.8 mm, that is equal to the specimen thickness and consequently the discontinuity between the thickest section of the trigger and the main section of the specimen. The presence of these peaks can be explained with the coarse discretization of the trigger used in the numerical model (figure 3.8): while in the experimental test the real trigger crushes smoothly and progressively, in the numerical model there are three well identified different sections, with relatively different behavior to the load applied.

It can be also observed that at the end of the transient state, the specific energy absorption of the the numerical model is not perfectly flat and overlapped to the experimental result, but oscillates around the test value. Once again it can be explained with the discretization of the specimen surface and the failure of the single finite elements.

In conclusion, the Abaqus progressive damage model achieves also the requirement of approximating with good precision the progression of the specific energy absorption of the experimental test.

Chapter 5

Conclusions

The main achievements of this thesis are the definition of a reliable experimental procedure for the quantification of the energy absorption capability of composite materials and the implementation of its numerical model.

This work constitutes also the first step of a building block approach program that, starting from experimental tests on small specimens and their numerical analysis, helps the designer to build the knowledge to better focus the study of more complex structures.

To pursue these aims, the work was articulated in two parts:

- experimental tests;
- numerical simulations.

In the experimental part, an extensive test campaign was performed to compare the most popular test methods, classified according to the kind of specimens they use as:

- flat specimens test method;
- self supporting specimens test method

and then evaluate their reliability.

The results obtained from the test campaign showed that the test method using self supporting specimens is more reliable and more consistent than the one that uses flat coupons. The self-supporting specimens test method, in fact, is not affected by external factors introduced by the anti-buckling fixture, necessary in the flat specimens test procedure.

Consequently to the comparison of the experimental results, a standard procedure is proposed according to requirements of:

- reliability;
- reproducibility of results;

- insensitivity to external factors.

The proposed method uses self supporting specimens crushed between two steel plates in quasi-static conditions.

In the numerical simulations part, a virtual model of the purposed standard test configuration is realized with Abaqus/Explicit.

The objectives of the numerical simulation are:

1. the representation of the macroscopic behavior of the experimental test during the crushing process;

2. the approximation of the experimental test specific energy absorption progress.

Two different progressive damage models were applied: a native Abaqus progressive damage model for fabric reinforced composites and a custom progressive damage material model implemented in Abaqus through a VUMAT, but only the Abaqus model gave results comparable with the ones of the experimental tests.

The comparison between the results obtained from the experimental tests and the numerical simulation with the Abaqus progressive damage model shows a progressive failure of the specimen during the crushing process that macroscopically reproduces the behavior of the real specimen and, moreover, it shows a good agreement between the relative energy absorptions.

Bibliography

[1] VV. AA. Chapter 14 – Crashworthiness and energy management. *MIL-HDBK-17-3F*, 3:1–10, Dec 2005.

[2] US Dept. of Transportation FAA. Advisory Circular 20-107b. pages 1–37, Sep 2009.

[3] G. C. Jacob, J. F. Fellers, S. Simunovic, and J. M. Starbuck. Energy absorption in polymer composites for automotive crashworthiness. *Journal of Composite Materials*, 36(07):813–850, Mar 2002.

[4] J. J. Carruthers, A. P. Kettle, and A. M. Robinson. Energy absorption capability and crashworthiness of a composite material - a review. *Applied Mechanics Review*, 51(10):635–649, May 1998.

[5] G. L. Farley and R. M. Jones. Energy-absorption capability of composite tube and beams. *NASA Technical Publications*, TM 101634:1–248, Jun 1989.

[6] J. A. Lavoie and J. Morton. Design and application of a quasistatic crush test fixture for investigating scale effects in energy absorbing composite plates. *NASA Technical Publications*, CR 4526:1–68, Jun 1993.

[7] J. A. Lavoie and S. Kellas. Dynamic crush tests of energy-absorbing laminated composite plates. *Composites: Part A*, 27(6):467 – 475, Sep 1996.

[8] S. Cauchi Savona and P. J. Hogg. Investigation of plate geometry on the crushing of flat composite plates. *Composites Science and Technology*, pages 1–12, Dec 2005.

[9] L. Daniel, P. J. Hogg, and P. T. Curtis. The relative effects of through-thickness properties and fibre orientation on energy absorption by continuous fibre composites. *Composites Part B*, 30:257–266, Mar 1998.

[10] D. Kohlgrüber and A. Kamoulakos. Validation of numerical simulation of composite helicopter subfloor structures under crush loading. *Proceedings of the 54th AHS Annual Forum*, Washington, DC, May 20-22:340–349, 1998.

[11] A. O. Bolukbasi and D. H. Laananen. Energy absorption in composite stiffeners. *Composites*, 26(4):291–301, Aug 1995.

[12] A. G. Mamalis, M. Robinson, D. E. Manolakos, G. A. Demosthenous, M. B. Ioannidis, and J. J. Carruthers. Crashworthy capability of composite material structures (review). *Composite Structures*, 37:109–134, Apr 1997.

[13] A. G. Mamalis, D. E. Manolakos, M. B. Ioannidis, and D. P. Papapostolou. Crashworthy characteristics of axially statically compressed thin-walled square cfrp composite tubes: experimental. *Composite Structures*, 63:347–360, Dec 2003.

[14] VV. AA. Chapter 4 – Carbon fiber composites. *MIL-HDBK-17-2F*, pages 1–29, Apr 2007.

[15] J. Tomblin, J. Sherraden, W. Seneviratne, and K. S. Raju. A-basis and B-basis design allowables for epoxy-based prepreg TORAY T700SC-12k-50C/#2510 Plain Weave fabric [SI units]. *AGATE-WP3.3-033051-134*, pages 1–258, Feb 2002.

[16] T. J. Brimhall. Measurement of static and dynamic friction energy absorption in carbon/vinyl ester composite. pages 1–13, Aug 2006.

[17] VV. AA. Volume 3 - Polymer matrix composites materials usage, design and analysis. *MIL-HDBK-17-3F*, pages 1–693, Jul 2002.

[18] P. Maimì, P. P. Camanho, J. A. Mayugo, and C. G. Davila. A continuum damage model for composite laminates: Part i – constitutive model. *Mechanics of Materials*, 39:897–908, Jun 2007.

[19] D. W. Sleight. Progressive failure analysis methodology for laminated composite structures. *NASA Technical Publications*, TP-1999-209107:1–92, Feb 1999.

[20] D. H. Laananen and A. O. Bolukbasi. Prediction of energy absorption in composite stiffeners. *Composite Structures*, 32:173–186, Apr 1995.

[21] E. Deletombe, D. Delsart, D. Kohlgrüber, and A. F. Johnson. Improvement of numerical methods for crash analysis in future composite aircraft design. *Aerospace Science and Technology*, 4:189–199, Apr 2000.

[22] P. B. Bogert, A. Satyanarayana, and P. B. Chunchu. Comparison of damage path predictions for composite laminates by explicit and standard finite element analysis tools. pages 1–28, Mar 2006.

[23] P. Maimì, P. P. Camanho, J. A. Mayugo, and C. G. Davila. A continuum damage model for composite laminates part ii – computational implementation and validation. *Mechanics of Materials*, 39:909–919, Jun 2007.

[24] N. F. Knight. User-defined material model for progressive failure analysis. *NASA Technical Publications*, CR-2006-214526:1–93, Dec 2006.

[25] C. G. Davila and P. P. Camanho. Failure criteria for FRP laminates in plane stress. *NASA Technical Publications*, TM-2003-212663:1–28, Oct 2003.

[26] Dassault Systèmes. *Abaqus 6.9 Documentation*. Jul 2009.

[27] G. Caligiana and F. Cesari. *I materiali compositi*. Pitagora editrice Bologna, 2002.

[28] A. F. Johnson. Modeling fabric reinforced composites under impact loads. *Composites: Part A*, 32:1197–1206, Aug 2001.

[29] S. T. Pinho, P. Robinson, and L. Iannucci. Fracture toughness of the tensile and compressive fibre failure modes in laminated composites. *Composites Science and Technology*, 66:2069–2079, Jul 2006.

[30] ASTM Standard D3039. Standard test method for tensile properties of polymer matrix composite materials. *ASTM International*, 2008.

[31] ASTM Standard D695. Standard test method for compressive properties of rigid plastics. *ASTM International*, 2008.

[32] ASTM Standard D7078. Standard test method for shear properties of composite materials by V-notched rail shear method. *ASTM International*, 2005.

Publications

P. Feraboli, F. Garattoni. "Development of a test method for composite materials energy absorption: corrugated specimens". 48th AIAA/ASME/ASCE/AHS/ASC Structures, Dynamics and Materials Conference, No. 2007-2011, Waikiki, HI (USA) – Apr. 2007

P. Feraboli, F. Garattoni, F. Deleo. "Toward the development of test standards for characterizing the energy absorption of composite materials: Part II". 7th SPE Automotive Composites Conference, Troy, MI (USA) – Sep. 2007

P.Feraboli, F. Deleo, F. Garattoni. "Efforts in the Standardization of Composite Materials Crashworthiness Energy Absorbtion". 22nd ASC Technical Conference, Seattle, WA (USA) – Sep. 2007

F. Garattoni, E. Troiani. "An experimental method and numerical simulation for composite materials energy absorption determination". 27th International Congress of the Aeronautical Sciences, Nice, France – Sep. 2010

F. Garattoni, G. Molinari, E. Troiani. "Development of a reliable test to support and validate a numerical model of progressive damage for composite materials". 2nd Aircraft structural design conference, Royal Aeronautical Society, London, UK – Oct. 2010

F. Garattoni, G. Molinari, E. Troiani. "Composite materials energy absorption determination: development of a reliable test and its numerical simulation ". Journal of Aerospace Engineering (Ready for submission)